Encapsulation strategy with whey protein isolate to improve bioaccessibility and targeted release of bioactive ingredients during (*in vitro*) digestion

By

Qianyu Ye

Master of Science (Chemistry)

Bachelor of Science (Chemistry)

A thesis submitted for the degree of Doctor of Philosophy at Monash University in 2021

Department of Chemical Engineering

Clayton Campus, Australia

March 2021

Copyright notice

Abstract

Numerous bioactive ingredients have received recognition for the benefits to human health. They may be sensitive to light, heat, or acid. Microencapsulation is a strategy to protect them from detrimental conditions and to achieve controlled release *in vivo*. Spray drying is timesaving, easy for production scale-up, and widely used in the food industry. Therefore, a versatile microencapsulation strategy *via* spray drying, utilising whey protein isolate (WPI) as the wall material, was proposed to improve the bioaccessibility and targeted release of bioactive ingredients.

Firstly, a method of ethanol desolvation and calcium crosslinking of WPI was established to fabricate riboflavin-WPI microparticles by spray drying. Desolvation exposed the buried apolar amino acids on WPI to riboflavin (a hydrophilic model drug), promoting the WPI-riboflavin complexation. The modification of WPI conformation *via* desolvation and crosslinking was retained in the spray-dried state, to obtain the microparticles with adjustable release profiles by changing the ethanol and Ca^{2+} concentrations from 0-50% v/v and from 0-2 mM, separately. The samples desolvated with 30% v/v ethanol without crosslinking showed rapid gastric release in 30 min. The particles desolvated with 30% v/v ethanol and cross-linked with 1 mM Ca^{2+} displayed remarkable gastric resistance and intestinal release.

Following this work, curcumin was selected as a core material with low bioaccessibility due to poor water solubility and stability. Curcumin-WPI complexation *via* desolvation was retained and enhanced by spray drying, reducing the content of uncomplexed curcumin to < 5% wt in the dry state, producing microparticles with better water solubility, stability, and bioaccessibility than raw curcumin. The desolvated microparticles allowed tenfold more curcumin to be loaded than those without desolvation. Upon integration into yogurt, the rapid-release sample discharged 87% curcumin, while the targeted-release formula liberated 44% after 1-hour simulated gastric digestion using a standard static protocol. Most of the yogurt sensory properties were not negatively impacted. This methodology allows food ingredients containing hydrophobic bioactive small molecules to be incorporated into a food matrix to improve bioaccessibility and targeted release, without affecting the sensory properties.

Simulating the *in vivo* pH evolution, gastric emptying, and digestion of the aforementioned curcumin-enriched yogurt in before/after-meal states was conducted, using a near-real dynamic *in vitro* human stomach (DIVHS), imitating the anatomical structures, peristalsis, and chemical environments of a human stomach. The effects of peristalsis, dilution, and proteolysis on digesta rheology were quantified, suggesting the decisive role of dilution and proteolysis. During digestion using the DIVHS, the peak release of curcumin was 43% at 120 min in the before-meal state, and 16% at 180 min in the after-meal state. The release difference resulted from the emptying kinetics in each state. Slower emptying in the after-meal state caused slower yogurt proteolysis and microparticle disintegration.

The thesis demonstrates that the microencapsulation strategy *via* spray drying can be used for both hydrophilic and hydrophobic bioactive small molecules, forming microparticles with improved bioaccessibility and targeted release for functional food applications. The active ingredient release could be measured using DIVHS in a near-real scenario without the invasive procedures and financial risks of *in vivo* studies.

Publications during enrolment

The following peer-reviewed publications arose from the involvement of the dissertation author in projects during the research degree enrolment:

Ye, Q., Georges, N., & Selomulya, C. (2018). Microencapsulation of active ingredients in functional foods: From research stage to commercial food products. Trends in food science & technology, 78, 167-179
https://doi.org/10.1016/j.tifs.2018.05.025

Ye, Q., Woo, M. W., & Selomulya, C. (2019). Modification of molecular conformation of spray-dried whey protein microparticles improving digestibility and release characteristics. Food chemistry, 280, 255-261.
https://doi.org/10.1016/j.foodchem.2018.12.074

Ye, Q., Ge, F., Wang, Y., Woo, M. W., Wu, P., Chen. C. X., & Selomulya, C. (2020). On improving bioaccessibility and targeted release of curcumin-whey protein complex microparticles in food. Food Chemistry, 346, 128900-128900
https://doi.org/10.1016/j.foodchem.2020.128900

Ye, Q., Ge, F., Wang, Y., Wu, P., Chen. C. X., & Selomulya, C. (2021). Digestion of curcumin-fortified yogurt in before/after-meal states using a near real dynamic *in vitro* human stomach. (Under review and revision)

Thesis including published works declaration

I hereby declare that this thesis contains no material which has been accepted for the award of any other degree or diploma at any university or equivalent institution and that, to the best of my knowledge and belief, this thesis contains no material previously published or written by another person, except where due reference is made in the text of the thesis.

This thesis includes three original papers published in peer reviewed journals and one submitted publication. The core theme of the thesis is Encapsulation strategy for improving bioaccessibility and targeted release of functional food ingredients during (*in vitro*) digestion. The ideas, development and writing up of all the papers in the thesis were the principal responsibility of myself, the student, working within the Department of Chemical Engineering, Monash University under the supervision of Prof. Cordelia Selomulya (main), Assoc. Prof. Meng Wai Woo, and Assoc. Prof. Victoria Haritos.

The inclusion of co-authors reflects the fact that the work came from active collaboration between researchers and acknowledges input into team-based research.

In the case of four chapters listed below, my contribution to the work involved the following:

Thesis Chapter	Publication Title	Status	Nature and % of student contribution*	Co-author names Nature and % of Co-authors' contribution*	Co-authors, Monash student
2	Microencapsulation of active ingredients in functional foods: From research stage to commercial food products.	Published	80% Conceptualization, Methodology, Software, Validation, Formal Analysis, Investigation, Data Curation, Visualization, Writing -Original Draft, -Review & Editing.	1. Nicolas Georges (2%): Funding Acquisition, Writing - Review & Editing. 2. Cordelia Selomulya (18%): Supervision, Conceptualization, Funding Acquisition, Project Administration, Writing - Original Draft, Writing - Review & Editing.	No No
3	Modification of molecular conformation of spray-dried whey protein microparticles improving digestibility and release	Published	80% Conceptualization, Methodology, Software, Validation, Formal Analysis, Investigation, Data Curation,	1. Meng Wai Woo (4%): Funding Acquisition, Writing - Review & Editing. 2. Cordelia Selomulya (16%): Supervision, Conceptualization, Funding Acquisition, Project Administration,	No No

Thesis Chapter	Publication Title	Status	Nature and % of student contribution*	Co-author names Nature and % of Co-authors' contribution*	Co-authors, Monash student
	characteristics.		Visualization, Writing -Original Draft, -Review & Editing.	Writing - Original Draft, Writing - Review & Editing.	
4	On improving bioaccessibility and targeted release of curcumin-whey protein complex microparticles in food.	Published	80% Conceptualization, Methodology, Software, Validation, Formal Analysis, Investigation, Data Curation, Visualization, Writing -Original Draft, -Review & Editing.	1. Fangzi Ge (1%): Writing - Review & Editing. 2. Yong Wang (4%): Funding Acquisition, Writing - Original Draft, Writing - Review & Editing. 3. Meng Wai Woo (2%): Funding Acquisition, Writing - Review & Editing. 4. Peng Wu (2%): Funding Acquisition, Writing - Review & Editing. 5. Xiao Dong Chen (2%): Funding Acquisition, Writing - Review & Editing. 6. Cordelia Selomulya (9%): Supervision, Conceptualization, Funding Acquisition, Project Administration, Writing - Original Draft, Writing - Review & Editing.	No No No No No No

I have renumbered sections of submitted or published papers in order to generate a consistent presentation within the thesis.

Student Signature: **Date**:

I hereby certify that the above declaration correctly reflects the nature and extent of the student's and co-authors' contributions to this work. In instances where I am not the responsible author I have consulted with the responsible author to agree on the respective contributions of the authors.

Main Supervisor Signature: **Date**:

Acknowledgements

First and foremost, I would like to express my deepest gratitude to my supervisors Prof. Cordelia Selomulya, Assoc. Prof. Meng Wai Woo, and Assoc. Prof. Victoria Haritos. Sincere thanks to my main supervisor Prof. Cordelia Selomulya for the support, encouragement, patience, motivation, and immense knowledge in my research throughout all the years during my PhD. I would like to also thank Assoc. Prof. Meng Wai Woo for his professional feedback on my work and sharing the knowledge on thermodynamics. I also thank Assoc. Prof. Victoria Haritos. Her knowledge on protein has provided critical guidance to my research. Thank Prof. Nicolas Georges for interviewing me when I was a Master student struggling to apply for a PhD position. I would also like to convey my thanks to Prof. Xiao Dong Chen to share his wisdom and kindly allow access to Soochow University. Finally, I would like to thank Dr. Yong Wang for his selfless guidance on rheology and for his endless patience and carefulness.

Secondly, I would like to show my gratitude to my friends. Thank Dr. Ruohui Lin for her generous help, cheerful personality, and being a reliable friend. Thank Dr. Jonathan Yekwai Chow, Dr. Grace Talbot-Walsh, Alina Tong Wu, Melissa Mace, and Jindi Yang, for the priceless and happy days in our small office. Thank my mentally matched friend Dr. Ruosang Qiu for her support and understanding. My heartfelt appreciation goes to my colleagues, Dr. Daisy Yang, Rachel Xueqing Liu, Mitra Nosratpour, Christine Darmali, Michael Kian Siang Lim, Dr. Huadong Peng, Kevin Nguyen Khai, Dr. Xingya Li, Dr. Yang Li, and Dr. Shanaz Mansouri. Particularly, I must express my appreciations to Chang Liu for the continuous support on enzyme kinetics.

I must thank my panel chair and examiners Prof. Ravi Jagadeeshan, Assoc. Prof. Victoria Haritos, Assoc. Prof. Louise Bennett, and Dr. Sushil Dhital, for being on my milestone committee and giving me suggestions on my project. I also acknowledge the administrative staff at Department of Chemical Engineering, Lilyanne Price, Tracy Groves, Kim Phu, Trina Olcorn, and Jill Crisfield.

I am thankful to the Australian Government Department of Industry, Innovation, and Science to support my project through the Australia-China Science and Research Fund (ACSRF48154), and the Australia-China Joint Research Centre in Future Dairy Manufacturing (http://acjrc.eng.monash.edu/). I wish to acknowledge Monash

University for Monash Graduate Scholarship (MGS) and Monash International Postgraduate Scholarship (MIPRS) for the PhD scholarship provided.

Most importantly, I would finally like to express sincere gratitude to my parents and grandparents for your unceasing encouragement and support. Special thanks to Yi for your inexhaustible love.

Contents

Chapter 1

Introduction

1.1 Background

Functional foods have received much attention with increasing demand for improving health and well-being. Numerous active ingredients *e.g.,* vitamins, lactic acid bacteria, unsaturated fatty acids, and polyphenols, have been proposed to provide health benefits. The process of adding the functional components to food and beverage products to enrich them with nutrients is referred to as food fortification. The global food fortification ingredients market had a 30.50 billion U.S. dollars valuation in 2016, and is projected to reach 100.84 billion U.S. dollars by 2025. Fortified foods have been identified as one of the strategies to prevent or reduce malnutrition, specifically in backward areas, by the Food and Agricultural Organization (FAO) and World Health Organization (WHO). The demand of customers for food fortification in developed countries is market-driven and growing exceptionally due to the increasing awareness about healthcare.

However, these aforementioned bioactive substances to some extent show susceptibility on exposure to high temperature and pressure during processing, oxygen, moisture, and light during storage, and physiological conditions during digestion. When integrating into food products, the components may possess off-flavours (*e.g.,* fish oil) and low palatability (some dietary fibre), which potentially reduce consumer acceptance. Microencapsulation is an extensively used technological solution to improve the preservation, palatability, and controlled release of functional ingredients. Besides, it shows significant advantages in enhancing the stability of nutrients, decreasing losses and overages during processing, and improving bioaccessibility and bioavailability during digestion. The key challenges in microencapsulation for food products can be classified into four categories. The first one is to produce microencapsulated active ingredients of food grade in a large scale *i.e.,* the scale-up for commercial production. The second issue is to reduce the cost of equipment and encapsulants, making the microparticles more economically advantageous. Another challenge is to incorporate the microcapsulated bioactive

ingredients into proper foods and to investigate the interaction between them *i.e.,* the development and optimisation of formulated functional foods. The last one is to ensure the release of bioactive components from the microparticles and formulated foods in the target site in human bodies. The grand challenge in target release of compounds in digestion system is firstly associated with the low stability, solubility, or bioavailability of some actives under various physiological conditions. This requires wall materials to provide the corresponding protections or functional properties to achieve controlled release. Additionally, there still exists a gap between *in vitro* and *in vivo* digestion methods. To make the *in vitro* digestion results as realistic as the *in vivo* ones, reproducing the dynamic *in vivo* conditions (*e.g.,* pH variation, digestive secretion, gastric emptying kinetics, gastric sieving effect, and gastrointestinal peristalsis) has become another challenge.

Technologies employed in the microencapsulation field can be classified into physical methods (*i.e.,* spray drying, supercritical fluid-based techniques, solvent evaporation, and lyophilisation/freeze drying), physico-chemical methods (liposomes, ionic gelation and coacervation), and chemical methods (interfacial polymerisation and molecular inclusion complexation). Spray drying is a one-step and continuous process widely applied in the food industry, capable of producing microparticles, nanoparticles, liposomes, and lipospheres in a large scale. A microcapsule or microparticle is characteristically a few microns in diameter, composed of core and wall materials. The typical core materials can be solids, liquids, and mixtures of them. Regarding food microencapsulation, the wall materials should be abundant, low-cost, and most importantly, safe for consumption in large quantities. Hence, food-grade natural polymers, synthetic polymers, and hybrid materials are commonly applied. The resulting structures can be divided into mono/multi-core shell and matrix type at which the core material is dispersed inside wall material network. The application of microparticles mainly depends on the core material, while the wall material affects the functional properties, including water solubility, particle size, mechanical strength, chemical stability, encapsulation efficiency, digestibility*, etc*. A combined effect of these properties determines the release characteristics, and target site of microparticles in human bodies. Many efforts have been made to tailor wall materials to meet the functional requirements of a specific core material.

The ultimate goal of microencapsulation of bioactive food components is to allow them to be efficiently released during *in vivo* digestion. However, upon food ingestion,

human gastric emptying kinetics and secretion rate are dependent on intake volume, viscosity, nutrient density, ingestion patterns, *etc*. The study of the food matrix breakdown and active ingredient release is challenging on human subjects because of invasive procedures or sophisticated tracer techniques. Using a dynamic digestive system model before any *in vivo* studies could be an alternative solution to evaluating targeted release in foods under various physiological conditions

1.2 Research aims

The focus of this project was to establish a simple microencapsulation strategy for core materials with different physicochemical properties, to enable the control of functional properties and release profiles of the microparticles for functional food applications. Riboflavin and curcumin were studied as two representatives of hydrophilic and lipophilic core materials, respectively. From a viewpoint of health benefits, riboflavin belongs to the B-vitamin family, with various biological effects *e.g.,* anti-aging, anti-inflammatory, and anti-cancer properties. Likewise, curcumin is a polyphenol extracted from the rhizome of turmeric plant, with pharmacological effects such as anti-inflammatory, antioxidant, anti-tumour, anti-proliferative, and anti-angiogenic activities. Whey protein isolate (WPI) as a typical dairy protein, was selected as the wall material due to the aqueous solubility, amphiphilicity, low cost, safety, and high nutritional value. The microparticles were incorporated into a food matrix and evaluated in an advanced near-real dynamic *in vitro* human stomach (DIVHS) to simulate *in vivo* release characteristics.

The hypothesis of this project was whether the scope of functional food design can be expanded, covering from the initial parameter optimisation of the microparticles added, to the integration into food matrix, the food breakdown during digestion, and further to the controlled release of active food ingredients in the target organ. The specific research aims are:

Chapter 3: to propose a simple methodology by which gastric digestibility, release sites, and release profiles of spray-dried riboflavin-WPI complex microparticles can be tuned *via* desolvation and crosslinking.

Chapter 4: to propose a strategy in which food ingredients containing hydrophobic bioactive small molecules can be incorporated into a food matrix to improve bioaccessibility and targeted release, without affecting their sensory properties.

Chapter 5: to explore the possible mechanisms for controlling the release of curcumin from yogurt, by utilising an *in vitro* digestion system that closely mimic the behaviour *in vivo*.

1.3 Thesis structure and chapter outline

This thesis is organised into 6 sections, as shown below:

Chapter 1 – Introduction

Chapter 2 – Literature review

Chapter 3 – Modification of molecular conformation of spray-dried whey protein microparticles improving digestibility and release characteristics. (Part 1)

Chapter 4 - On improving bioaccessibility and targeted release of curcumin-whey protein complex microparticles in food. (Part 2)

Chapter 5 - Digestion of curcumin-fortified yogurt in before/after-meal states: A study using a near-real dynamic *in vitro* human stomach. (Part 3)

Chapter 6 – Conclusions and recommendations.

Chapter 2

Literature Review

Part of this chapter has been published as a peer reviewed research paper by Trends in Food Science & Technology on 06 June 2018:
Ye, Q., Georges, N., & Selomulya, C. (2018). Microencapsulation of active ingredients in functional foods: From research stage to commercial food products. Trends in food science & technology, 78, 167-179
https://doi.org/10.1016/j.tifs.2018.05.025

2.1 Abstract

Twelve categories of active ingredients have been recognised to enhance human health. They are to some extent susceptible to certain conditions such as heat, light and low pH. To reduce their susceptibility and achieve controlled release at the target site, various microencapsulation strategies have been introduced. In this chapter, the chemical structures, physicochemical properties, and beneficial effects of the active components are summarised. Different encapsulation techniques and tailored shell materials have been investigated to optimise the functional properties of microcapsules. Several encapsulated constituents (*e.g.,* amino acids) have been successfully incorporated into food products while others such as lactic acid bacteria are mostly used in the free format. Encapsulating some of these active ingredients will extend their ability to withstand process conditions such as heat and shear, and prolong their shelf stability. The functional properties of a microcapsule are encapsulation efficiency, size, morphology, stability, release characteristics, *etc*. Several microencapsulation strategies include the use of double emulsions, hybrid wall materials and crosslinkers, increasing intermolecular attraction between shell and core, physical shielding of shell materials, and the addition of certain ions. Other approaches such as the use of hardening agents, nanoencapsulation, or secondary core materials, and the choice of shell materials possessing specific interactions with the core may be used to achieve targeted release of active ingredients. The physicochemical properties of shell materials influence where the active ingredients

will be released *in vivo*. A suitable microencapsulation strategy of active ingredients will therefore expand their applications in the functional foods industry.

2.2 Introduction

In the last decades, the concept of food has changed greatly. Nutrition is not only to sustain life, supply energy, or promote growth, but also to prevent disease and enhance physical and mental health. In the latter fields, “functional food” especially has attracted increasing attention.

Generally, functional foods are closely regulated but not recognised by law in most countries, resulting in no statutory definition. There is a working definition adopted by the European Commission Concerted Action *i.e.,* “a food can be regarded as ‘functional’ if it satisfactorily demonstrates to improve beneficially one or more target functions in the body, beyond the adequate nutritional effects in a way that is relevant to either an improved state of health and well-being and/or reduction of risk of disease” (Action, 1999). With respect to legal supervision, functional foods are regulated by Food and Drug Administration (FDA) in the USA but they are not specifically defined by law. Food Standards Australia New Zealand defines novel foods and food for special medical purposes. Japan regulates and oversees functional foods, named “Foods with Health Claims,” under the provision of a specific regulatory approval process. According to the Japanese Ministry of Health and Welfare, twelve broad categories of ingredients have been regarded to promote human health: dietary fibre; oligosaccharides; sugar alcohols; amino acids, peptides and proteins; glucosides; alcohols; isoprenes and vitamins; cholines; lactic acid bacteria; minerals; unsaturated fatty acids; and others *e.g.,* phytochemicals and antioxidants (Goldberg, 2012).

The supplementation of these active ingredients into food and dairy products is a commonly used method in the food industry to improve the nutritional value. Many of the ingredients have been researched and manufactured to produce functional foods such as orange juice with added calcium, eggs with increased omega-3 content, and sunflower seeds with guarana. In some of the cases, however, the active ingredients and their true effects on physiological functions in humans have not been fully deciphered. Considerable epidemiological, *in vivo*, *in vitro*, and clinical trials have been conducted but the results obtained are controversial and often contradictory. For example, the isoflavones extracted from soy were considered to be responsible for the

cholesterol-lowering effect of soy on blood lipids (Potter, 1998). However other reports showed no dependence of isoflavones on the hypocholesterolemic effect (Nestel et al., 1997). Furthermore, several active ingredients *e.g.,* probiotic bacteria, Vitamin B, conjugated linoleic acid and dairy proteins show instability on exposure to heat, acid, oxygen, or daylight. These issues lead to technological challenges and research opportunities including identification, separation, maximal recovery, and preservation of the active ingredients. Microencapsulation is a technological solution to optimise the preservation of active ingredients in raw materials and in foods during processing and storage.

Microencapsulation of functional components is a process of entrapping functional components within one or more classes of shell materials to fabricate a capsule, typically a few microns in diameter, referred as microcapsules. The microencapsulation process is to uniformly coat the functional ingredients with food-grade and biodegradable materials to separate the internal phase and the surrounding matrix. The separation is used to enhance nutrition, mask off-flavours, facilitate storage, and extend shelf life without adverse influence on their physical, chemical, or functional properties. Microencapsulation can be done *via* spray drying (Li et al., 2017), with the potential of tuning the colloidal and surface properties from the feed material, and their controlled release behaviour. Current methods used for microencapsulation consist of spray drying, spray cooling/chilling, layer-by-layer assembly, ultrasonic encapsulation, microfluidic encapsulation, homogenisation, simple extrusion, centrifugal extrusion, ionic gelation, thermal gelation, fluidised bed coating, lyophilisation/freeze drying, molecular inclusion complexation, coacervation, emulsion phase separation, liposome entrapment, solvent evaporation, polymer-polymer incompatibility (phase separation), supercritical fluid-based techniques, interfacial polymerisation, pan coating, air-suspension coating, spinning disk, vibrational nozzle, and sol-gel methods (Jamekhorshid et al., 2014; Jyothi et al., 2012; Ozkan et al., 2019; Suganya & Anuradha, 2017). Common techniques that have been widely used to fabricate microcapsules in the food industry are physical methods (*i.e.,* spray drying, supercritical fluid-based techniques, solvent evaporation, and lyophilisation/freeze drying), physico-chemical methods (liposomes, ionic gelation and coacervation), and chemical methods (interfacial polymerisation and molecular inclusion complexation) (Ozkan et al., 2019).

Microcapsules possess various functional properties including encapsulation efficiency, size, size distribution and morphology during preparation, stability under storage, and *in vitro* and *in vivo* release characteristics. The control of functional properties of microcapsules and the crosslinking mechanisms of shell materials play a vital role in the stability and the release characteristics, and thus have drawn much attention. Microcapsules with proper properties exhibit the potentials to increase viability and stability of core materials. Therefore, this chapter will focus on the definition, shell material selection and resulting functional properties of microparticles and their encapsulation strategies, and also provide a summary of active constituents *i.e.,* twelve categories of active ingredients approved as functional ingredients in Japan (Goldberg, 2012), which can be encapsulated and integrated into food products.

2.3 Microencapsulation

2.3.1 Microcapsules

In terms of a microcapsule, the substance entrapped within the carrier is known as the core material and the substance encapsulating the core material is named the shell/matrix material. Microcapsules are generally particles of size ranging from 1 to 1000 microns. The structure of microcapsules can be classified into mono-core shell, multi-core shell and matrix type at which the core material is dispersed as small droplets within the matrix material.

In order for the core material to be active and useful, many factors need to be considered, including molecular structure (molecular weight and electrical charge), physical state (boiling and melting point), biological structure (antimicrobial activity and bioactivity), solubility and surface activity, optical properties and chemical stability (oxidation and hydrolysis). For food ingredient production, the typical core materials are liquids and solids.

Ideal encapsulant materials are supposed to be biocompatible, biodegradable, non-toxic, and low cost. The characteristics of each type of encapsulant materials are summarised in **Table 2.1** below. The mechanisms behind the formation of shell/matrix structure can be divided into four categories based on the type of materials. Polymer chains are interconnected by covalent crosslinking into a hydrogel like membrane. Lipids are stabilised by hydrophobic and van der Waals interactions. Proteins are held together through hydrophobic interaction and covalent disulphide crosslinking. Sol-

driven metal alkoxides and silica are hydrolysed and polycondensed to form dense matrixes. Therefore, the release of the core material results from various mechanisms, ranging from physical fragmentation to chemical or enzymatic degradation. In a word, the double functionalities of cores and shells that can be independently adjusted cause various applications.

Table 2.1: Advantages and drawbacks of various encapsulant materials

Encapsulant materials	Organic materials			Inorganic materials
	Biological polymers	Synthetic polymers	Hybrid materials	
Advantages	Abundant, biodegradable, and biocompatible (Angelova & Hunkeler, 1999).	Easy to tune properties.	Obtaining the desired functionalities from a limited palette; lower cost than that of new polymer synthesis (Angelova & Hunkeler, 1999).	Higher chemical and mechanical stability.
Drawbacks	Unstable quality of products due to batch to batch variations (Angelova & Hunkeler, 1999).	Low biocompatibility and biodegradability (Angelova & Hunkeler, 1999).	Phase separation or plasticizer redistribution due to the low entropy of mixed systems.	Hard to adjust the microstructure of the microcapsules; high temperature processing; biocompatibility should be carefully tuned (Anglin et al., 2008).
Examples	Chitosan (Goycoolea et al., 2012); whey protein (O'Neill et al., 2015).	Poly (L-lactide-co-glycolide) (Morita et al., 2000).	Alginate–montmorillonite mixture (Kaygusuz & Erim, 2013).	Porous silicon (Anglin et al., 2008).

2.3.2 Functional properties of microcapsules

For a microcapsule loading one or more bioactive ingredients, the key functional properties include encapsulation efficiency, size and morphology during preparation,

stability under storage, and *in vitro* and *in vivo* release characteristics. Microcapsule size differs in a broad range, from submicron to millimetre with variation of encapsulation techniques. Extensive research has been conducted to tune the size of microcapsules by varying process parameters, amount and concentration of core and shell materials. For example, the size, encapsulation efficiency and hydrophobicity of casein hydrolysate-loaded microcapsules were tuned by varying shell materials and degree of hydrolysis of core materials (Morais et al., 2004). This section focuses on their stability under storage and *in vitro* and *in vivo* release characteristics.

Stability under storage includes oxidative stability, thermal stability, hygroscopicity, *etc*. For encapsulation of oxygen-labile core materials, double emulsion, and hybrid wall materials with/without crosslinkers are frequently used methods. Double emulsion possessing multilayer coating and thick layers provides protection against oxidative degradation. Regarding wall material, polysaccharide is the most popular candidate. It is cheap and useful for enhancing the water-solubility of hydrophobic core materials, which is vital for increasing bioavailability. However, shells made of some polysaccharides may have relatively large pores, causing the exposure or diffusion of entrapped substances (Zhang et al., 2016). Therefore other compounds are added into a single polysaccharide system to form a hybrid shell with compact structure to improve the resistance to oxygen (Hosseini et al., 2014). Commonly used crosslinkers include glutaraldehyde to chitosan, transglutaminase to protein hydrolysate, and $CaCl_2$ to alginate and whey protein isolate bead. Crosslinking enables to suppress the autoxidation and release of core materials.

Thermal stability is critical to certain core materials (*e.g.,* volatile aroma) and thermally sensitive enzyme when heat treatments are used. Intermolecular attraction between shell and core (Bernela et al., 2014), physical shield of wall materials (Rodriguez-Nogales & Delgadillo, 2005), and certain ions (*e.g.,* K^+ from KCl solution at 5 w/v%) (Zhang et al., 2016) stabilising the enzyme architecture are the main methods to improve thermal stability. To reduce hygroscopicity, core materials can be incorporated into encapsulants with high molecular weights (MW) to increase the glass transition temperature (Kurozawa et al., 2009).

Release characteristics of a microcapsule refer to release rate, release profile and target site. Many efforts have been made to control the rate of release. It includes hardening agents (Mank et al., 1996), secondary core materials (Mank et al., 1996), hybrid materials with/without crosslinkers (O'Neill et al., 2015), double emulsions

(Bonnet et al., 2010), multilayer coating (Tomaszewska & Jarosiewicz, 2006), capsules in nanoscale instead of microscale (Lin et al., 2013), and shell materials showing strong interaction with core (O'Neill et al., 2015). For a microcapsule with controlled release, its release profile is classified into: 1) initially burst and then sustained release and 2) thoroughly prolonged release. The first type is commonly observed in microcapsules with large pores on surface or weak interaction between shell and core materials. The interaction is associated with hydrophobicity, hydrophilicity, charge density, and molecular structure of materials. People normally favour the second type which is found in microcapsules containing strong interaction. Due to the surface distribution of core materials, matrix microcapsules have a stronger possibility of the first type release than core/shell ones. Target site of microcapsules depends on the physicochemical properties of shell materials. Eudragit L-100 and alginate are excellent candidates for target delivery to the intestine due to their pH-sensitive characters. Liposome and liposphere have the similar functionality since the majority of lipid metabolism in humans occurs in the small intestine. Additionally crosslinked whey protein isolates show resistance to digestion in the gastric fluid with pepsin (O'Neill et al., 2015). Upon crosslinking and aggregation, whey proteins lose their secondary structure. The high resistance of whey protein aggregates to digestion is presumably because most of the cleavage sites of the globular proteins are buried in the hydrophobic cores of the aggregates.

The final aim of microencapsulation of active ingredients is to release the components in a way in which they can be digested and absorbed efficiently in human digestive system. Due to the complexity of *in vivo* human studies and their high costs, *in vitro* controlled release studies are often done instead. Ideally, *in vitro* digestion systems are supposed to accurately reproduce the *in vivo* digestive behaviours (*e.g.,* gastrointestinal (GI) secretion, emptying, and peristaltic contractions) of various foods in different ingestion patterns. Over the past decades, a large amount of *in vitro* digestion systems have been created, ranging from single static bioreactors to multi-compartmental dynamic models, primarily focusing on gastric digestion simulation (Kong & Singh, 2008). Static *in vitro* models are normally made up of a series of stirred reactors due to the low cost, simple operation, bulk testing, and application to mechanistic studies and hypothesis development with certain applications (Minekus et al., 2014). However, the digestive physiology in the static models was too simplified to imitate the *in vivo* digestion behaviours of GI secretion, peristaltic, and emptying

simultaneously (Bornhorst & Paul Singh, 2014). To simulate the dynamic digestion process effectively, various dynamic digestion systems have been established, including the TNO's GI model (TIM-1) (Minekus et al., 1995), the dynamic gastric model (DGM) (Mercuri et al., 2008), the human gastric simulator (HGS) (Kong & Singh, 2010), the simulator of the human intestinal microbial ecosystem (SHIME) (De Boever et al., 2000; Molly et al., 1993), the *in vitro* mechanical gastric system (IMGS) (Barros et al., 2016), the dynamic rat stomach-duodenum system (DRS) (Wu, Bhattarai, et al., 2017; Wu et al., 2014; Wu, Deng, et al., 2017; Wu, Liao, et al., 2017), the dynamic human stomach-intestine system (DHSI) (Chen et al., 2016b; Wang et al., 2019), and the human gastric digestion simulator (GDS) (Kozu et al., 2014).

The models mentioned above simulate the physicochemical conditions in the GI tract, whereas several dynamic human digestion systems further mimic the stomach anatomy, morphology, and inner wrinkled structures, including rope-driven *in vitro* human stomach (RD-IV-HSM) (Chen et al., 2016a), and near real dynamic *in vitro* human stomach (DIVHS) (Wang et al., 2019). Development of *in vitro* model is based on the understanding of human digestive system. The system includes the GI tract and the accessory organs of digestion, which possess their own characteristics. Briefly, the inner layer of stomach is full of wrinkles, necessary for accommodating meals and peristalsis movement. Gastric juice provides a low pH condition (1.5-3.5) and pepsin secreted in the stomach hydrolyses proteins into small peptides. The small intestine contains bile, pancreatic juice, and intestinal juice. Pancreatic juice has high concentration of HCO_3^- and various enzymes. The HCO_3^- raises the low pH of the gastric juice to 7 and the enzymes catalyse the degradation of carbohydrates, proteins, and lipids. On the other hand, bile salts and phospholipids are crucial components of bile, accounting for emulsifying fats. The emulsification provides fats with a larger contact area with water-soluble pancreatic lipase. The absorptive surface area of the small intestine is largely increased due to the villi and the microvilli of enterocyte where the small intestine enzymes are anchored. Consequently, not only the physicochemical environment but also the morphological characteristics plays a role in the release, digestion, and absorption of active ingredients. For *in vitro* studies, the physicochemical environment *e.g.,* temperature, enzyme, and electrolyte concentration, is relatively easy to cope with. The major challenge is to mimic the morphological characteristics and movement type of the GI tract mentioned above. RD-IV-HSM is a dynamic model by incorporating the gastric morphology containing complex geometrical shape and

interior wrinkles to the *in vitro* human stomach model (Chen et al., 2016a). Peristalsis movement of the gastric wall is mimicked based on the rope-driven mechanism. The distribution and emptying order of buckwheat meal in the RD-IV-HSM agreed well with those reported from *in vivo* data (Burton et al., 2005; Malagelada et al., 1979; Moore et al., 1981). This indicates that the meal emptying was prolonged with an initial lag period by the solid fractions, while the liquid fractions left from the stomach model immediately after food intake. However, the RD-IV-HSM failed to disintegrate the large solid particles to achieve the gastric sieving effect, resulting from a lack of pylorus valve to control the opening/closure of the pylorus, as well as the insufficient peristaltic movements produced by the model (Chen et al., 2016a). In **Fig. 2.1**, the novel DIVHS was able to reproduce the peristaltic contractions moving chyme toward the pylorus and small intestine, with the aid of a separate roller-eccentric wheel subsystem. After ingestion of beef stew mixed with orange juice, the DIVHS could reproduce the dynamic gastric pH changes, emptying and sieving effect, and particle disintegration (Wang et al., 2019).

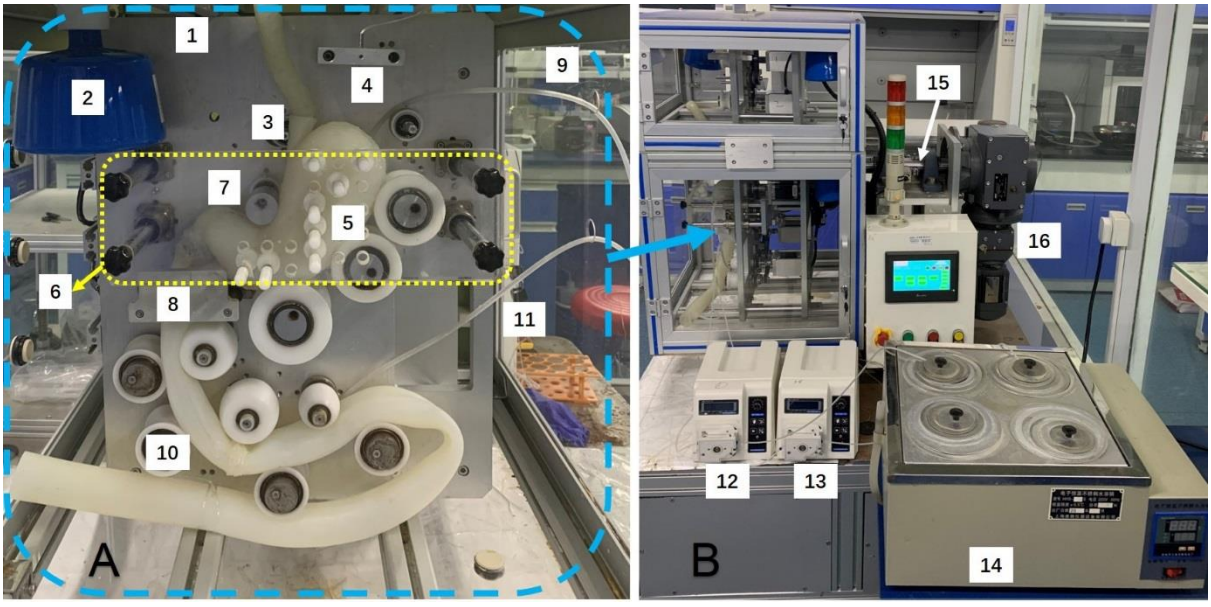

Fig. 2.1. Image of the DIVHS. (A) 1: fixed plate; 2: heat preservation lamp; 3: oesophagus model; 4: thermal sensor; 5: 3D-printed soft-elastic human stomach model; 6: transparent acrylic plate (yellow dashed box); 7: roller/eccentric wheel; 8: pylorus extrusion plate; 9: SGF secretion tube; 10: duodenum model; 11: SIF secretion tube. (B): the whole stomach system in the blue dashed box in (A) is installed in the metal/glass box in (B) as indicated by the blue arrow; (12) peristalsis pump used for

pumping the SGF; (13) peristalsis pump for the SIF; (14) water bath for warming the simulated digestive fluids; (15) auxiliary emptying device; (16) motor.

2.3.3 Microencapsulation methods for food application

Microencapsulation methods normally applied to prepare microparticles in the food industry include physical methods (*i.e.,* spray drying, supercritical fluid-based techniques, solvent evaporation, and lyophilisation/freeze drying), physico-chemical methods (liposomes, ionic gelation and coacervation), and chemical methods (interfacial polymerisation and molecular inclusion complexation) (Ozkan et al., 2019). The advantages and drawbacks of these methods are summarised in **Table 2.2** in detail.

In this project, the encapsulation technique used was the coupling between spray drying and desolvation. Spray drying is a method of atomising a feed liquid into a dry powder using an injector and a hot drying gas stream (Rattes & Oliveira, 2007). The feed liquid can be a solution, an emulsion, or a suspension, containing a wall and core material. Wall materials could be water-soluble polysaccharides *e.g.,* chitosan (Ye et al., 2018), gum *Arabic,* and maltodextrin (Minemoto et al., 2002), and various proteins *e.g.,* whey protein isolates (Ye et al., 2021), pea protein isolates (Ye et al., 2016), and sodium caseinate (Li et al., 2017). Typical core material are the twelve categories of bioactive food ingredients summarised in section 2.4. The key parameters in spray drying are wall material selection, solvent volatility, inlet/outlet temperatures, feed viscosity, feed solid content, feed surface tension, feed flow rate, feed temperature, dehumidified air flow rate, and sort of carrier and crosslinker (Mahdavi et al., 2014). When a microfluidic piezo atomiser is employed, microparticle characteristics also depend on nozzle conditions including atomiser orifice, resonance frequency, and amplitude.

These parameters significantly influence the functional properties of microparticles such as encapsulation efficiency, hygroscopicity, water dispersibility, yield, moisture content, *etc*. For example, under the same spray drying condition, propolis extract rich in polyphenols and flavonoids was microencapsulated with pea protein, soybean protein, rice protein, and ovalbumin upon spray drying, separately (Jansen-Alves et al., 2018). The encapsulation efficiency was evaluated based on polyphenols retained and entrapped. The encapsulation efficiency of the propolis

microparticles ranged from 70% to 90%, because both propolis polyphenols and these four proteins have high polarity, leading to a good affinity between them. Amongst them, the microparticles entrapped with rice protein had highest encapsulation efficiency around 90%, presumably due to its 7% carbohydrate content which affected the encapsulation process. The microparticles covered with rice and soy proteins possessed higher aggregation, hygroscopicity, and thus particle size, due to the nature of wall materials. The larger particle size of the microparticles produced with rice and soy proteins showed the lower water solubility and water absorption, explained by their lower specific surface area for hydration (Jansen-Alves et al., 2018; Kuck & Noreña, 2016). When concentrated pea protein was used at varying contents, the propolis microparticles covered with 2% pea protein had significantly higher encapsulation efficiency than those with 4% and 6% protein (Jansen-Alves et al., 2019). The encapsulation efficiency was also measured from the retention of flavonoids and phenolic compounds in propolis extract. It seems that the droplets dry faster at lower protein contents, accompanied by the faster generation of an external crust withholding more phenolic compounds. This phenomenon, in turn, led to the fact that the microparticles covered with less protein possessed higher moisture content, because the external crust hampers water evaporation (Jansen-Alves et al., 2019). Additionally, lower protein contents may shorten the exposure of core materials to high temperatures during spray drying, reducing the degradation risk of the flavonoids and phenolics contained (Ezhilarasi et al., 2014). Regarding the operational conditions of spray drying, it has been reported that increasing feed flow rate from 5 g/min to 25 g/min reduced the yield of açai (Euterpe oleraceae Mart.) microparticles entrapped within maltodextrin, caused by the insufficient atomisation and slower heat and mass transfer at higher feed flow rates (Tonon et al., 2008). Whereas rising inlet temperature from 138°C to 202°C increased the yield due to higher efficiency of heat and mass transfer at higher inlet temperature. When it comes to dehumidified air flow rate (*i.e.,* aspirator capacity), greater aspiration resulted in more sufficient particle separation in the cyclone, better thermal conductivity in the chamber, larger aerodynamic drag force, and thus an increase in the powder yield (Gallo et al., 2011; Ståhl et al., 2002).

Desolvation, another necessary procedure in this project, is defined as a thermodynamically driven self-assembly phenomenon of polymers. These polymeric molecules undergo separation and coacervation by means of adding desolvating agents *e.g.,* acetone and ethanol (Soppimath et al., 2001). The crucial parameters of

desolvation process include volume ratio of desolvating agent to water, the rate of adding desolvating agent, pH, ionic content, polymer concentration, and thermal treatment. Increasing volume ratio of desolvating agent/water can significantly increase the mean size of polymer nanoparticles generated (Doan & Ghosh, 2019; Gülseren et al., 2012a; Langer et al., 2003; Von Storp et al., 2012). The average size of zinc-loaded whey protein nanoparticles rose from 76.42±2.53 to 222.41±12.22 nm when the volume ratio of ethanol/water increased from 1 to 5 (Shao et al., 2018). It is because the addition of ethanol alters the dielectric constant of solvent bulk and thus leads to the shift of protein secondary structure (Dufour et al., 1994). This causes the exposure of protein hydrophobic fractions and the resulting coacervation and aggregation (Dalgalarrondo et al., 1995; Hirota-Nakaoka & Goto, 1999). The rate of ethanol addition had negligible effect on the mean size of human serum albumin nanoparticles (~280 nm), whereas it affected the polydispersity of particle size (Langer et al., 2003). With increasing ethanol addition rates from 0.5 ml/min to 2.0 ml/min, the polydispersity indices reduced from 0.10 to around 0.01, possibly due to more rapid coacervation and separation of protein molecules at higher desolvation rates. pH value is another key parameter that can be used in desolvation techniques for controlling particle size (Jun et al., 2011). When pH shifts towards the isoelectric point (pI) of protein selected, the protein-protein interactions become stronger, which promotes protein coacervation and causes the generation of larger particles. In other words, if pH changes in the opposite direction to the pI, the increasing protein-water interactions would limit coacervation, responsible for the formation of smaller nanoparticles. Regarding ionic content, this factor is associated with the surface charge shielding of proteins (Ikeda & Morris, 2002). The addition of salts such as NaCl increased the size of bovine serum albumin nanoparticles during desolvation, since the decreasing net charge on the proteins reduced the repulsion and facilitated the coacervation (Jun et al., 2011). Protein concentrations can slightly affect particle size (Langer et al., 2003). The more proteins added, the stronger electrostatic and hydrophobic interactions might occur, leading to the formation of larger nanoparticles (Jun et al., 2011). For thermal treatment, heating from 40°C to 90°C increased the average size of WPI nanoparticles from 183±34 nm to 4294±139 nm after ethanol desolvation, because high temperatures facilitate aggregation and protein-protein interactions (Gülseren et al., 2012a). Desolvation process efficiently improved the encapsulation and loading

efficiency of protein particles loaded with riboflavin (Ye et al., 2019), curcumin (Ye et al., 2021), and zinc ion (Gülseren et al., 2012b; Shao et al., 2018). This may be because the binding of these substances to proteins causes complex formation upon desolvation, reducing the loss of actives during encapsulation process. On the other hand, increasing volume ratios of desolvating agent/water from 1 to 5 raised the encapsulation and loading efficiency of zinc ions, implying that the larger nanoparticle size formed at higher desolvation degree can entrap more zinc ions (Gülseren et al., 2012b; Shao et al., 2018).

Table 2.2: Advantages and disadvantages of microencapsulation methods for food application

Microencapsulation methods	Advantages	Disadvantages
Spray drying (physical method)	A continuous process, rapid, simple, economic, reproducible, and easy to scale up, compared to other drying processes *e.g.,* freeze drying (Gong et al., 2014). Low moisture content and water activity. High physico-chemical and microbial stability due to no final drying step required (Gula et al., 2013).	Powder loss in the wall of drying chamber. Polydisperse microparticles (Dalmoro et al., 2012). High drying temperatures may damage heat-sensitive components (Gao & Yang, 2016). Low water solubility of some polysaccharides and proteins limits the feed solid contents (Desai & Park, 2005). Sugar rich materials only can be spray-dried with the addition of carrier agents, due to the low glass transition temperature and stickiness behaviour (Bhandari et al., 1997).
Lyophilisation/freeze drying (physical method)	A simple process, low operating temperature without air to reduce oxidation or chemical modification of products (Anwar & Kunz, 2011).	Long operating time and high cost; expensive storage and transport of products (Maroof et al., 2020). Porous microstructure of powders attributed to ice sublimation during process.

Microencapsulation methods	Advantages	Disadvantages
	Products with prolonged and superior quality (Anwar & Kunz, 2011). Suitable for dehydration of thermo-sensitive and water-soluble ingredients (Desai & Park, 2005).	Hence, grinding after drying is required, causing a broad size distribution of microparticles (Anandharamakrishnan et al., 2010). Potential exposure of active substances encapsulated to air due to the porous structure mentioned above (Baldwin et al., 2011).
Solvent evaporation (physical method)	A simple process, low-cost and easy to scale up. Monodisperse particles can be obtained (Maroof et al., 2020).	Preventing crystal growth by adding surfactants (Geetha et al., 2014). The active ingredients encapsulated should be soluble at least in one solvent (Geetha et al., 2014). Active ingredients can be unstable under heating and drying (Maroof et al., 2020).
Supercritical fluid-based techniques (physical method)	Nontoxicity, non-flammability, low cost, and ease of solvent removal by depressurisation (Reverchon & Adami, 2006). Monodisperse powder, less degradation of heat-sensitive ingredients, higher encapsulation efficiency, and precipitation yield, compared to traditional methods (Santos & Meireles, 2010). Complex purification steps during post-processing are not required (Martín et al., 2007).	Supercritical process depends on the solubility of core and wall materials in the supercritical fluids (Bahrami & Ranjbarian, 2007).
Liposomes (physico-chemical method)	High bioavailability, biodegradability, biocompatibility, and cell membrane permeability (Slingerland et al., 2012).	Scaling up is limited by high cost, low physico-chemical stability, polydisperse microparticle, and lipid oxidation (Tan & Misran, 2013).

Microencapsulation methods	Advantages	Disadvantages
	Suitable for encapsulating oil-soluble and amphiphilic substances (da Silva Malheiros et al., 2010).	Complex post-treatment steps are required (Trucillo et al., 2018).
Ionic gelation (physico-chemical method)	Mild operating conditions without extreme pH, high temperatures, organic solvents, or sonication (Calvo et al., 1997). Crosslinkers of low toxicity and cost (de Pinho Neves et al., 2014).	Microbeads fabricated have high porosity, potentially leading to burst release of active substances (Maroof et al., 2020).
Coacervation (physico-chemical method)	No specific equipment required (Gomez-Estaca et al., 2016) Low temperature and agitation, non-toxic solvent (Jain et al., 2016); thus suitable for entrapping heat-sensitive compounds (Maroof et al., 2020). High loading efficiency, low thermal degradation, and controlled release of functional ingredients (Taneja & Singh, 2012).	Poor stability of complex co-acervates (Maroof et al., 2020). Expensive cost of particle isolation process; technique complexity (Gouin, 2004).
Interfacial polymerisation (chemical method)	A simple and low-cost process, easy to scale up. Microparticles with adjustable size and size distribution, membrane thickness with stable mechanical and chemical properties, and high loading efficiency (Perignon et al., 2015).	Proteins or enzymes may denature during polymerisation, adverse to the formation of large oil-water interface (Yeo et al., 2001). Low reproducibility of yield and quality of polymer membrane (Yeo et al., 2001). Removal of monomers, by-products, organic solvents and surfactants by washing steps, may cause functional compound loss (Yeo et al., 2001).

Microencapsulation methods	Advantages	Disadvantages
		Acid-sensitive substances become unstable, when HCl is formed as a by-product (Yeo et al., 2001). Extreme pH, toxic monomers, solvents, and reaction products (Perignon et al., 2015).
Molecular inclusion complexation (chemical method)	Improved stability against oxidation, heating, and light; faster dissolution rate and higher bioavailability (Li & McGuffin, 2007). Longer product shelf-life by prolonged release of bioactive components (Li & McGuffin, 2007). Masking of bitter taste and unpleasant odors; reducing volatility of aromas (Ezhilarasi et al., 2013).	Molecular inclusion efficiency is highly limited by 1) the geometrical dimensions of cyclodextrin and guest actives, 2) the molecular structure, charge, and polarity between them, and 3) the operating temperature and solvent during complexation (Astray et al., 2009).

2.4 Active ingredients and their microencapsulation strategies.

This section concentrates on the chemical structures, physicochemical properties, and other potentially beneficial effects of the active components on human health, and their microencapsulation and integration strategy into commercial food products. Based on their physiological functions, the twelve ingredients can be classified into four categories in **Fig. 2.2**.

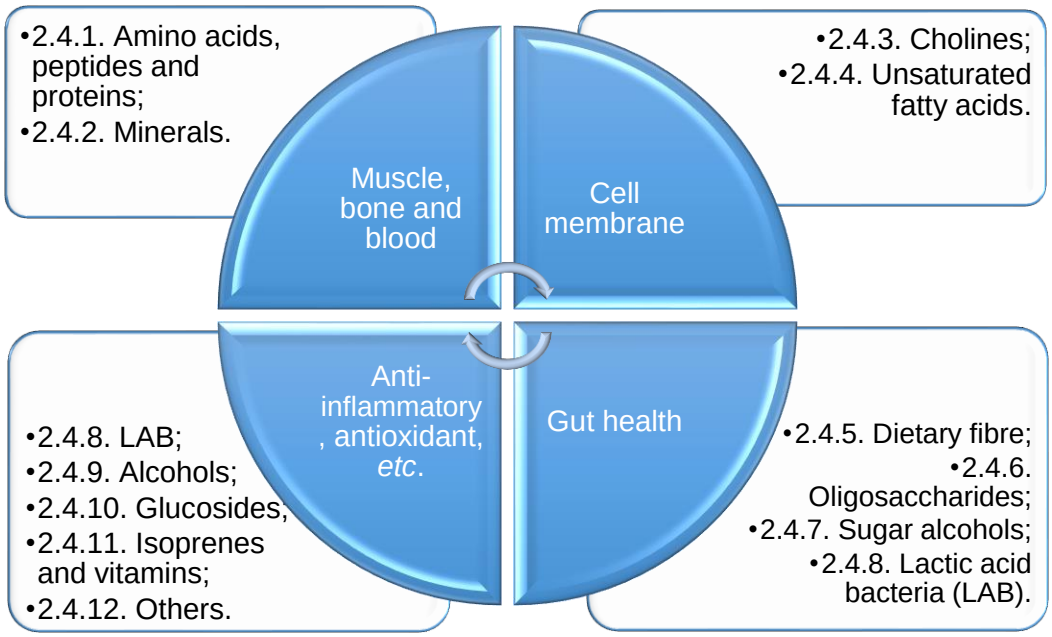

Fig. 2.2. Physiological functions and classification of active ingredients.

2.4.1 Amino acids, peptides and proteins

Amino acids, peptides and proteins play a critical role in health maintenance. Proteins are hydrolysed by digestive proteases to peptides and amino acids. Large peptides are converted by peptidases to give small peptides. In terms of human nutrition, there are twenty standard amino acids connected with the synthesis of proteins and other biomolecules and the oxidation to urea and CO_2 to supply energy. Among the twenty standard amino acids, nine cannot be synthesised *in vivo* and must be ingested from exogenous sources to meet the need of normal growth, known as essential amino acids. Apart from the primary role as amino acid supplier, some proteins and their hydrolytic products also carry out the task of health restoration. Therefore, certain proteins and peptides and amino acids are recognised as active ingredients in functional foods.

2.4.1.1 Amino acids

Regarding amino acid functionality, numerous therapeutic effects have been proposed and extensively investigated *e.g.,* methionine metabolism in liver disease (Mato et al., 2008). In some cases, non-essential amino acids are also incorporated into functional foods due to their role of building blocks of some biologically active

compounds. For example, β-alanine was added into beverage as a carnosine precursor (Wyzisk & Sloggett, 2014). Additionally, leucine, isoleucine, and valine, known as branched-chain amino acids (BCAAs) are among the nine essential amino acids. BCAAs occupy 35-40% of the essential amino acids in muscle protein and approximately 14% of the total amino acids in skeletal muscle protein. Their beneficial effects include anti-fatigue, burn treatment, *etc*.

Several amino acids including BCAAs are poorly water-soluble. Exposure of hydrophobic amino acid residues to taste receptors are responsible for the bitter taste (Ishibashi et al., 1988). This causes unacceptable taste, poor wettability, and slow dissolution in the GI tract, which affects bioavailability and restricts their beverage applications for energy drinks and other nutritional products. The insolubility confines the supplementation of certain amino acids in their free form. To circumvent these challenges, microencapsulation can be applied in this area.

Hydrophilic amino acids, peptides, or proteins were encapsulated with biocompatible copolymers by phase separation (Mank et al., 1996). Interestingly, the release behaviour of microcapsules was controlled by the coating material as well as oils selected as hardening agents. Both oil viscosity and their residual content in the microcapsules affected the control release.

Hydrophobic amino acids especially BCAAs are used as human supplements and have received much attention over the past few decades. BCAAs products are provided in capsule, tablet, and powder formats in current markets. The dosage to satisfy customers' daily needs is 5-20 g and BCAAs are ground down into microparticles (50 μm), causing a high specific volume (≥ 2.0 mL/g) (Sakai et al., 2006). It means a minimal volume of 10 mL in powder format or at least sixteen 300 mg tablets or capsules is needed daily. Due to the hydrophobicity, it takes 20 minutes to humidify and dissolve 2 g of BCAAs into 100 mL water at 25°C (Wu et al., 2013). It is inconvenient for customers, compared with the forms of ready-to-mix or ready-to-drink. Recently several patents have been disclosed in this field. Organic acid was added into BCAAs to decrease the specific volume and to improve solubility to produce granules (Sakai et al., 2006). However, capsules and tablets are associated with medication by customers and are difficult to swallow. Using granulation and extrusion, gum *Arabic*, carboxy methyl starch sodium and polyglycerol fatty acid ester (Wu et al., 2013) were applied to prepare dissolvable or instantised BCAAs microparticles.

2.4.1.2 Peptides

Certain peptides are bioactive compounds *e.g.,* casomorphins, exhibiting antihypertensive activity (Pihlanto-Leppälä, 2000). Besides the active peptides, protein hydrolysates enriched in low MW peptides, in particular di- and tripeptides, have shown huge potential in field of nutritional supplements for people unable to digest intact proteins. For example, infants with cow's milk protein intolerance require an extensively hydrolysed formula with lessened immunological reactivity.

Bioactive peptide and protein hydrolysate products in current market include infant formula, soft drink, soup, drink powder, confectionery, dry milk protein hydrolysate, fermented milk, and whey protein hydrolysate. Being marketed as functional foods with health claim notwithstanding, some of them remain traditional foods. The innovation and commercialisation of peptide products is hindered by the perishability, chemical instability, bitterness, hygroscopicity and poor bioavailability. Considering structural heterogeneity of the peptides and protein hydrolysates, the related microencapsulation applications will be discussed from the type of matrix/shell materials *i.e.,* proteins, polysaccharides, and lipids.

Protein-based carriers:

Protein carriers are regarded as a nutrient-dense system providing essential amino acids and to be versatile in solubility, gelation, film formation, foaming, emulsification, and water binding capacity. However, structural similarity between matrices and cores may give rise to poor protection of protein walls against instability issues. Not only single materials but also hybrid materials have been introduced to overcome this challenge. Casein hydrolysate microcapsules were coated with soybean protein (Ortiz et al., 2009) and soybean protein-gelatin blend (Favaro-Trindade et al., 2010). They were considered to be less bitter than the free hydrolysates. Although the first example reported elevated hygroscopicity after encapsulation, the latter showed reduced hygroscopicity due to an increase in glass transition temperature. The increase was caused by the incorporation of materials with high MW into peptides and protein hydrolysates containing low MW (Kurozawa et al., 2009).

Corn zein-glycerol blend was employed to coencapsulate nisin and thymol by spray drying, in order to achieve controlled release of nisin while thymol acted as an

antimicrobial and assisted with the prolonged release of nisin (Xiao et al., 2011). However, nisin encapsulation efficiency decreased tremendously from around 84% to 36% when the thymol content increased from 0.02% to 1% w/v, indicating high stickiness of the delivery system to spray drying chambers. Selectivity of protein-based carriers for the core materials was investigated (O'Neill et al., 2014, 2015). Tryptophan, riboflavin, dipeptide and pentapeptide were encapsulated within whey protein microbeads crosslinked by $CaCl_2$, respectively. The higher encapsulation efficiency, higher equilibrium constant, and the lower release rate constants were observed in the relatively hydrophobic pentapeptide microcapsules (O'Neill et al., 2014, 2015). The migration of these four core materials into protein carriers was driven by concentration gradient and diffusion, and thus influenced by the affinity between core and shell materials (*e.g.,* hydrophobicity) in the partition process.

Polysaccharide-based carriers:

Polysaccharide is thought to be a low-cost, highly water-soluble, and structurally stable delivery system, mainly including maltodextrin, gum *Arabic*, chitosan, β-cyclodextrin, and alginate. Maltodextrin and gum *Arabic* possess low viscosity at high solid content and in aqueous solution, respectively, as well as good emulsifying ability. They have been extensively investigated to incorporate with materials which are difficult to dehydrate. For example, a mixture of maltodextrin and gum *Arabic* has been designed as shell material to prepare casein hydrolysate microcapsules (Rao et al., 2016) and chicken meat protein hydrolysate microcapsules (Kurozawa et al., 2009) by spray drying. The former exhibited an initial burst and fast release of core material under simulated GI environments. It indicated the weak interaction between the hydrolysates and the highly aqueous-soluble polysaccharide blends. In the latter case, the blend addition improved the final product stability due to the substantially increased glass transition temperature and reduced hygroscopicity. These examples show the typical merits and drawbacks of polysaccharide mixtures as carrier agents.

Other combinations *e.g.,* alginate-based carriers also have been widely studied. Alginate is a structurally simple anionic hydrogel with excellent biodegradability and biocompatibility. The microstructure of alginate capsules is of pH-sensitivity, porosity, and hydrophilicity. Due to pore shrinkage at low pH, alginate capsules undergo release of core materials in aqueous solution but relatively low release in acidic environment like the gastric fluid. A blend of alginate and resistant starch using as shell material to

coat nisin showed a comparatively sustained release profile in distilled water medium, compared to that of pure alginate microcapsules (Hosseini et al., 2014). This delaying release was also found in microencapsulation of polyphenol with alginate-starch blend (Córdoba et al., 2013). The encapsulation efficiency of core materials raised progressively by the addition of starch in both cases. Additionally, alginate-chitosan blend has received much attention due to the biodegradability, biocompatibility, and antimicrobial characteristics of chitosan. Pluronic F68 was mixed with chitosan-alginate blend to encapsulate nisin (Bernela et al., 2014). Pluronic F68 is a non-ionic di-functional triblock copolymer, used in the food industry as a surfactant and additive. The release characteristics appeared to be in an initially rapid and subsequently sustained manner. By contrast, nanoencapsulation of nisin coated with alginate-chitosan blend exhibited relatively rapid release behaviour (Zohri et al., 2010). It reveals that a strong interaction between shell and core enables to retard the release. Analogous slowing release was observed in the encapsulation of bovine serum albumin (BSA) with alginate–montmorillonite mixture, where alginate was the major component by weight (Kaygusuz & Erim, 2013).

Lipid-based carriers:

Compared with other delivery systems, lipid-based carriers possess higher cell membrane affinity and thus can enhance the bioavailability of core materials. Lipid-based carriers include liposome and liposphere. Liposomes are vesicular structures consisting of one or multi-phospholipid bilayers coating an aqueous core. Because of the presence of lipids and aqueous media, liposomes enable to encapsulate, deliver, and release hydrophilic, hydrophobic, and amphiphilic materials. The chief bottlenecks of liposomal application in the food industry are the scaling up of manufacturing processes, the high-cost of phospholipids, and the instability of liposomes. Liposomes in an aqueous environment may be subject to lipid hydrolysis to yield fatty acids and lysophosphatidylcholines during processing and storage. Lysophosphatidylcholines are possibly further degraded to form fatty acids and glycerophospho compounds. This causes a reduction in physical and chemical stability of liposomes. It was reported that compared with the ionic strength of the buffer and the presence of oxygen in the container headspace, pH values of buffer system exerted more significant influence on the hydrolysis rate of liposomes (Zhang & Pawelchak, 2000).

Liposomes were used to encapsulate marine hydrolysates (da Rosa Zavareze et al., 2014; Mosquera et al., 2014). Antioxidant activity or angiotensin I-converting enzyme inhibitory activity of each hydrolysates kept unchanged subsequent to nanoencapsulation. For emulsions and suspensions, zeta-potential is associated with surface charge density of the dispersed phase. Aggregation occurs when it is close to the isoelectric point, when there are opposite charges as there are little repulsion between them. If the suspensions are highly positive or negative, they will be stable. However, storage stability *i.e.,* zeta-potential in each case mentioned above was different, indicating high heterogeneity and different charge distribution of peptides. Chitosan was introduced in the liposomal entrapment of antidiabetic marine peptides (Li et al., 2015). Chitosan coating layer elevated the electrostatic repulsive force and stability of liposomes. A prolonged release of the peptides in simulated GI tract was observed.

Liposphere contains a matrix type inner layer composed by fatty acid and core material and an outer layer formed by the hydrophilic part of the fatty acid or phospholipid. Compared to casein hydrolysate-loaded liposome, the liposphere one exhibited larger particle size, higher encapsulation efficiency and less hydrophobicity (Morais et al., 2004). The encapsulation efficiency of casein hydrolysates raised with increasing hydrophobicity of the peptide fractions, indicating that hydrophobic interaction between lipid and peptide plays a crucial role on the formation of lipospheres (Barbosa et al., 2004).

2.4.1.3 Proteins

Compared with low MW materials, proteins are large molecules with complex architectures that are inherently less stable. They have secondary, tertiary and/or quaternary structure containing chemically reactive groups. Denaturation and aggregation due to exposure to heat, light, oxygen, acidic or basic conditions may result in loss of activity or of immunogenicity. Technologies *e.g.,* membrane separation, lyophilisation and microencapsulation have been applied in protein purification, concentration, stabilisation, shelf-life extension, and sustained delivery. Currently encapsulation is implemented on three categories of proteins: β-galactosidase in the dairy industry, proteinase and lipase in the ripening process of cheese, and human therapeutic protein in the pharmaceutical industry. β-galactosidase is an acid-labile

enzyme to hydrolyse lactose into glucose and galactose and ideally should be released in the small intestine. Proteinase and lipase are encapsulated and incorporated to cheese to shorten the maturation time. Encapsulation of human therapeutic proteins is associated with sustained release.

β-Galactosidase:

β-Galactosidase is an enzyme produced in the small intestine, responsible for hydrolysing lactose (5 w/w % in the milk) into glucose and galactose. Due to a lack of β-galactosidase, over 70% of the world population cannot easily digest milk, known as lactose intolerance. To circumvent this issue, the lactose content in milk and dairy products is normally reduced *via* enzymatic or chemical hydrolysis. The enzymatic hydrolysis of lactose does not impair the nutritional value of dairy products and produces fewer nasty flavours, odours, and colours than the chemical hydrolysis. However, the direct addition of free or immobilised β-galactosidase into milk results in the hydrolysis action to generate the constituent monosaccharides, glucose and galactose, which make the milk too sweet. To maintain the characteristic taste of whole milk and protect the enzyme activity from proteolysis in the stomach, the microencapsulation of β-galactosidase has been investigated by many researchers (Ahn et al., 2013; Kim et al., 1999; Kwak et al., 2001; Rodriguez-Nogales & Delgadillo, 2005).

Due to the mild conditions used and the characteristics of lipolysis, the liposomal entrapment of β-galactosidase have received much attention. It was found that liposomal β-galactosidase exhibited higher thermal stability and stability with time but lower affinity to the substrates than the free enzyme (Rodriguez-Nogales & Delgadillo, 2005). Trehalose acting as cryoprotectant was incorporated into β-galactosidase liposomes to prevent fusion and leakage (Kim et al., 1999). The liposomes showed high resistance to the simulated gastric fluids with pepsin and allowed targeted delivery to the small intestine.

Compared with liposomes, β-galactosidase lipospheres had higher encapsulation efficiency. Kwak et al. (2001) used medium-chain triacylglycerol (MCT) and polyglycerol monostearate (PGMS) to encapsulate β-galactosidase. With the optimisation of coating to core ratio, the encapsulation efficiency was up to 98% (the enzyme-MCT lipospheres) and 73% (the enzyme-PGMS lipospheres). Since the lipospheres efficiently isolated β-galactosidase from lactose present in the milk and

lipid digestion basically occurs in the small intestine, no changes in sweetness and off-taste were found until 8-day and 3-day storage of the MCT and PGMS lipospheres, respectively.

Besides lipids, polysaccharides and proteins also have been utilised to coat β-galactosidase. β-galactosidase was encapsulated with MCT as the internal shell material and with whey protein isolate, maltodextrin, or gum *Arabic* as the external shell (Ahn et al., 2013). The encapsulation efficiency was optimised to 99.5%. The microcapsules with whey protein isolate displayed faster release of enzyme in the simulated intestinal fluids than that coated with maltodextrin. Zhang et al. (2016) demonstrated the impact of K^+ ion on the activity of β-galactosidase entrapped in κ-carrageenan hydrogel. The pore size of the hydrogel was large enough for H^+ to diffuse in and out the matrix, resulting to inactivation of the acid-labile enzyme. But the high concentration K^+ inside the hydrogel increased the enzyme activity and thermal stability under moderate pH and mild temperature conditions. Apart from K^+, previous reports show that some cations including Mn^{2+}, Mg^{2+}(Wheatley et al., 2015), Ca^{2+}(Garman et al., 1996), and Na^+(Jurado et al., 2004) also can alter the enzyme activity.

Proteinase and lipase:

Coagulation, draining, and ripening are three main stages of cheese production. Ripening is of importance for the development of flavour, texture, and aroma of cheese. It is the consequence of proteolysis, lipolysis, and glycolysis during aging period. The maturation time varies from 6 months to 2 years according to the cheese variety, which means a high cost in handling and capital. Accelerating cheese ripening without sacrificing its quality can bring numerous technological and economic benefits. Many attempts including addition of enzymes, addition of cheese slurry, and increased aging temperatures, have been made to circumvent the challenging. Direct addition of enzyme to the cheese matrix, however, causes deficient enzyme distribution in curd, enzyme loss in whey, and cheese of poor quality and low yield. Enzyme microencapsulation enables to isolate the enzyme from the curd during clotting and to release the enzyme during ripening upon microcapsule collapse.

Flavourzyme was coated with gellan, κ-carrageenan and milk fat individually to accelerate cheese ripening (Kailasapathy & Lam, 2005). The encapsulation efficiency was higher in κ-carrageenan (55.6%) and gellan coating capsules (48.2%) than in milk

fat ones (38.9%). While these two gel beads showed greater enzyme leakage due to their large pore size. Over 70% of encapsulated enzyme was retained after incorporating into cheese matrix and undergoing 16-h press.

Human therapeutic protein:

Protein therapeutics usually refer to human therapeutic proteins *e.g.,* growth hormone, nerve growth factor, and vascular endothelial growth factor. To be a successful therapeutic protein, it must be highly purified, concentrated and commonly lyophilised, with a long shelf life (≥ 2 years). Low oral and transdermal bioavailability of the protein limits its administration to frequent injection or infusion. Development of sustained-release formulation has been a longstanding focus in the pharmaceutical industry. Most work in this field involves protein encapsulation using a biodegradable polymer *i.e.,* poly(lactic-co-glycolic acid) (PLGA) (Morita et al., 2000). Other materials like poly(lactic acid) (PLA) and polyethylene glycol (PEG) (Morita et al., 2000) have also been tried. However, the high price of these materials restricts their applications in the food industry. Development of therapeutic protein encapsulation will not be discussed in detail herein.

2.4.2 Minerals

Dietary minerals are classified by the amount people need: major and trace elements. The former includes calcium, phosphorus, magnesium, sodium, potassium, chloride, and sulphur. The latter consist of iron, manganese, copper, iodine, zinc, cobalt, fluoride, and selenium. Deficiency in these minerals may lead to osteoporosis, cardiovascular diseases, anaemia, iodine deficiency disorders, *etc*.

At present mineral supplements mainly provide calcium, iron, zinc, magnesium, chromium, selenium, and iodine, which are deficient in populations. The prevalent form of mineral fortification is addition of mineral acids and salts, which may be unstable during storage (iodine) or result in quick release, chemical degradation, protein aggregation and unpleasant taste sensations (magnesium and ferrous). Magnesium chloride was entrapped within a W/O/W double emulsion to achieve controlled release (Bonnet et al., 2010). A commercial granular fertilizer also showed decrease in release rate after being coated with polysulfone (Tomaszewska & Jarosiewicz, 2006).

To summarise, proteins and minerals are the major building blocks of muscle, bone, and blood. Amino acids, peptides, and proteins face a greater challenge of target release, architecture, and stability than minerals. The next two sections 2.4.3 and 2.4.4 will concentrate on cholines and unsaturated fatty acids, which are important constituents of cell membrane.

2.4.3 Cholines

Choline is a water-soluble white crystalline powder, belonging to vitamin-B family. It is considered as an essential dietary nutrient, critical for human cell growth and reduction of chronic disease risk.

Multivitamin and mineral tablets loaded with unentrapped choline salts are unstable during storage due to entrapped hygroscopic choline salts and poorly entrapped non-hygroscopic choline salts (Richardson & Hernandez, 2002). It is presumably because of the interaction between the choline and heavy metals present in the tablets, accounting for the reduced choline activity and shelf life, fishy odour, and discoloration development. To overcome the challenge, choline bitartrate was coated with hydrogenated soya bean oil, showing stability over 6 months and encapsulation efficiency of 54-61% (Gangurde et al., 2015).

2.4.4 Unsaturated fatty acids

According to the degree of saturation, unsaturated fatty acids are divided into mono-unsaturated fatty acids and poly-unsaturated fatty acids (PUFA). Monounsaturated fatty acids are composed of oleic acid, erucic acid, *etc*. They are colourless, odourless, and oxygen-labile substances, which are major or minor ingredients of certain vegetable oils such as olive oil, rapeseed oil, and macadamia oil. Maillard reaction products of sodium caseinate and lactose was used as shell materials to suppress lipid oxidation (Li et al., 2017). Apart from the use of common foods, ricinoleic oil exhibits pro- or anti-inflammatory and analgesic activities in the topical application. It was entrapped within crosslinked chitosan/liposome matrix to limit the oxidative degradation and prolong its release for local anaesthetic agent (Azeem & Nada, 2015).

PUFA may be identified by the location of the first double bond in the backbone. PUFA omega-3 consist of α-linolenic acid, eicosapentaenoic acid (EPA),

docosahexaenoic acid (DHA), *etc*. They play a vital role in normal growth and reducing the risk of coronary heart disease. Spray dried α-linolenic acid microcapsules were blended into biscuits, showing elevated storage stability and acceptable mouthfeel (Umesha et al., 2015). EPA and DHA are bioactive compounds present in fish oil. Many efforts have been made to mask the fishy odour and to enhance the water solubility and oxygen sensitivity. The relevant encapsulation methods include spray drying (Chen et al., 2013), freeze drying (El-Messery et al., 2020), fluidised bed drying (Ponginebbi & Puglisi, 2008), extrusion (Gouin, 2004), simple coacervation and spray-drying (Wu & Xiao, 2005), inclusion complexation (Choi et al., 2010), liposome entrapment (Kubo et al., 2003), complex coacervation and freeze drying (Liu et al., 2010), complex coacervation (Zhang et al., 2012), double emulsification and subsequent enzymatic gelation (Cho et al., 2003), electrostatic layer-by-layer deposition and spray drying (Klinkesorn et al., 2006), ultrasonic atomisation and freeze drying (Klaypradit & Huang, 2008), electrospraying (Torres‐Giner et al., 2010), spray granulation and fluid bed film coating (Anwar et al., 2010), and spray granulation (Anwar & Kunz, 2011). They provided good protection against oxidation. The encapsulated fish oil possessed equivalent or enhanced bioavailability.

As PUFA omega-6, arachidonic acid, linoleic acid, and conjugated linoleic acid (CLA) are active ingredients fortifying functional foods. Using spray drying, linoleic acid was coated with gum *Arabic* or maltodextrin to retard its autoxidation (Minemoto et al., 2002). Besides the use of shell materials, ascorbate was also added into linoleic acid prior to encapsulation for the same reason (Watanabe et al., 2002). With respect of CLA, it is an aqueous insoluble and oxygen-labile PUFA omega-6, possessing anticancer properties and numerous biological benefits. Shell materials such as various cyclodextrin (Kim et al., 2000) were demonstrated to improve the oxidative stability of CLA. A blend of maltodextrin and pea protein concentrate was used as a shell material to provide microcapsules with better functional properties over the single protein or polysaccharide material (Costa et al., 2015).

High proportions of cholines and unsaturated fatty acids provide mammalian cell membranes with excellent fluidity and permeability to various ions. Microencapsulation has been introduced to weaken their susceptibility to moisture content, heavy metals, and oxygen. The following sections from 2.4.5 to 2.4.7 will focus on ingestible or fermentable oligo- and polysaccharides which are vital to gut flora. Ingestion of lactic

acid bacteria is also considered as an alternative way to improve gut health, thus discussed in section 2.4.8.

2.4.5 Dietary fibre

Briefly, dietary fibre is a kind of carbohydrate indigestible for humans. The main fractions are composed of cellulose, hemicellulose, pectins, β-glucans, resistant starch, non-digestible oligosaccharide (*e.g.,* inulin), other synthetic carbohydrate compounds (*e.g.,* methyl cellulose), gums and mucilages, lignin, and other minor components *e.g.,* phytic acid.

In accordance with the FDA health claim, high levels of dietary fibres are required to add into food and beverage formulations. It causes the increase in unpalatability and viscosity of the final products. Some refined fibre constituents such as polydextrose were developed as substitutes but the high cost restricted a wider application. The optimisation of palatability and water absorption during formulation and processing spurred the development of microencapsulation. When the fibres are microencapsulated using materials which can decrease hydration and water absorption, the final high-fibre products meet the consumer trend without compromising on mouthfeel, flavour, and colour. For example, chitooligosaccharide microcapsules coated with polyacylglycerol monostearate were produced successfully (Choi et al., 2006). The encapsulation efficiency reached 88.08% and only 7.6% of chitooligosaccharide was released during 15 days at 4°C. Milk added with such microcapsules showed similar physicochemical and sensorial properties such as viscosity, colour, astringency, and bitterness with the commercial milk.

2.4.6 Oligosaccharides

Certain types of mono- and oligosaccharides are used as bulk sucrose substitutes to provide bulk properties, sweetness, and beneficial effects in functional foods. They include various oligosaccharides, three disaccharides, and three monosaccharides. Similar with dietary fibres, the saccharides are applied in the food industry without encapsulation and thus will not be discussed in detail herein.

2.4.7 Sugar alcohols

Sugar alcohols are the reduction products of sugar, implying all carbonyl groups (in aldehydes or ketones) in a single sugar molecule are reduced to hydroxyl groups. They normally have at least three hydroxyl groups, known as polyhydric alcohols. They are classified into acyclic polyols and cyclic polyols. The former are the sugar alcohols discussed in this section *e.g.,* sorbitol and xylitol, while an example of cyclic polyols is *myo*-inositol.

Sugar alcohols are used commonly without encapsulation in the food industry due to the pleasant sweet taste. However, xylitol microcapsules coated with gum *Arabic*-gelatin mixtures by complex coacervation were used to extend the sweetness and cooling sensation (Santos et al., 2015). Over 70% xylitol was released from the microcapsules within 20 min in saliva simulant. As cooling agents, menthol and xylitol were coencapsulated using similar methodology and the resulting microcapsules were incorporated into chewing gum (Santos et al., 2014). The cooling sensation was enhanced by the sustained release of these two components.

2.4.8 Lactic acid bacteria

"Lactic acid bacteria" (LAB) represent a functional grouping of non-pathogenic, non-sporing, gram positive bacteria, which produce lactic acid as a primary metabolic end-product and are widely used in food fermentations (Goldberg, 2012). LAB are comprised of species of *Lactococcus*, *Lactobacillus*, *Streptococcus*, *Leuconostoc*, and *Pediococcus*. Regarding to health promotion, a new concept of probiotics including LAB and *Bifidobacterium* and *Enterococcus* species was established. It is described by FAO and WHO as "live microorganisms which when consumed in adequate amounts as part of food confer a health benefit on the host" (FAO/WHO, 2001).

Viable probiotic microorganisms have been proven scientifically and clinically effective in treating diarrhea and lactose intolerance symptoms, facilitating the intestinal microbial balance by antimicrobial activity. Functional foods containing probiotics are one of the most promising fields in the food industry. For a health claim, the number of probiotic microorganisms at the end of shelf-life is required to exceed 107 colony forming units (cfu)/ml, according to the Fermented Milks and Lactic Acid Bacteria Beverages Association in Japan. Furthermore, the bacteria should enable to proliferate and colonise in the intestinal ecosystem. The probiotics, however, are

anaerobic and cannot tolerate high temperature and/or air exposure during processing, acidic conditions of the stomach, and the bile concentrations encountered in the intestine.

To further enhance the cell viability, microencapsulation technology has been introduced, which consists of spray drying, freeze drying, emulsification, phase separation-coacervation, and gel beads. The encapsulants involved include skim milk powder, alginate, κ-carrageenan, gelatin, starch, and gum acacia.

In freeze drying processing, researchers investigated various encapsulants *e.g.,* skim milk powders to suspend the cells (Sinha et al., 1974). This technique in the encapsulants caused low survival percentages of *Lactobacillus bulgaricus*, less than 30%, due to cell membrane damage during drying process (Castro et al., 1997).

The primary limitation of spray drying in probiotic encapsulation is the high mortality due to the simultaneous dehydration and thermal inactivation. Various thermo-protectors have been developed to improve cell viability during drying and storage, including reconstituted non-fat milk solids or adonitol (Selmer ‐ Olsen et al., 1999) and gum acacia (Desmond et al., 2002). The protective effect of inorganic salts such as Ca^{2+} on LAB bacteria upon spray drying was demonstrated and presumably explained by the physicochemical properties of Mg^{2+} and Ca^{2+} (Gao & Yang, 2016). Apart from the LAB strains mentioned above, Huang et al. (2016) cultivated and spray dried *Lactobacilllus casei* and *Propionibacteria. freudenreichii*. They demonstrated that the hyperconcentrated sweet whey used facilitated the overexpression of key stress proteins and accumulation of intracellular storage molecules and compatible solutes. It caused an increase in tolerance for heat, acid, bile salts and spray drying on *Propionibacteria*. Following this methodology, a one-stage/multi-stage pilot scale spray drying was conducted in *L. casei* and *P. freudenreichii* (Huang et al., 2017). In this work, even 100% survival was reached regardless of the probiotic strain when they were spray-dried at lower temperatures. Moreover, spray drying enhanced the tolerance for simulated intestinal environment on *P. freudenreichii*, presumably owing to strain-dependent cellular stress response (Huang et al., 2017).

Chemical methods have been applied to probiotic encapsulation *e.g.,* phase separation-coacervation and gel beads. *Lactobacillus acidophilus* loaded in calcium alginate beads (Chandramouli et al., 2004) and in κ-carrageenan gel beads (Tsen et al., 2004) withstood the gastric conditions and exhibited better fermentation efficiency

than free cells, respectively. In the case of LAB entrapped in gel beads, the batch process becomes the main restriction on scale-up for commercial production.

In conclusion, the ingestible or fermentable saccharides are used to increase satiety with lower energy and to selectively stimulate the growth of certain gut flora. LAB supplements are also regarded as a way to improve the population of probiotic microorganisms. The low viability of encapsulated LAB is still a key problem. Improvements in probiotic encapsulation have been made to solve this problem during the past decades, shifting attention from drying or freezing conditions to factors *e.g.,* thermo-protectors, culture media, strain selection, and chemical encapsulation methods under mild conditions. However, further studies are required to evaluate the bioavailability and long-term effects. Besides the common active ingredients *i.e.,* LAB, proteins, saccharides and fatty acids, a family of substances showing antioxidant, anti-inflammatory, anti-cancer, and many other activities will be introduced in the following section 2.4.9-2.4.12.

2.4.9 Alcohols

Alcohols are organic compounds where a hydroxyl group is attached to a saturated carbon atom. Polyphenol and phytosterol mentioned in the section 2.4.12 have attracted considerable interest, as well as sugar alcohols in 2.4.7.

Fatty alcohols, particularly very long-chain fatty alcohols *i.e*., C24-C34 alcohols have been reported to decrease serum total cholesterol in humans (Hargrove et al., 2004). Lim et al. (2016) incorporated policosanols into reconstituted high-density lipoproteins to synergistically exhibit the anti-senescence and longevity effects. Capsaicinoid is a family of hydrophobic and pungent vanilloids present in chilli peppers for the treatment of arthritis and diabetic neuropathy. To improve its oral bioavailability, capsaicinoid was encapsulated by emulsification with chitosan (Goycoolea et al., 2012), by liposomal nanoformulation (Zhu et al., 2015), and by thin-film dispersion method with polymeric micelles (Zhu et al., 2014).

2.4.10 Glucosides

Glucosides are commonly extracted from plants and may be classified into five major types of derivatives (**Table 2.3**). Various glucosides are bioactive compounds, used as an anti-inflammatory (salicin), an antioxidant (cucurbitacin B + E glucosides),

a skin-whitening agent, a urinary antiseptic and diuretic (arbutin), a cathartic (jalapin), *etc*.

Sinigrin and sinalbin can be found in black and white pepper, respectively, resulting in a pungent taste. As important ingredients of seasonings, glucosides are used without encapsulation in the food industry. Most of the glucoside-related encapsulation is applied in the pharmaceutical and cosmetic industry. For example, esculin is a styrolene derivative of glucosides, acting as a therapeutic compound to treat nephrolithiasis. It is sensitive to acidic conditions *e.g.,* the upper GI tract in humans. Esculin was entrapped within alginate-chitosan hydrogel matrix by extrusion and gelation for target delivery to the intestine (Tsirigotis-Maniecka et al., 2016).

Table 2.3: Screening on glucosides (Kulka, 1967).

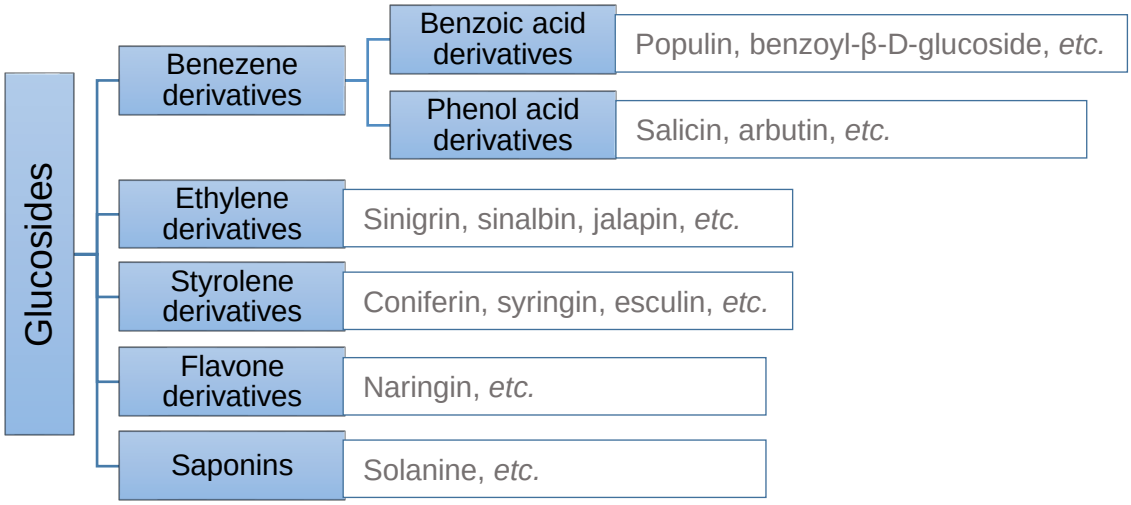

2.4.11 Isoprenes and vitamins

2.4.11.1 Isoprenoids

An isoprene is an organic compound with the formula $CH_2=C(CH_3)-CH=CH_2$. Isoprenoids are subdivided into numerous categories according to the number of isoprene units in a molecule. In the food industry, the noteworthy are monoterpenes used as aromas, diterpenes as vitamins and vitamin precursors, triterpenes including steroids and squalenes, and tetraterpenes referring to carotenoids.

Monoterpenes such as citral, linalool, myrcene, limonene, and pinene are significant but volatile flavour ingredients in essential oils. Microencapsulation has been introduced to prolong the aroma release in food matrix and to enhance the

oxidative stability of these olefinic compounds. Limonene as a model flavour was coated with diverse shell materials to investigate release profile and storage stability (Soottitantawat et al., 2005). It was found that aroma concentration and storage temperature (Bertolini et al., 2001) played a role in the retention of various monoterpene compounds.

Squalene is a triterpene which may serve as a potent antioxidant and a free radical scavenger, due to its multi-conjugated double bonds. However, it is heat- and oxygen-labile during processing and storage. Squalene and diphencyprone were co-entrapped within nanostructured lipid carriers to treat Alopecia Areata (Lin et al., 2013).

2.4.11.2 Vitamins and carotenoids

Vitamins B and C are water-soluble compounds, whereas vitamins A, D, E, K and carotenoids are liposoluble ones. All of them are naturally-occurring molecules in food and are labile when exposed to light, oxidising agents, reducing agents, heat, humidity, acids, and alkalis. There exist numerous chemical forms of vitamins and carotenoids based on the location in the organism and function. Their physiological benefits have been extensively studied and fully discussed (Gonnet et al., 2010), wherefore this section concentrates on the related encapsulation strategies.

Low aqueous solubility of vitamins A, D, E, K and carotenoids is associated with inadequate absorption and poor bioavailability. To overcome this issue, vitamin D3 was bound to α-lactalbumin to form a complex (Delavari et al., 2015). Carboxymethyl chitosan and soy protein isolate mixtures were used to encapsulate vitamin D3 (Teng et al., 2013). Compared with single protein or polysaccharide, the hybrid material provided better protection to vitamin D3 under simulated gastric condition and elevated release in simulated intestinal fluid. The low solubility of vitamin B9 also becomes a bottleneck in its use for fortification of food products. Vitamin B9 was encapsulated with β-lactoglobulin-lactoferrin aggregates or coacervates *via* co-assembly, with high entrapment and good storage protection for vitamin B9 (Chapeau et al., 2017).

Amongst various well-known carotenoids, lycopene is a novel and high-profile one with sensitive unsaturated bonds, exhibiting anti-cancer and cardiovascular protective effects. Blanch et al. (2007) reported a one-pot methodology named supercritical fluid extraction process. The extraction, fractionation and encapsulation of lycopene was completed in one step with an encapsulation efficiency of 67.6%.

Regarding water-soluble vitamins, dried microbeads containing vitamin B2 coated with whey protein isolates were crossed by $CaCl_2$ (O'Neill et al., 2015). *In vivo* release of vitamin B2 was evaluated in piglets. 26%, 21% and 12% of riboflavin was retained in microbeads after 1-hour ingestion in the stomach, duodenum, and jejunum, respectively, indicating the resistance of protein wall to the gastric environment.

2.4.12 Others *e.g.,* phytochemicals

Phytochemicals refer to various compounds which are extracted from plants and physiologically active when consumed. They are composed of polyphenols, phytosterols, alkaloids, derivatives of isoprene, and numerous other chemicals. This section focuses on polyphenols and phytosterols due to their relevance in the food industry.

2.4.12.1 Polyphenols

A broad classification of polyphenols is shown in **Table 2.4**. The most noteworthy are resveratrol and curcumin. Despite exhibiting potent antioxidant, platelet anti-aggregate, cancer chemopreventive activities and cardiovascular protective effects, resveratrol is an oxygen-sensitive and photo-sensitive compound. As a result of encapsulation, researchers enabled to enhance the permeability of resveratrol on cells (Sessa et al., 2014) and photostability (Davidov-Pardo & McClements, 2015). Curcumin shows antioxidant, anti-inflammatory, antiseptic and analgesic activities. However, its low oral bioavailability arising from the physicochemical instability and aqueous insolubility hampered the efficacy and clinical usage. Curcumin was coated with peptide to increase the bioavailability (Altunbas et al., 2011). Its release rate and therapeutic efficacy could be readily tuned by varying the peptide concentration. Curcumin nanoparticles covered with polyvinylpyrrolidone were prepared by sonication, solvent evaporation, and grinding (Almeida et al., 2018). Three curcumin formulations including the nanoparticle, a curcumin powder (65% pure grade), and a commercial water-dispersible curcumin, were incorporated into yogurts as colorants, respectively. Prior to integration, the curcumin powder possessed the best antioxidant, anti-inflammatory, cytotoxic and antibacterial properties. This implies that the other two formulations decreased the accessibility to curcumin in short-term. After incorporation into yogurts, these curcumin-enriched yogurts exhibited different but

appealing yellow appearances, with negligible changes in the nutritional composition during 15-day storage (Almeida et al., 2018). Curcumagalactomannoside, a novel food-grade formulation of curcumin, was synthesised by ultrasound-mediated gel phase impregnation of curcumin into a non-digestible, fermentable, and soluble fibre-protein composite extracted from fenugreek (Liju et al., 2015). Curcumagalactomannosides were used as a bioactive hydrocolloid-based food ingredient and integrated into soup, chocolate, yogurt, cookies, honey, and juice, respectively. These formulated foods had well-accepted tastes and appearances, and 7-10 times higher bioavailability of curcumin by evaluating the post-blood plasma curcumin levels in humans. Additionally, curcumin was entrapped within β-cyclodextrin by kneading, coprecipitation, and simple mixing (Marcolino et al., 2011). The formed curcumin-β-cyclodextrin complexes with improved colour and water solubility were incorporated into cheese and yogurt, with appealing sensory properties. Based on these studies on curcumin encapsulation, a project on improving bioaccessibility and targeted release of curcumin-protein complex microparticles in food was proposed without complicated synthesis of curcumin derivatives or multi-batch processes, which would be presented in chapter 4.

2.4.12.2 Phytosterols

Sterols of plants and animals are known as phytosterols and zoosterols, respectively. Phytosterols include campesterol, sitosterol, and stigmasterol, exhibiting cholesterol lowering properties, antioxidation, anti-inflammatory, anti-atherogenicity, and anti-cancer activities. Stanols are the hydrogenated forms of sterols with similar physiological effects. Cholesterol is a representative type of zoosterols. The structure comparison of β-sitosterol, β-sitostanol and cholesterol is shown in **Fig. 2.3**.

The oxidation risk of phytosterols rises on exposure to heat, oxygen, and light. Microcapsules of phytosterols coated with milk proteins (Chen et al., 2013) by spray drying showed acceptable retention and storage stability.

Table 2.4: Screening on polyphenols.

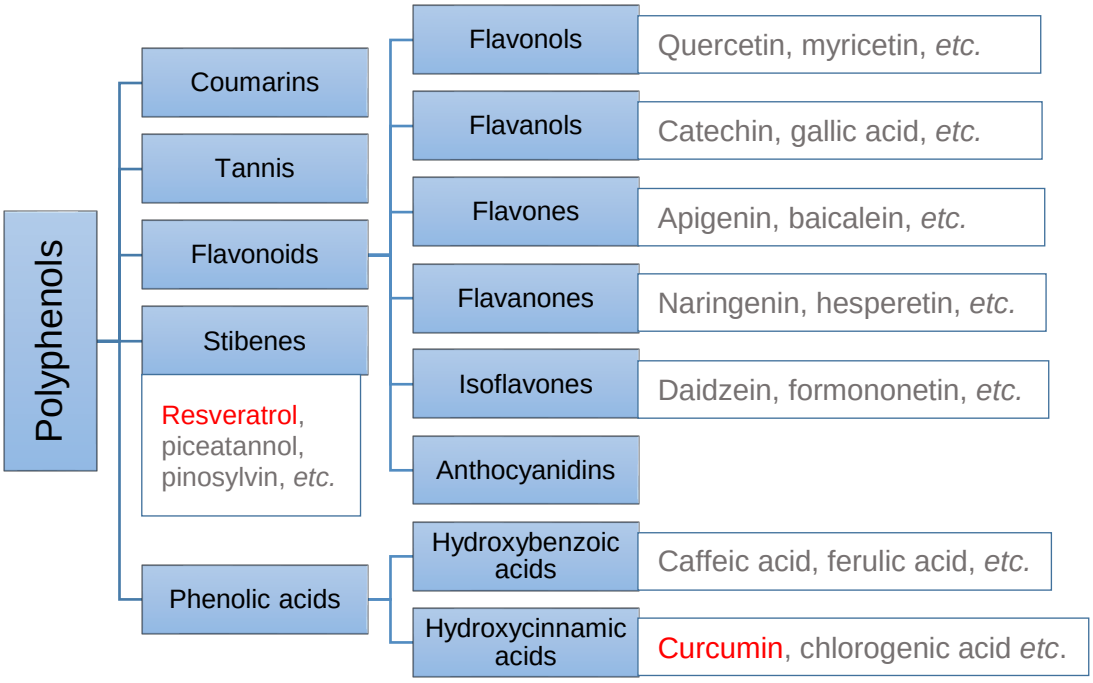

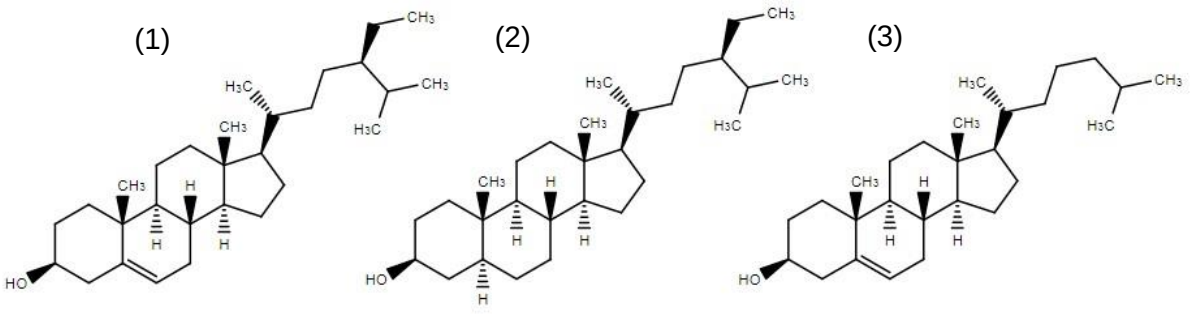

Fig. 2.3. Structures of β-sitosterol (1), β-sitostanol (2), and cholesterol (3).

2.5 Summary and remarks

The key challenge of incorporating bioactive ingredients into functional foods is to keep the constituents stable and to release them into the target site of human bodies. Microencapsulation is a currently used approach in industry and can be done *via* spray drying, coacervation, and other routes. For scale up of production, a continuous process like spray drying saves cost, time and energy and thus offers more advantages than the batch process like coacervation. These different routes have specific conditions *e.g.,* high temperature, shear force, and pH, which may in turn affect the preservation of the ingredients. Thus, it is important to develop microencapsulation strategies by screening on active constituents with desired beneficial effects, formulating shell materials with expected functional properties, and

selecting encapsulation techniques and adjusting the processing conditions suitable for the core materials.

Certain microcapsules have been incorporated into commercial food products. However, most remain in the research stage where the functional properties of microcapsules like encapsulation efficiency and storage stability have been optimised but the evaluation of controlled release and bioavailability has rarely been studied. At present, there exist two possible trends: 1) employing shell materials with specific functionality; 2) applying dynamic digestion systems to evaluate the food breakdown and active ingredient release. The former involves the usage of shell materials with higher nutritional values like proteins or with certain characteristics like indigestible dietary fibres. The latter can obtain the release profiles as realistic as possible under the effect of physiological processes such as GI motility, secretion, and emptying.

Therefore, the main focus of this thesis was on establishing a simple microencapsulation strategy in which the microparticles prepared can deliver core materials with different properties and susceptibilities, and exhibit adjustable functional properties and release profiles. Riboflavin and curcumin were encapsulated as two representatives of hydrophilic and lipophilic core materials, respectively. WPI were used as the wall material because of the water solubility, surface amphiphilicity, low cost, safety, and high nutritional value. The methodologies proposed will be introduced in detail in chapter 3 and 4. Then, the microparticles loaded with curcumin would be integrated into a food matrix *i.e.,* yogurt. The yogurt digestion and curcumin release were evaluated using the DIVHS to mimic the *in vivo* release profiles in before- and after-meal states, which would be presented in chapter 5.

2.6 References

Action, E. (1999). Scientific concepts of functional foods in Europe: consensus document. *British Journal of Nutrition, 81*(1), 1-27.

Ahn, S.-I., Lee, Y.-K., & Kwak, H.-S. (2013). Optimization of water-in-oil-in-water microencapsulated β-galactosidase by response surface methodology. *Journal of microencapsulation, 30*(5), 460-469.

Almeida, H. H., Barros, L., Barreira, J. C., Calhelha, R. C., Heleno, S. A., Sayer, C., Miranda, C. G., Leimann, F. V., Barreiro, M. F., & Ferreira, I. C. (2018). Bioactive evaluation and application of different formulations of the natural colorant curcumin (E100) in a hydrophilic matrix (yogurt). *Food Chemistry, 261*, 224-232.

Altunbas, A., Lee, S. J., Rajasekaran, S. A., Schneider, J. P., & Pochan, D. J. (2011). Encapsulation of curcumin in self-assembling peptide hydrogels as injectable drug delivery vehicles. *Biomaterials, 32*(25), 5906-5914.

Anandharamakrishnan, C., Rielly, C. D., & Stapley, A. G. (2010). Spray-freeze-drying of whey proteins at sub-atmospheric pressures. *Dairy Science & Technology, 90*(2), 321-334.

Angelova, N., & Hunkeler, D. (1999). Rationalizing the design of polymeric biomaterials. *Trends in biotechnology, 17*(10), 409-421.

Anglin, E. J., Cheng, L., Freeman, W. R., & Sailor, M. J. (2008). Porous silicon in drug delivery devices and materials. *Advanced drug delivery reviews, 60*(11), 1266-1277.

Anwar, S. H., & Kunz, B. (2011). The influence of drying methods on the stabilization of fish oil microcapsules: Comparison of spray granulation, spray drying, and freeze drying. *Journal of food engineering, 105*(2), 367-378.

Anwar, S. H., Weissbrodt, J., & Kunz, B. (2010). Microencapsulation of fish oil by spray granulation and fluid bed film coating. *Journal of Food Science, 75*(6), E359-E371.

Astray, G., Gonzalez-Barreiro, C., Mejuto, J. C., Rial-Otero, R., & Simal-Gandara, J. (2009). A review on the use of cyclodextrins in foods. *Food Hydrocolloids, 23*(7), 1631-1640.

Azeem, R. A. E., & Nada, A. A. (2015). Chitosan Liposomal microspheres for Ricinoleic acid Encapsulation.

Bahrami, M., & Ranjbarian, S. (2007). Production of micro-and nano-composite particles by supercritical carbon dioxide. *The Journal of supercritical fluids, 40*(2), 263-283.

Baldwin, E. A., Hagenmaier, R., & Bai, J. (2011). *Edible coatings and films to improve food quality*. CRC press.

Barbosa, C., Morais, H. A., Delvivo, F. M., Mansur, H. S., De Oliveira, M. C., & Silvestre, M. P. (2004). Papain hydrolysates of casein: molecular weight profile and encapsulation in lipospheres. *Journal of the Science of Food and Agriculture, 84*(14), 1891-1900.

Barros, L., Retamal, C., Torres, H., Zúñiga, R. N., & Troncoso, E. (2016). Development of an in vitro mechanical gastric system (IMGS) with realistic peristalsis to assess lipid digestibility. *Food Research International, 90*, 216-225.

Bernela, M., Kaur, P., Chopra, M., & Thakur, R. (2014). Synthesis, characterization of nisin loaded alginate–chitosan–pluronic composite nanoparticles and

evaluation against microbes. *LWT-Food Science and Technology, 59*(2), 1093-1099.

Bertolini, A., Siani, A., & Grosso, C. (2001). Stability of monoterpenes encapsulated in gum arabic by spray-drying. *Journal of agricultural and food chemistry, 49*(2), 780-785.

Bhandari, B. R., Datta, N., & Howes, T. (1997). Problems associated with spray drying of sugar-rich foods. *Drying technology, 15*(2), 671-684.

Blanch, G. P., del Castillo, M. L. R., del Mar Caja, M., Pérez-Méndez, M., & Sánchez-Cortés, S. (2007). Stabilization of all-trans-lycopene from tomato by encapsulation using cyclodextrins. *Food chemistry, 105*(4), 1335-1341.

Bonnet, M., Cansell, M., Placin, F., Anton, M., & Leal-Calderon, F. (2010). Impact of sodium caseinate concentration and location on magnesium release from multiple W/O/W emulsions. *Langmuir, 26*(12), 9250-9260.

Bornhorst, G. M., & Paul Singh, R. (2014). Gastric digestion in vivo and in vitro: how the structural aspects of food influence the digestion process. *Annu Rev Food Sci Technol, 5*, 111-132.

Burton, D. D., Kim, H. J., Camilleri, M., Stephens, D. A., Mullan, B. P., O'Connor, M. K., & Talley, N. J. (2005, Aug). Relationship of gastric emptying and volume changes after a solid meal in humans. *Am J Physiol Gastrointest Liver Physiol, 289*(2), G261-266.

Calvo, P., Remunan‐Lopez, C., Vila‐Jato, J. L., & Alonso, M. (1997). Novel hydrophilic chitosan‐polyethylene oxide nanoparticles as protein carriers. *Journal of Applied Polymer Science, 63*(1), 125-132.

Castro, H., Teixeira, P., & Kirby, R. (1997). Evidence of membrane damage in Lactobacillus bulgaricus following freeze drying. *Journal of Applied Microbiology, 82*(1), 87-94.

Chandramouli, V., Kailasapathy, K., Peiris, P., & Jones, M. (2004). An improved method of microencapsulation and its evaluation to protect Lactobacillus spp. in simulated gastric conditions. *Journal of microbiological methods, 56*(1), 27-35.

Chapeau, A.-L., Hamon, P., Rousseau, F., Croguennec, T., Poncelet, D., & Bouhallab, S. (2017, 2017/08/01/). Scale-up production of vitamin loaded heteroprotein coacervates and their protective property. *Journal of Food Engineering, 206*, 67-76.

Chen, L., Xu, Y., Fan, T., Liao, Z., Wu, P., Wu, X., & Chen, X. D. (2016a, 2016/08/01/). Gastric emptying and morphology of a ‘near real’ in vitro human stomach model (RD-IV-HSM). *Journal of Food Engineering, 183*, 1-8.

Chen, L., Xu, Y., Fan, T., Liao, Z., Wu, P., Wu, X., & Chen, X. D. (2016b). Gastric emptying and morphology of a 'near real'in vitro human stomach model (RD-IV-HSM). *Journal of food engineering, 183*, 1-8.

Chen, Q., McGillivray, D., Wen, J., Zhong, F., & Quek, S. Y. (2013). Co-encapsulation of fish oil with phytosterol esters and limonene by milk proteins. *Journal of food engineering, 117*(4), 505-512.

Cho, Y., Shim, H., & Park, J. (2003). Encapsulation of fish oil by an enzymatic gelation process using transglutaminase cross‐linked proteins. *Journal of Food Science, 68*(9), 2717-2723.

Choi, H., Ahn, J., Kim, N., & Kwak, H. (2006). The effects of microencapsulated chitooligosaccharide on physical and sensory properties of the milk. *Asian Australasian Journal of Animal Sciences, 19*(9), 1347.

Choi, M.-J., Ruktanonchai, U., Min, S.-G., Chun, J.-Y., & Soottitantawat, A. (2010). Physical characteristics of fish oil encapsulated by β-cyclodextrin using an aggregation method or polycaprolactone using an emulsion–diffusion method. *Food Chemistry, 119*(4), 1694-1703.

Córdoba, A. L., Deladino, L., & Martino, M. (2013). Effect of starch filler on calcium-alginate hydrogels loaded with yerba mate antioxidants. *Carbohydrate polymers, 95*(1), 315-323.

Costa, A., Nunes, J., Lima, B., Pedrosa, C., Calado, V., Torres, A., & Pierucci, A. (2015). Effective stabilization of CLA by microencapsulation in pea protein. *Food chemistry, 168*, 157-166.

da Rosa Zavareze, E., Telles, A. C., El Halal, S. L. M., da Rocha, M., Colussi, R., de Assis, L. M., de Castro, L. A. S., Dias, A. R. G., & Prentice-Hernández, C. (2014). Production and characterization of encapsulated antioxidative protein hydrolysates from Whitemouth croaker (Micropogonias furnieri) muscle and byproduct. *LWT-Food Science and Technology, 59*(2), 841-848.

da Silva Malheiros, P., Daroit, D. J., & Brandelli, A. (2010). Food applications of liposome-encapsulated antimicrobial peptides. *Trends in Food Science & Technology, 21*(6), 284-292.

Dalgalarrondo, M., Dufour, E., Chobert, J.-M., Bertrand-Harb, C., & Haertlé, T. (1995, 1995/01/01/). Proteolysis of β-lactoglobulin and β-casein by pepsin in ethanolic media. *International dairy journal, 5*(1), 1-14.

Dalmoro, A., Barba, A. A., Lamberti, G., & d'Amore, M. (2012). Intensifying the microencapsulation process: Ultrasonic atomization as an innovative approach. *European Journal of Pharmaceutics and Biopharmaceutics, 80*(3), 471-477.

Davidov-Pardo, G., & McClements, D. J. (2015). Nutraceutical delivery systems: resveratrol encapsulation in grape seed oil nanoemulsions formed by spontaneous emulsification. *Food chemistry, 167*, 205-212.

De Boever, P., Deplancke, B., & Verstraete, W. (2000). Fermentation by gut microbiota cultured in a simulator of the human intestinal microbial ecosystem is improved by supplementing a soygerm powder. *The Journal of nutrition, 130*(10), 2599-2606.

de Pinho Neves, A. L., Milioli, C. C., Müller, L., Riella, H. G., Kuhnen, N. C., & Stulzer, H. K. (2014). Factorial design as tool in chitosan nanoparticles development by ionic gelation technique. *Colloids and Surfaces A: Physicochemical and Engineering Aspects, 445*, 34-39.

Delavari, B., Saboury, A. A., Atri, M. S., Ghasemi, A., Bigdeli, B., Khammari, A., Maghami, P., Moosavi-Movahedi, A. A., Haertlé, T., & Goliaei, B. (2015). Alpha-lactalbumin: a new carrier for vitamin D 3 food enrichment. *Food Hydrocolloids, 45*, 124-131.

Desai, K. G. H., & Park, J. H. (2005). Recent developments in microencapsulation of food ingredients. *Drying technology, 23*(7), 1361-1394.

Desmond, C., Ross, R., O'callaghan, E., Fitzgerald, G., & Stanton, C. (2002). Improved survival of Lactobacillus paracasei NFBC 338 in spray‐dried powders containing gum acacia. *Journal of Applied Microbiology, 93*(6), 1003-1011.

Doan, C. D., & Ghosh, S. (2019). Formation and stability of pea proteins nanoparticles using ethanol-induced desolvation. *Nanomaterials, 9*(7), 949.

Dufour, E., Genot, C., & Haertlé, T. (1994). β-Lactoglobulin binding properties during its folding changes studied by fluorescence spectroscopy. *Biochimica et Biophysica Acta (BBA)-Protein Structure and Molecular Enzymology, 1205*(1), 105-112.

El-Messery, T. M., Altuntas, U., Altin, G., & Özçelik, B. (2020). The effect of spray-drying and freeze-drying on encapsulation efficiency, in vitro bioaccessibility and oxidative stability of krill oil nanoemulsion system. *Food Hydrocolloids, 106*, 105890.

Ezhilarasi, P., Karthik, P., Chhanwal, N., & Anandharamakrishnan, C. (2013). Nanoencapsulation techniques for food bioactive components: a review. *Food and Bioprocess Technology, 6*(3), 628-647.

Ezhilarasi, P. N., Indrani, D., Jena, B. S., & Anandharamakrishnan, C. (2014). Microencapsulation of Garcinia fruit extract by spray drying and its effect on bread quality. *Journal of the Science of Food and Agriculture, 94*(6), 1116-1123.

FAO/WHO. (2001). Health and nutritional properties of probiotics in food including powder milk with live lactic acid bacteria. *Prevention, 5*(1), 1-34.

Favaro-Trindade, C., Santana, A., Monterrey-Quintero, E., Trindade, M., & Netto, F. (2010). The use of spray drying technology to reduce bitter taste of casein hydrolysate. *Food Hydrocolloids, 24*(4), 336-340.

Gallo, L., Llabot, J. M., Allemandi, D., Bucalá, V., & Piña, J. (2011). Influence of spray-drying operating conditions on Rhamnus purshiana (Cáscara sagrada) extract powder physical properties. *Powder Technology, 208*(1), 205-214.

Gangurde, A. B., Fule, R. A., Javeer, S. D., Patole, R. K., Pawar, J. N., & Amin, P. D. (2015). Microencapsulation using aqueous dispersion of lipid matrix by fluidized bed processing technique for stabilization of choline salt. *Journal of Pharmaceutical Investigation, 45*(2), 209-221.

Gao, Y., & Yang, W. (2016). Capture of a third Mg2+ is essential for catalyzing DNA synthesis. *Science, 352*(6291), 1334-1337.

Garman, J., Coolbear, T., & Smart, J. (1996). The effect of cations on the hydrolysis of lactose and the transferase reactions catalysed by β-galactosidase from six strains of lactic acid bacteria. *Applied microbiology and biotechnology, 46*(1), 22-27.

Geetha, G., Poojitha, U., & Khan, K. A. A. (2014). Various techniques for preparation of nanosuspension-A Review. *International Journal of Pharma Research & Review, 3*(9), 30-37.

Goldberg, I. (2012). *Functional foods: designer foods, pharmafoods, nutraceuticals*. Springer Science & Business Media.

Gomez-Estaca, J., Comunian, T., Montero, P., Ferro-Furtado, R., & Favaro-Trindade, C. (2016). Encapsulation of an astaxanthin-containing lipid extract from shrimp waste by complex coacervation using a novel gelatin–cashew gum complex. *Food Hydrocolloids, 61*, 155-162.

Gong, P., Zhang, L., Han, X., Shigwedha, N., Song, W., Yi, H., Du, M., & Cao, C. (2014). Injury mechanisms of lactic acid bacteria starter cultures during spray drying: a review. *Drying technology, 32*(7), 793-800.

Gonnet, M., Lethuaut, L., & Boury, F. (2010). New trends in encapsulation of liposoluble vitamins. *Journal of Controlled Release, 146*(3), 276-290.

Gouin, S. (2004). Microencapsulation: industrial appraisal of existing technologies and trends. *Trends in Food Science & Technology, 15*(7-8), 330-347.

Goycoolea, F. M., Valle-Gallego, A., Stefani, R., Menchicchi, B., David, L., Rochas, C., Santander-Ortega, M. J., & Alonso, M. J. (2012). Chitosan-based nanocapsules: physical characterization, stability in biological media and capsaicin encapsulation. *Colloid and Polymer Science, 290*(14), 1423-1434.

Gula, A., Ren, L., Zhou, Z., Lu, D., & Wang, S. (2013). Design and evaluation of biodegradable enteric microcapsules of amifostine for oral delivery. *International journal of pharmaceutics, 453*(2), 441-447.

Gülseren, İ., Fang, Y., & Corredig, M. (2012a). Whey protein nanoparticles prepared with desolvation with ethanol: Characterization, thermal stability and interfacial behavior. *Food Hydrocolloids, 29*(2), 258-264.

Gülseren, İ., Fang, Y., & Corredig, M. (2012b). Zinc incorporation capacity of whey protein nanoparticles prepared with desolvation with ethanol. *Food Chemistry, 135*(2), 770-774.

Hargrove, J. L., Greenspan, P., & Hartle, D. K. (2004). Nutritional significance and metabolism of very long chain fatty alcohols and acids from dietary waxes. *Experimental Biology and Medicine, 229*(3), 215-226.

Hirota-Nakaoka, N., & Goto, Y. (1999). Alcohol-induced denaturation of β-lactoglobulin: a close correlation to the alcohol-induced α-helix formation of melittin. *Bioorganic & medicinal chemistry, 7*(1), 67-73.

Hosseini, S. M., Hosseini, H., Mohammadifar, M. A., German, J. B., Mortazavian, A. M., Mohammadi, A., Shojaee-Aliabadi, S., & Khaksar, R. (2014). Preparation and characterization of alginate and alginate-resistant starch microparticles containing nisin. *Carbohydrate polymers, 103*, 573-580.

Huang, S., Méjean, S., Rabah, H., Dolivet, A., Le Loir, Y., Chen, X. D., Jan, G., Jeantet, R., & Schuck, P. (2017). Double use of concentrated sweet whey for growth and spray drying of probiotics: Towards maximal viability in pilot scale spray dryer. *Journal of food engineering, 196*, 11-17.

Huang, S., Rabah, H., Jardin, J., Briard-Bion, V., Parayre, S., Maillard, M.-B., Le Loir, Y., Chen, X. D., Schuck, P., & Jeantet, R. (2016). Hyperconcentrated Sweet Whey, a New Culture Medium That Enhances Propionibacterium freudenreichii Stress Tolerance. *Applied and environmental microbiology, 82*(15), 4641-4651.

Ikeda, S., & Morris, V. J. (2002). Fine-stranded and particulate aggregates of heat-denatured whey proteins visualized by atomic force microscopy. *Biomacromolecules, 3*(2), 382-389.

Ishibashi, N., Kouge, K., Shinoda, I., Kanehisa, H., & Okai, H. (1988). A mechanism for bitter taste sensibility in peptides. *Agricultural and Biological Chemistry, 52*(3), 819-827.

Jain, A., Thakur, D., Ghoshal, G., Katare, O., & Shivhare, U. (2016). Characterization of microcapsulated β-carotene formed by complex coacervation using casein and gum tragacanth. *International Journal of Biological Macromolecules, 87*, 101-113.

Jamekhorshid, A., Sadrameli, S., & Farid, M. (2014). A review of microencapsulation methods of phase change materials (PCMs) as a thermal energy storage (TES) medium. *Renewable and Sustainable Energy Reviews, 31*, 531-542.

Jansen-Alves, C., Fernandes, K. F., Crizel-Cardozo, M. M., Krumreich, F. D., Borges, C. D., & Zambiazi, R. C. (2018). Microencapsulation of propolis in protein matrix using spray drying for application in food systems. *Food and Bioprocess Technology, 11*(7), 1422-1436.

Jansen-Alves, C., Maia, D. S., Krumreich, F. D., Crizel-Cardoso, M. M., Fioravante, J. B., da Silva, W. P., Borges, C. D., & Zambiazi, R. C. (2019). Propolis microparticles produced with pea protein: Characterization and evaluation of antioxidant and antimicrobial activities. *Food Hydrocolloids, 87*, 703-711.

Jun, J. Y., Nguyen, H. H., Chun, H. S., Kang, B.-C., & Ko, S. (2011). Preparation of size-controlled bovine serum albumin (BSA) nanoparticles by a modified desolvation method. *Food Chemistry, 127*(4), 1892-1898.

Jurado, E., Camacho, F., Luzón, G., & Vicaria, J. (2004). Kinetic models of activity for β-galactosidases: influence of pH, ionic concentration and temperature. *Enzyme and Microbial Technology, 34*(1), 33-40.

Jyothi, S. S., Seethadevi, A., Prabha, K. S., Muthuprasanna, P., & Pavitra, P. (2012). Microencapsulation: a review. *Int. J. Pharm. Biol. Sci, 3*, 509-531.

Kailasapathy, K., & Lam, S. (2005). Application of encapsulated enzymes to accelerate cheese ripening. *International Dairy Journal, 15*(6), 929-939.

Kaygusuz, H., & Erim, F. (2013). Alginate/BSA/montmorillonite composites with enhanced protein entrapment and controlled release efficiency. *Reactive and Functional Polymers, 73*(11), 1420-1425.

Kim, C.-K., Chung, H.-S., Lee, M.-K., Choi, L.-N., & Kim, M.-H. (1999). Development of dried liposomes containing β-galactosidase for the digestion of lactose in milk. *International journal of pharmaceutics, 183*(2), 185-193.

Kim, S. J., Park, G. B., Kang, C. B., Park, S. D., Jung, M. Y., Kim, J. O., & Ha, Y. L. (2000). Improvement of oxidative stability of conjugated linoleic acid (CLA) by microencapsulation in cyclodextrins. *Journal of agricultural and food chemistry, 48*(9), 3922-3929.

Klaypradit, W., & Huang, Y.-W. (2008). Fish oil encapsulation with chitosan using ultrasonic atomizer. *LWT-Food Science and Technology, 41*(6), 1133-1139.

Klinkesorn, U., Sophanodora, P., Chinachoti, P., Decker, E. A., & McClements, D. J. (2006). Characterization of spray-dried tuna oil emulsified in two-layered interfacial membranes prepared using electrostatic layer-by-layer deposition. *Food Research International, 39*(4), 449-457.

Kong, F., & Singh, R. P. (2008, Jun). Disintegration of solid foods in human stomach. *J Food Sci, 73*(5), R67-80.

Kong, F., & Singh, R. P. (2010, Nov-Dec). A human gastric simulator (HGS) to study food digestion in human stomach. *J Food Sci, 75*(9), E627-635.

Kozu, H., Nakata, Y., Nakajima, M., Neves, M. A., Uemura, K., Sato, S., Kobayashi, I., & Ichikawa, S. (2014). Development of a Human Gastric Digestion Simulator Equipped with Peristalsis Function for the Direct Observation and Analysis of the Food Digestion Process. *Food Science and Technology Research, 20*(2), 225-233.

Kubo, K., Sekine, S., & Saito, M. (2003). Docosahexaenoic acid-containing phosphatidylethanolamine in the external layer of liposomes protects docosahexaenoic acid from 2, 2′-azobis (2-aminopropane) dihydrochloride-mediated lipid peroxidation. *Archives of biochemistry and biophysics, 410*(1), 141-148.

Kuck, L. S., & Noreña, C. P. Z. (2016). Microencapsulation of grape (Vitis labrusca var. Bordo) skin phenolic extract using gum Arabic, polydextrose, and partially hydrolyzed guar gum as encapsulating agents. *Food Chemistry, 194*, 569-576.

Kulka, K. (1967). Aspects of functional groups and flavor. *Journal of agricultural and food chemistry, 15*(1), 48-57.

Kurozawa, L. E., Park, K. J., & Hubinger, M. D. (2009). Effect of carrier agents on the physicochemical properties of a spray dried chicken meat protein hydrolysate. *Journal of food engineering, 94*(3), 326-333.

Kwak, H., Ihm, M., & Ahn, J. (2001). Microencapsulation of β-galactosidase with fatty acid esters. *Journal of Dairy Science, 84*(7), 1576-1582.

Langer, K., Balthasar, S., Vogel, V., Dinauer, N., Von Briesen, H., & Schubert, D. (2003). Optimization of the preparation process for human serum albumin (HSA) nanoparticles. *International journal of pharmaceutics, 257*(1-2), 169-180.

Li, K., Woo, M. W., Patel, H., & Selomulya, C. (2017). Enhancing the stability of protein-polysaccharides emulsions via Maillard reaction for better oil encapsulation in spray-dried powders by pH adjustment. *Food hydrocolloids, 69*, 121-131.

Li, X., & McGuffin, V. L. (2007). Thermodynamics and Kinetics of Chiral Separations with β‐Cyclodextrin Stationary Phase: I. Effect of Mobile Phase Composition. *Journal of liquid chromatography & related technologies, 30*(5-7), 937-964.

Li, Z., Paulson, A. T., & Gill, T. A. (2015). Encapsulation of bioactive salmon protein hydrolysates with chitosan-coated liposomes. *Journal of Functional Foods, 19*, 733-743.

Liju, V. B., Jeena, K., Kumar, D., Maliakel, B., Kuttan, R., & Krishnakumar, I. (2015). Enhanced bioavailability and safety of curcumagalactomannosides as a dietary ingredient. *Food & function, 6*(1), 275-285.

Lim, S.-M., Yoo, J.-A., Lee, E.-Y., & Cho, K.-H. (2016). Enhancement of high-density lipoprotein cholesterol functions by encapsulation of policosanol exerts anti-senescence and tissue regeneration effects via improvement of anti-glycation, anti-apoptosis, and cholesteryl ester transfer inhibition. *Rejuvenation research, 19*(1), 59-70.

Lin, Y.-K., Al-Suwayeh, S. A., Leu, Y.-L., Shen, F.-M., & Fang, J.-Y. (2013). Squalene-containing nanostructured lipid carriers promote percutaneous absorption and hair follicle targeting of diphencyprone for treating alopecia areata. *Pharmaceutical research, 30*(2), 435-446.

Liu, S., Low, N., & Nickerson, M. T. (2010). Entrapment of flaxseed oil within gelatin‐gum arabic capsules. *Journal of the American Oil Chemists' Society, 87*(7), 809-815.

Mahdavi, S. A., Jafari, S. M., Ghorbani, M., & Assadpoor, E. (2014). Spray-drying microencapsulation of anthocyanins by natural biopolymers: A review. *Drying technology, 32*(5), 509-518.

Malagelada, J.-R., Go, V., & Summerskill, W. (1979). Different gastric, pancreatic, and biliary responses to solid-liquid or homogenized meals. *Digestive Diseases and Sciences, 24*(2), 101-110.

Marcolino, V. A., Zanin, G. M., Durrant, L. R., Benassi, M. D. T., & Matioli, G. (2011). Interaction of curcumin and bixin with β-cyclodextrin: complexation methods, stability, and applications in food. *Journal of agricultural and food chemistry, 59*(7), 3348-3357.

Maroof, K., Lee, R. F., Siow, L. F., & Gan, S. H. (2020). Microencapsulation of propolis by spray drying: A review. *Drying technology*, 1-20.

Martín, A., Mattea, F., Gutiérrez, L., Miguel, F., & Cocero, M. J. (2007). Co-precipitation of carotenoids and bio-polymers with the supercritical anti-solvent process. *The Journal of supercritical fluids, 41*(1), 138-147.

Mato, J. M., Martínez-Chantar, M. L., & Lu, S. C. (2008). Methionine metabolism and liver disease. *Annu. Rev. Nutr., 28*, 273-293.

Mercuri, A., Curto, A., Wickham, M., Craig, D., & Barker, S. A. (2008, 01/01). Dynamic gastric model (DGM): A novel in vitro apparatus to assess the impact of gastric digestion on the droplet size of self-emulsifying drug-delivery systems. *J. Pharm. Pharmacol., 60*.

Minekus, M., Alminger, M., Alvito, P., Ballance, S., Bohn, T., Bourlieu, C., Carrière, F., Boutrou, R., Corredig, M., Dupont, D., Dufour, C., Egger, L., Golding, M., Karakaya, S., Kirkhus, B., Le Feunteun, S., Lesmes, U., Macierzanka, A., Mackie, A., Marze, S., McClements, D. J., Ménard, O., Recio, I., Santos, C. N., Singh, R. P., Vegarud, G. E., Wickham, M. S. J., Weitschies, W., & Brodkorb, A. (2014). A standardised static in vitro digestion method suitable for food - an international consensus. *Food Funct, 5*(6), 1113-1124.

Minekus, M., Marteau, P., Havenaar, R., & Veld, J. (1995, 03/01). A multicompartmental dynamic computer-controlled model simulating the stomach and small intestine. ATLA Altern Lab Anim. *Alternatives to laboratory animals: ATLA, 23*, 197-209.

Minemoto, Y., Hakamata, K., Adachi, S., & Matsuno, R. (2002). Oxidation of linoleic acid encapsulated with gum arabic or maltodextrin by spray-drying. *Journal of microencapsulation, 19*(2), 181-189.

Molly, K., Woestyne, M. V., & Verstraete, W. (1993). Development of a 5-step multi-chamber reactor as a simulation of the human intestinal microbial ecosystem. *Applied microbiology and biotechnology, 39*(2), 254-258.

Moore, J. G., Christian, P. E., & Coleman, R. E. (1981, Jan). Gastric emptying of varying meal weight and composition in man. Evaluation by dual liquid- and solid-phase isotopic method. *Dig Dis Sci, 26*(1), 16-22.

Morais, H. A., Da Silva Barbosa, C. M., DELVIVO, F. M., MANSUR, H. S., CRISTINA DE OLIVEIRA, M., & SILVESTRE, M. P. C. (2004). Comparative study of microencapsulation of casein hydrolysates in lipospheres and liposomes. *Journal of food biochemistry, 28*(1), 21-41.

Morita, T., Sakamura, Y., Horikiri, Y., Suzuki, T., & Yoshino, H. (2000). Protein encapsulation into biodegradable microspheres by a novel S/O/W emulsion method using poly (ethylene glycol) as a protein micronization adjuvant. *Journal of Controlled Release, 69*(3), 435-444.

Mosquera, M., Giménez, B., da Silva, I. M., Boelter, J. F., Montero, P., Gómez-Guillén, M. C., & Brandelli, A. (2014). Nanoencapsulation of an active peptidic fraction from sea bream scales collagen. *Food chemistry, 156*, 144-150.

Nestel, P. J., Yamashita, T., Sasahara, T., Pomeroy, S., Dart, A., Komesaroff, P., Owen, A., & Abbey, M. (1997). Soy isoflavones improve systemic arterial compliance but not plasma lipids in menopausal and perimenopausal women. *Arteriosclerosis, Thrombosis, and Vascular Biology, 17*(12), 3392-3398.

O'Neill, G. J., Jacquier, J. C., Mukhopadhya, A., Egan, T., O'Sullivan, M., Sweeney, T., & O'Riordan, E. D. (2015). In vitro and in vivo evaluation of whey protein hydrogels for oral delivery of riboflavin. *Journal of Functional Foods, 19*, 512-521.

O'Neill, G. J., Egan, T., Jacquier, J. C., O'Sullivan, M., & O'Riordan, E. D. (2014). Whey microbeads as a matrix for the encapsulation and immobilisation of riboflavin and peptides. *Food chemistry, 160*, 46-52.

O'Neill, G. J., Egan, T., Jacquier, J. C., O'Sullivan, M., & O'Riordan, E. D. (2015). Kinetics of immobilisation and release of tryptophan, riboflavin and peptides from whey protein microbeads. *Food chemistry, 180*, 150-155.

Ortiz, S. E. M., Mauri, A., Monterrey-Quintero, E. S., Trindade, M. A., Santana, A. S., & Favaro-Trindade, C. S. (2009). Production and properties of casein hydrolysate microencapsulated by spray drying with soybean protein isolate. *LWT-Food Science and Technology, 42*(5), 919-923.

Ozkan, G., Franco, P., De Marco, I., Xiao, J., & Capanoglu, E. (2019). A review of microencapsulation methods for food antioxidants: Principles, advantages, drawbacks and applications. *Food Chemistry, 272*, 494-506.

Perignon, C., Ongmayeb, G., Neufeld, R., Frere, Y., & Poncelet, D. (2015). Microencapsulation by interfacial polymerisation: membrane formation and structure. *Journal of microencapsulation, 32*(1), 1-15.

Pihlanto-Leppälä, A. (2000). Bioactive peptides derived from bovine whey proteins: opioid and ace-inhibitory peptides. *Trends in Food Science & Technology, 11*(9-10), 347-356.

Potter, S. M. (1998). Soy protein and cardiovascular disease: the impact of bioactive components in soy. *Nutrition reviews, 56*(8), 231-235.

Rao, P. S., Bajaj, R. K., Mann, B., Arora, S., & Tomar, S. (2016). Encapsulation of antioxidant peptide enriched casein hydrolysate using maltodextrin–gum arabic blend. *Journal of food science and technology, 53*(10), 3834-3843.

Rattes, A. L. R., & Oliveira, W. P. (2007). Spray drying conditions and encapsulating composition effects on formation and properties of sodium diclofenac microparticles. *Powder Technology, 171*(1), 7-14.

Reverchon, E., & Adami, R. (2006). Nanomaterials and supercritical fluids. *The Journal of supercritical fluids, 37*(1), 1-22.

Rodriguez-Nogales, J. M., & Delgadillo, A. (2005). Stability and catalytic kinetics of microencapsulated β-galactosidase in liposomes prepared by the dehydration–rehydration method. *Journal of Molecular Catalysis B: Enzymatic, 33*(1), 15-21.

Santos, D. T., & Meireles, M. A. A. (2010). Carotenoid pigments encapsulation: fundamentals, techniques and recent trends. *The Open Chemical Engineering Journal, 4*(1).

Santos, M. G., Bozza, F. T., Thomazini, M., & Favaro-Trindade, C. S. (2015). Microencapsulation of xylitol by double emulsion followed by complex coacervation. *Food chemistry, 171*, 32-39.

Santos, M. G., Carpinteiro, D. A., Thomazini, M., Rocha-Selmi, G. A., da Cruz, A. G., Rodrigues, C. E., & Favaro-Trindade, C. S. (2014). Coencapsulation of xylitol and menthol by double emulsion followed by complex coacervation and microcapsule application in chewing gum. *Food Research International, 66*, 454-462.

Selmer‐Olsen, E., Birkeland, S. E., & Sørhaug, T. (1999). Effect of protective solutes on leakage from and survival of immobilized Lactobacillus subjected to drying, storage and rehydration. *Journal of Applied Microbiology, 87*(3), 429-437.

Sessa, M., Balestrieri, M. L., Ferrari, G., Servillo, L., Castaldo, D., D'Onofrio, N., Donsì, F., & Tsao, R. (2014). Bioavailability of encapsulated resveratrol into nanoemulsion-based delivery systems. *Food chemistry, 147*, 42-50.

Shao, S., Shen, X., & Guo, M. (2018). Zinc‐loaded whey protein nanoparticles prepared by enzymatic cross‐linking and desolvation. *International Journal of Food Science & Technology, 53*(9), 2205-2211.

Sinha, R., Dudani, A., & Ranganathan, B. (1974). Protective effect of fortified skim milk as suspending medium for freeze drying of different lactic acid bacteria. *Journal of Food Science, 39*(3), 641-642.

Slingerland, M., Guchelaar, H.-J., & Gelderblom, H. (2012). Liposomal drug formulations in cancer therapy: 15 years along the road. *Drug discovery today, 17*(3-4), 160-166.

Soottitantawat, A., Bigeard, F., Yoshii, H., Furuta, T., Ohkawara, M., & Linko, P. (2005). Influence of emulsion and powder size on the stability of encapsulated D-limonene by spray drying. *Innovative Food Science & Emerging Technologies, 6*(1), 107-114.

Soppimath, K. S., Aminabhavi, T. M., Kulkarni, A. R., & Rudzinski, W. E. (2001). Biodegradable polymeric nanoparticles as drug delivery devices. *Journal of controlled release, 70*(1-2), 1-20.

Ståhl, K., Claesson, M., Lilliehorn, P., Lindén, H., & Bäckström, K. (2002). The effect of process variables on the degradation and physical properties of spray dried insulin intended for inhalation. *International journal of pharmaceutics, 233*(1-2), 227-237.

Suganya, V., & Anuradha, V. (2017). Microencapsulation and nanoencapsulation: a review. *International Journal of Pharmaceutical and Clinical Research, 9*(3), 233-239.

Tan, H. W., & Misran, M. (2013). Polysaccharide-anchored fatty acid liposome. *International journal of pharmaceutics, 441*(1-2), 414-423.

Taneja, A., & Singh, H. (2012). Challenges for the delivery of long-chain n-3 fatty acids in functional foods. *Annual review of food science and technology, 3*, 105-123.

Teng, Z., Luo, Y., & Wang, Q. (2013). Carboxymethyl chitosan–soy protein complex nanoparticles for the encapsulation and controlled release of vitamin D 3. *Food chemistry, 141*(1), 524-532.

Tomaszewska, M., & Jarosiewicz, A. (2006). Encapsulation of mineral fertilizer by polysulfone using a spraying method. *Desalination, 198*(1-3), 346-352.

Tonon, R. V., Brabet, C., & Hubinger, M. D. (2008). Influence of process conditions on the physicochemical properties of açai (Euterpe oleraceae Mart.) powder produced by spray drying. *Journal of food engineering, 88*(3), 411-418.

Torres‐Giner, S., Martinez‐Abad, A., Ocio, M. J., & Lagaron, J. M. (2010). Stabilization of a nutraceutical omega‐3 fatty acid by encapsulation in ultrathin electrosprayed zein prolamine. *Journal of Food Science, 75*(6), N69-N79.

Trucillo, P., Campardelli, R., & Reverchon, E. (2018). Production of liposomes loaded with antioxidants using a supercritical CO2 assisted process. *Powder Technology, 323*, 155-162.

Tsen, J.-H., Lin, Y.-P., & King, V. A.-E. (2004). Fermentation of banana media by using κ-carrageenan immobilized Lactobacillus acidophilus. *International journal of food microbiology, 91*(2), 215-220.

Tsirigotis-Maniecka, M., Gancarz, R., & Wilk, K. A. (2016). Preparation and characterization of sodium alginate/chitosan microparticles containing esculin. *Colloids and Surfaces A: Physicochemical and Engineering Aspects, 510*, 22-32.

Umesha, S., Manohar, R. S., Indiramma, A., Akshitha, S., & Naidu, K. A. (2015). Enrichment of biscuits with microencapsulated omega-3 fatty acid (Alpha-linolenic acid) rich Garden cress (Lepidium sativum) seed oil: Physical, sensory and storage quality characteristics of biscuits. *LWT-Food Science and Technology, 62*(1), 654-661.

Von Storp, B., Engel, A., Boeker, A., Ploeger, M., & Langer, K. (2012). Albumin nanoparticles with predictable size by desolvation procedure. *Journal of microencapsulation, 29*(2), 138-146.

Wang, J., Wu, P., Liu, M., Liao, Z., Wang, Y., Dong, Z., & Chen, X. D. (2019). An advanced near real dynamic in vitro human stomach system to study gastric digestion and emptying of beef stew and cooked rice. *Food & function, 10*(5), 2914-2925.

Watanabe, Y., Fang, X., Minemoto, Y., Adachi, S., & Matsuno, R. (2002). Suppressive effect of saturated acyl L-ascorbate on the oxidation of linoleic acid encapsulated with maltodextrin or gum arabic by spray-drying. *Journal of agricultural and food chemistry, 50*(14), 3984-3987.

Wheatley, R. W., Juers, D. H., Lev, B. B., Huber, R. E., & Noskov, S. Y. (2015). Elucidating factors important for monovalent cation selectivity in enzymes: E. coli β-galactosidase as a model. *Physical Chemistry Chemical Physics, 17*(16), 10899-10909.

Wu, K. G., & Xiao, Q. (2005). Microencapsulation of fish oil by simple coacervation of hydroxypropyl methylcellulose. *Chinese Journal of Chemistry, 23*(11), 1569-1572.

Wu, P., Bhattarai, R. R., Dhital, S., Deng, R., Chen, X. D., & Gidley, M. J. (2017). In vitro digestion of pectin-and mango-enriched diets using a dynamic rat stomach-duodenum model. *Journal of food engineering, 202*, 65-78.

Wu, P., Chen, L., Wu, X., & Chen, X. D. (2014). Digestive behaviours of large raw rice particles in vivo and in vitro rat stomach systems. *Journal of food engineering, 142*, 170-178.

Wu, P., Deng, R., Wu, X., Wang, Y., Dong, Z., Dhital, S., & Chen, X. D. (2017). In vitro gastric digestion of cooked white and brown rice using a dynamic rat stomach model. *Food Chemistry, 237*, 1065-1072.

Wu, P., Liao, Z., Luo, T., Chen, L., & Chen, X. D. (2017). Enhancement of digestibility of casein powder and raw rice particles in an improved dynamic rat stomach model through an additional rolling mechanism. *Journal of Food Science, 82*(6), 1387-1394.

Xiao, D., Davidson, P. M., & Zhong, Q. (2011). Spray-dried zein capsules with coencapsulated nisin and thymol as antimicrobial delivery system for enhanced antilisterial properties. *Journal of agricultural and food chemistry, 59*(13), 7393-7404.

Ye, Q., Biviano, M., Mettu, S., Zhou, M., Dagastine, R., & Ashokkumar, M. (2016). Modification of pea protein isolate for ultrasonic encapsulation of functional liquids. *RSC advances, 6*(108), 106130-106140.

Ye, Q., Ge, F., Wang, Y., Woo, M. W., Wu, P., Chen, X. D., & Selomulya, C. (2021). On improving bioaccessibility and targeted release of curcumin-whey protein complex microparticles in food. *Food Chemistry, 346*, 128900.

Ye, Q., Mettu, S., Zhou, M., Dagastine, R., & Ashokkumar, M. (2018). Ultrasonically synthesized organic liquid-filled chitosan microcapsules: part 1: tuning physical & functional properties. *Soft matter, 14*(16), 3202-3208.

Ye, Q., Woo, M. W., & Selomulya, C. (2019). Modification of molecular conformation of spray-dried whey protein microparticles improving digestibility and release characteristics. *Food Chemistry, 280*, 255-261.

Yeo, Y., Baek, N., & Park, K. (2001). Microencapsulation methods for delivery of protein drugs. *Biotechnology and Bioprocess Engineering, 6*(4), 213-230.

Zhang, J.-a. A., & Pawelchak, J. (2000). Effect of pH, ionic strength and oxygen burden on the chemical stability of EPC/cholesterol liposomes under accelerated conditions: Part 1: Lipid hydrolysis. *European journal of pharmaceutics and biopharmaceutics, 50*(3), 357-364.

Zhang, K., Zhang, H., Hu, X., Bao, S., & Huang, H. (2012). Synthesis and release studies of microalgal oil-containing microcapsules prepared by complex coacervation. *Colloids and Surfaces B: Biointerfaces, 89*, 61-66.

Zhang, Z., Zhang, R., Chen, L., & McClements, D. J. (2016, 2016/06/01/). Encapsulation of lactase (β-galactosidase) into κ-carrageenan-based hydrogel beads: Impact of environmental conditions on enzyme activity. *Food chemistry, 200*, 69-75.

Zhu, Y., Peng, W., Zhang, J., Wang, M., Firempong, C. K., Feng, C., Liu, H., Xu, X., & Yu, J. (2014). Enhanced oral bioavailability of capsaicin in mixed polymeric micelles: Preparation, in vitro and in vivo evaluation. *Journal of Functional Foods, 8*, 358-366.

Zhu, Y., Wang, M., Zhang, J., Peng, W., Firempong, C. K., Deng, W., Wang, Q., Wang, S., Shi, F., & Yu, J. (2015). Improved oral bioavailability of capsaicin via liposomal nanoformulation: preparation, in vitro drug release and pharmacokinetics in rats. *Archives of pharmacal research, 38*(4), 512-521.

Zohri, M., Alavidjeh, M. S., Haririan, I., Ardestani, M. S., Ebrahimi, S. E. S., Sani, H. T., & Sadjadi, S. K. (2010). A comparative study between the antibacterial effect of nisin and nisin-loaded chitosan/alginate nanoparticles on the growth of Staphylococcus aureus in raw and pasteurized milk samples. *Probiotics and Antimicrobial Proteins, 2*(4), 258-266.

Chapter 3

Modification of molecular conformation of spray-dried whey protein microparticles improving digestibility and release characteristics

This chapter has been published as a peer reviewed research paper by Food Chemistry, (2019), 280, 255-261.
https://doi.org/10.1016/j.foodchem.2018.12.074

According to the literature review in chapter 2, numerous active ingredients with different health benefits belong to water-soluble small molecules such as hydrophilic amino acid, peptides, minerals, cholines, oligosaccharides, sugar alcohols, *etc*. The research aim of this chapter is to propose a general methodology in which microparticles loaded with this type of nutrients could be produced with tunable functional properties and release profiles. Riboflavin *i.e.,* vitamin B2, was used as the model core material.

3.1 Abstract

This study reports on the preparation of riboflavin-loaded whey protein isolate (WPI) microparticles, using desolvation and then spray drying. Ethanol desolvation led to the exposure of embedded hydrophobic amino acids of WPI to riboflavin, facilitating the formation of riboflavin-WPI complexes. The extent of desolvation and cross-linking influenced the morphology of the spray-dried microparticles, while the moisture content of microparticles decreased with desolvation and increased with crosslinking. The modification of WPI conformation upon desolvation could be retained in the dry state *via* spray drying. The gastric resistance, release site and release characteristics of microparticles were readily adjusted by varying the ethanol and calcium ion contents from 0-50% v/v and from 0-2 mM, respectively. The sample prepared from 30% v/v ethanol without calcium crosslinking displayed rapid peptic digestion in less than 30 minutes. The samples from 30% v/v ethanol at 1 and 2 mM Ca^{2+} exhibited excellent gastric resistance and intestinal release.

Keywords: microencapsulation; desolvation; spray drying; targeted release; riboflavin

3.2 Introduction

Many efforts have been devoted to the research, design, and production of nutraceuticals and functional foods to provide public health benefits such as enhanced cognitive performance, gut immune function and improved anti-oxidant capabilities (Duffy et al., 2003). However, a great number of active components lack bioavailability by oral administration because of poor solubility and/or permeability in the gut (Varma et al., 2004). Moreover, some bioactives are unstable during food processing (exposure to heat, oxygen, light) or in the gastro-intestinal tract (due to acid, proteolysis, or interactions with other substances) (Arbos et al., 2002).

In the past decades, encapsulation strategies using food-grade carriers have been proposed to protect and incorporate active ingredients into functional foods. Whey protein isolates (WPI) are one type of extensively used milk proteins, considered as water-soluble, cheap, safe (GRAS *i.e.,* Generally Recognized As Safe, an American Food and Drug Administration designation), and nutrient-dense coating materials. It is a mixture of around 60% β-lactoglobulin, 22% α-lactalbumin, 5.5% bovine serum albumin and 9.1% immunoglobulins (Bryant & McClements, 1998). As the principal component, native β-lactoglobulin is not digested by pepsin since most cleavage sites of this globular protein for pepsin are buried in its hydrophobic cores (Dalgalarrondo et al., 1995; Kitabatake & Kinekawa, 1998). The low peptic digestion of WPI is regarded as the leading cause of its allergenicity (Schmidt et al., 1995). Many means *e.g.,* heat treatment, high pressure, esterification, sulfitolysis and desolvation, have been applied to improve the WPI susceptibility to enzymatic hydrolysis (Dalgalarrondo et al., 1995; Maynard et al., 1998). Desolvation induced by alcohols is proven to change the solvent bulk dielectric constant and form competing hydrogen bonds with proteins, causing the shift of protein secondary structure and exposure of cleavage sites of β-lactoglobulin for pepsin (Dalgalarrondo et al., 1995; Hirota-Nakaoka & Goto, 1999). The effect of desolvation on protein susceptibility to pepsin hydrolysis has been investigated in the aqueous suspension state but rarely in the dry state. The first aim of this study was to investigate the reversibility of protein susceptibility to pepsin *via* desolvation in the aqueous suspensions *versus* in the dry state.

Meanwhile, desolvation leads to the coacervation of protein molecules in the aqueous phase and formation of nanoparticles, which can act as drug delivery devices

(Soppimath et al., 2001). It has been reported that WPI can bind and transport various ligand molecules such as riboflavin (Diarrassouba et al., 2013) and resveratrol (Liang et al., 2007). However, very few studies have investigated the binding behaviour and generation of ligand-WPI complexes under desolvation condition. It is reported that a part of WPI and ligands generate complexes and the rest remain in the free form, causing dynamic fluorescence quenching in the pure water solvents (Diarrassouba et al., 2013). Hence, another aim of this study was to investigate the influence of desolvation on the protein bias in favour of the complex form or the free form and thus to understand the mechanism of formation of this complex system.

WPI possesses poor gastric digestibility, which should be ideal to deliver acid- or pepsin-labile active ingredients. However, its high solubility (Pelegrine & Gasparetto, 2005) leads to rapid release of core materials in the stomach. Calcium ion bridging, especially the cold-set gelation technique, is commonly used to crosslink WPI molecules to prepare gastro-resistant gel beads (Bryant & McClements, 1998; O'Neill et al., 2015). This methodology consists of heat denaturation, cooling, gelation, partitioning, and drying steps, which is a batch process and difficult for scale up of production. High viscosity and water-holding capacity of WPI after gelation possibly results in the fact that little attention has been paid to the fabrication of calcium-crosslinked WPI microparticles *via* spray drying, even though spray drying is a widely used continuous process in the food industry. Thereby, the last aim was to introduce a protocol to crosslink and spray dry active ingredient-filled WPI microparticles.

Thus, the overall objective was to propose a simple methodology by which the gastric digestibility, release sites, and release profiles of spray-dried WPI microparticles can be tuned *via* desolvation and crosslinking. Riboflavin is selected as the core material, also as the fluorescence probe to track the digestion process of WPI and as the ligand molecule to investigate the mechanism of ligand-WPI complex formation *via* desolvation.

3.3 Materials and methods

3.3.1 Materials

Instant whey protein isolate 894 (WPI) containing ≥90% w/w protein was provided by Fonterra (material number: 114266; batch number: 22839594). Riboflavin and pepsin from porcine gastric mucosa (catalog no. P6887, 3200-4500 units/mg protein)

were purchased from Sigma-Aldrich, USA. Potassium dihydrogen phosphate, sodium chloride, sodium hydroxide pellets, and calcium chloride (anhydrous) were purchased from Merck, Germany. Ethanol 99.5% and hydrochloric acid 32% were purchased from Univar, Germany. Milli-Q water was obtained from a Millipore system (18.2 MΩ cm^{-1} at 25°C). All chemicals were used without further purification.

3.3.2 Suspension preparation

WPI was reconstituted in Milli-Q water at 3% w/v. Note that if ethanol was added, equal volumes of water were subtracted to ensure the final concentration of WPI in the ethanol-water systems was still 3% w/v. The WPI solutions were stirred with a magnetic bar for 2 hours at 500 rpm at room temperature and then kept at 4 °C overnight for complete hydration. Riboflavin was added into the solutions at 0.1 mg/ml as a model core material.

The desolvation method was modified from Langer et al. (2003). Briefly, under stirring at 500 rpm at room temperature, the WPI solutions were transformed into sub-microparticle suspensions and made to 0%, 30% and 50% v/v ethanol by the dropwise addition of ethanol at a rate of 2 ml/min using a syringe pump (NE-1600 Syringe Pump, USA). It is reported that WPI susceptibility to pepsin reached its maximum in 30% v/v ethanol and then got inhibited at higher ethanol concentrations (≥40%) (Dalgalarrondo et al., 1995). The ethanol concentrations were varied from 0-50% v/v. After desolvation, anhydrous calcium chloride fine powders were added into the WPI suspensions at $[Ca^{2+}]$ =0, 0.5, 1, and 2 mM, respectively. The higher calcium ion concentration, the higher crosslinking extent and system viscosity. This may result in blockage in spray drying process and thus the calcium ion concentrations were controlled within 0 to 2 mM. The mixtures were kept stirred at 500 rpm for 4 hours for calcium ion crosslinking. The sample details were provided in **Table 3.1**.

3.3.3 Characterisation of suspensions

The viscosity measurement of WPI suspensions was carried out at room temperature using a DV1 Brookfield viscometer (Brookfield, USA). Spindle S61 was mounted to the viscometer, providing a torque value> 10%, with a motor speed at 100 rpm. The hydrodynamic diameter by volume *i.e.,* (D[4,3]) and polydispersity (PDI) was

evaluated using Zetasizer (Malvern). The refractive index of WPI used was 1.53 (Alawode, 2014).

3.3.4 Microfluidic jet spray drying

A triple nozzles micro-fluidic-jet spray dryer (MFJSD) (Nantong Dong Concept New Material Technology Ltd., China) was used to spray dry the WPI suspensions and produced monodisperse microparticles with uniform drying history. The WPI suspensions were pumped into a feed tank by dehumidified air and generated a jet from a nozzle. A microfluidic aerosol nozzle in the form of a tetrafluoroethylene tube with an orifice of 100 µm was selected. The jet broke up into monodisperse droplets with a sinusoidal pulse of 10 kHz from piezoceramics surrounding the nozzle tip. The feed rate was controlled by the dehumidified air flow from 8-12.5 psi based on the viscosity of each sample to generate uniform droplet. The image of the droplets was recorded by a digital SLR (Nikon D90). The drying chamber was 3.2 m in height with a concurrent drying air supply. For most of the samples, the inlet and outlet temperature were fixed at 180 °C and 80 °C, respectively. The inlet/outlet temperature for Samples 1 & 2 were 200 °C and 90 °C, respectively, due to their higher drying requirements, which will be explained in the later section.

3.3.5 Characterisation of spray-dried microparticles

The morphology, average size, and size distribution of the microparticles were evaluated using scanning electron microscopy (Phenom SEM XL), by measuring over 200 microparticles per sample. Plate reader (Infinite 200 PRO, Tecan) was employed to determine fluorescence emission spectra of the chromophores on WPI. Conformational aspects of the spray-dried WPI and WPI-riboflavin complex microparticles were examined using a Spectrum Two FTIR Spectrometer (Perkin Elmer).

3.3.5.1 Moisture content

0.1 g of microparticles was precisely weighted and oven-dried at 105 °C for 3 hours. The microparticles were cooled in a desiccator for 30 min to constant weight. Moisture content was calculated by Eq. (3.1):

$$Moisture(\%) = \frac{original\ sample - dried\ sample}{original\ sample} \times 100 \quad (3.1)$$

3.3.5.2 Riboflavin loading efficiency and encapsulation efficiency

Simulated gastric fluid (SGF) was made of 2.0 g sodium chloride and 1000 ml Milli-Q water, adjusted to pH 1.2 with hydrochloric acid 32% (Maltais et al., 2010). Specific activity of pepsin (catalog no. P6887) was determined to be 3500 units/mg by Li et al. (2003). The pepsin was dispersed into the SGF to approximately 2000 units/ml, according to the harmonised INFOGEST *in vitro* digestion method (Egger et al., 2016). 4 mg microparticles was accurately weighted and incubated in 1 ml the SGF with pepsin at 37 °C under vigorous shaking for 6 hours. Then the mixture was centrifuged at 10,000 rpm for 5 min at room temperature (Sigma 1-14 centrifuge). The concentration of riboflavin in the supernatant was examined from absorbance at 444 nm on a Spectramax M2E microplate reader using a calibration curve (Shu & Zhu, 2002). The loading efficiency (LE) and encapsulation efficiency (EE) of riboflavin were determined from Eq. (3.2) and (3.3):

$$Loading\ efficiency\ (LE)(\%) = \frac{the\ amount\ of\ riboflavin\ encapsulated\ in\ the\ microparticles}{the\ total\ amount\ of\ the\ microparticles} \times 100 \quad (3.2)$$

$$Encapsulation\ efficiency\ (EE)(\%) = \frac{the\ amount\ of\ riboflavin\ encapsulated\ in\ the\ microparticles}{the\ total\ amount\ of\ riboflavin\ in\ the\ microparticles} \times 100 \quad (3.3)$$

3.3.5.3 In vitro release studies

20 mg of microparticles was weighted precisely and incubated in 5 ml the SGF with pepsin or the simulated intestinal fluid (SIF) with trypsin, at 37 °C, 100 rpm, respectively (Incubator-Shaker, Thermoline Scientific). SIF was prepared by adding 6.8 g monobasic potassium phosphate to 250 ml Milli-Q water and mixing with 190 ml 0.2 M sodium hydroxide and 400 ml Milli-Q water, adjusted to pH 7.5 with 0.2 M sodium hydroxide. The final volume was diluted to 1000 ml with Milli-Q water (Piyakulawat et al., 2007). At designated time intervals, 200 µl solution was withdrawn, and 200 µl SGF with pepsin or SIF with trypsin was added into the solutions to keep the total solution volume unchanged. Riboflavin concentration was evaluated in the same method described in the riboflavin loading efficiency measurement.

3.3.6 Statistical analysis

All analyses were performed in triplicate on each sample. Average and error bars (*i.e.,* standard deviations) were determined from the statistical model using analysis of variance (ANOVA) with Microsoft Excel 2010.

Sample Number	Components				Before spray drying (in the feed solution state)		After spray drying (in the dry state)			
	WPI (w/v)	Ethanol (v/v)	$CaCl_2$ (mM)	Riboflavin (mg/ml)	Hydrodynamic Diameter (nm)	Viscosity* (cP)	Diameter (μm)	Moisture Content	Loading Efficiency	Encapsulation Efficiency (%)
1	3%	0%	0	0	522±21	/	74.7±10.1	7.5±0.6	/	/
2	3%	30%	0	0	195±2	/	74.6±12.2	6.3±0.5	/	/
3	3%	0%	0	0.1	495±37	/	69.4±7.2	5.5±0.2	0.25±0.01	70.1±2.0
4	3%	30%	0	0.1	168±0	/	68.3±9.1	3.5±0.8	0.32±0.03	90.0±7.8
5	3%	30%	0.5	0.1	389±5	/	69.4±13.7	5.2±0.4	0.33±0.00	94.6±0.2
6	3%	30%	1	0.1	1485±53	6.3±0.1	56.7±10.2	6.0±0.3	0.34±0.01	96.6±3.4
7	3%	30%	2	0.1	2383±626	12.7±0.2	53.7±9.7	6.9±1.1	0.33±0.01	94.8±2.8
8	3%	50%	2	0.1	2492±87	22.3±0.3	57.6±10.6	6.6±0.1	0.33±0.02	95.9±7.0

Table 3.1: Summary of parameters and composition of Sample 1-8 as prepared. (If the torque value < 10%, the corresponding viscosity* values were omitted.)

3.4 Results and discussion

3.4.1 Effect of ethanol desolvation on WPI suspensions.

Desolvation is considered as a thermodynamically driven self-assembly behaviour of polymers. These polymeric molecules are separated and coacervated with the addition of desolvating agents such as methanol and ethanol (Soppimath et al., 2001). Upon desolvation, sub-microparticles generated aggregated to larger size, scattering strongly and causing its opacity. **Insert. 3.1**A and B in **Fig. 3.1** show the change of appearance for WPI suspensions before and after desolvation.

The hydrodynamic diameter by volume (D[4,3]) and PDI of the suspended WPI sub-microparticles are summarised in **Table 3.1**. The plot of volume percentage *versus* size in **Fig. 3.2**, presents the size distributions with and without ethanol. The WPI sample in Milli-Q water possessed two peaks at values around 50 nm and 342 nm (D[4,3]= 199 nm). The addition of ethanol decreased the polydispersity (PDI) from 0.42 to 0.19 and provoked a shift in the size distribution to D[4,3]= 252 nm. The hydrodynamic diameter of WPI in sodium citrate buffer at pH 3 with filtration was reported to be ≤10 nm (Gülseren et al., 2012). The WPI sample we used was a commercial product, dispersed in Milli-Q water without further filtration, containing ≥90% w/w mixture protein and other impurities such as fat, lactose, and ash (Wang & Lucey, 2003). The comparatively high hydrodynamic diameter of our suspended WPI possibly resulted from the neutral pH selected, non-filtration, or impurities. When converting D[4,3] to hydrodynamic diameter by number, the peaks representing the large particles disappeared in both two systems, shown in **Fig. 3.2**(B). It indicates that the numbers of the large particles were negligible. The hydrodynamic diameter by number increased from 47 nm in Milli-Q water to 116 nm in 30% v/v ethanol. It is presumably due to a decrease in dielectric constant of solvents with the addition of ethanol, resulting in the destabilisation of protein hydration layers and hydrophobic cores and exposure of buried apolar amino acids (Dalgalarrondo et al., 1995; Dufour & Haertlé, 1993). Consequently, protein coacervation and aggregation occurred. With further calcium chloride fine powders dispersed, the hydrodynamic diameter of WPI elevated to micro scale (**Table 3.1**). It may result from the formation of ion crosslinking (Bryant & McClements, 1998; Hongsprabhas et al., 1999), ion-induced protein configuration alteration (Wang & Damodaran, 1991), increasing reactive thiol group content (Jeyarajah & Allen, 1994), and electrostatic shielding effect (Hongsprabhas & Barbut,

1997b). The crosslinking between WPI and calcium ions could also be supported by the increasing viscosity of suspensions (**Table 3.1**).

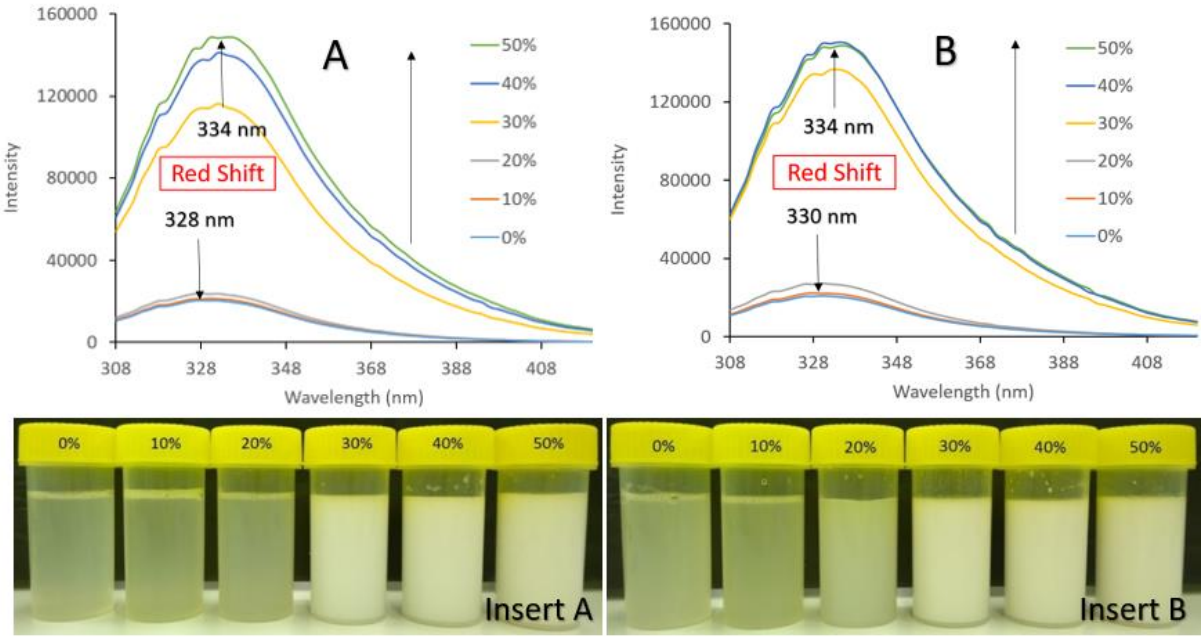

Fig. 3.1. Fluorescence emission spectra of WPI with increasing volume ratios of ethanol; (A) [WPI] = 3% w/v; (B) [WPI] = 6% w/v (Excitation wavelength: 280 nm, at room temperature). Inserts: Appearance of WPI suspensions upon desolvation with varying ethanol contents from 0% to 50% v/v; (A) [WPI] = 3% w/v; (B) [WPI] = 6% w/v.

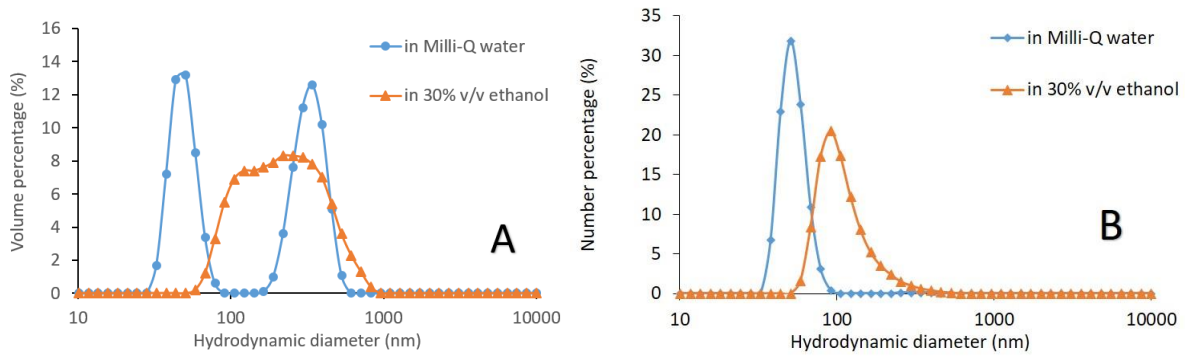

Fig. 3.2. Hydrodynamic diameter by volume (A) and number (B) for WPI in Milli-Q water and 30% v/v ethanol.

The strong intrinsic fluorescence emission peak of WPI at 330 nm upon excitation at 280 nm is ascribed to its tryptophan or tyrosine residues (Zhang & Zhong, 2012). Normally these apolar and aromatic amino acids are embedded in the hydrophobic core of proteins, protecting from proteolysis. The fluorescence spectra of 3% w/v and

6% w/v WPI increased with the addition of ethanol up to 50% v/v as observed in **Fig. 3.1** (A) and (B), implying the increase in tryptophan or tyrosine side chains that were exposed and solvated in the solvents of low polarity. A red shift of fluorescence emission maximum represents more exposure of fluorophores to solvent, *vice versa* (Pallarès et al., 2004). The red shifts (328 to 334 nm, and 330 to 334 nm) found in both two WPI concentrations further illustrate the change in protein conformational structure. It is demonstrated that ethanol desolvation at higher concentrations (>25% v/v) causes the shift of protein secondary structure (Dalgalarrondo et al., 1995; Hirota-Nakaoka & Goto, 1999). Hence, the WPI conformational modification observed in our case is presumably ascribed to its secondary structure shift.

The binding sites for riboflavin are close to tryptophan side chains on WPI (Liang et al., 2007). Thus, more binding sites would be available if more hydrophobic amino acids are exposed *via* desolvation. To confirm this analysis, fluorescence spectra of riboflavin-WPI suspensions were studied.

3.4.2 Effect of ethanol desolvation on WPI-riboflavin suspensions.

The interaction between proteins and ligands can be indicated by fluorescence spectroscopy due to the high sensitivity of fluorophore to its surrounding polarity (Tang et al., 2008). The fluorescence spectra of 3% w/v WPI in the presence of different concentrations of riboflavin in Milli-Q water and 30% ethanol systems are shown in **Fig. 3.3**, respectively. The fluorescence intensity of riboflavin increased with rising riboflavin concentrations (**Fig. 3.4**), while the WPI fluorescence in both solvents declined. This fluorescence quenching implies the interaction between riboflavin and tryptophan or tyrosine residues on WPI.

If the interaction merely caused dynamic quenching, resulting from collisions between fluorophore and quencher in the lifetime of excited state, no WPI-riboflavin complexes would be formed. Otherwise, there existed static quenching and the resulting WPI-riboflavin complexes. The Stern-Volmer equation can be employed to describe dynamic quenching, the Eq. (3.4):

$$F_0/F = 1 + K_q\tau_0[RF] = 1 + K_{SV}[RF] \quad (3.4)$$

Here, F_0 and F represent WPI fluorescence intensity without and with quencher, respectively. K_{SV} is the Stern-Volmer quenching constant. K_q and τ_0 are the dynamic

quenching rate constant of the biopolymer and the fluorophore lifetime in the absence of quencher, respectively. [RF] represents the riboflavin concentration.

According to Liang et al. (2007), τ_0 of tryptophan on β-lactoglobulin (the major component of WPI) under neutral condition is 1.28×10^{-9} s. Stern-Volmer plots of F_0/F against [RF] are shown in inserts of **Fig. 3.3**, exhibiting a linear trend. In **Table 3.2**, the computed values of dynamic quenching rate constant (K_q) were 1.0×10^{12} $M^{-1}s^{-1}$ and 1.3×10^{12} $M^{-1}s^{-1}$ in pure Milli-Q water and 30% v/v ethanol systems at 25°C, respectively. They are much larger than the collisional quenching constant of different quenchers upon biopolymer, being approximately 2.0×10^{10} $M^{-1}s^{-1}$ (Guo et al., 2009). This indicates the dominant role of static quenching in our case, with and/or without desolvation.

On the other hand, dynamic and static quenching have different dependence on temperature and viscosity. Rising temperature leads to greater diffusion coefficients and dynamic quenching *i.e.,* a larger dynamic quenching constant (K_q). High temperature may also be responsible for the destabilisation of complexes, causing a reduction of the static quenching constant. The plots of riboflavin quenching upon WPI at various temperatures (25, 35 and 42°C) are shown in **Table 3.2**. The Stern-Volmer quenching constants (K_{SV}) in pure water increased with elevating temperature, implying the existence of dynamic quenching between WPI and riboflavin. By comparison, the K_{SV} values deceased with increasing temperature in the 30% v/v ethanol system, suggesting that instead of dynamic collision, complex generation initiates the fluorescence quenching of WPI (Lakowicz, 1999). It further demonstrates that desolvation provides a better environment for the formation of ground-state WPI-riboflavin complexes.

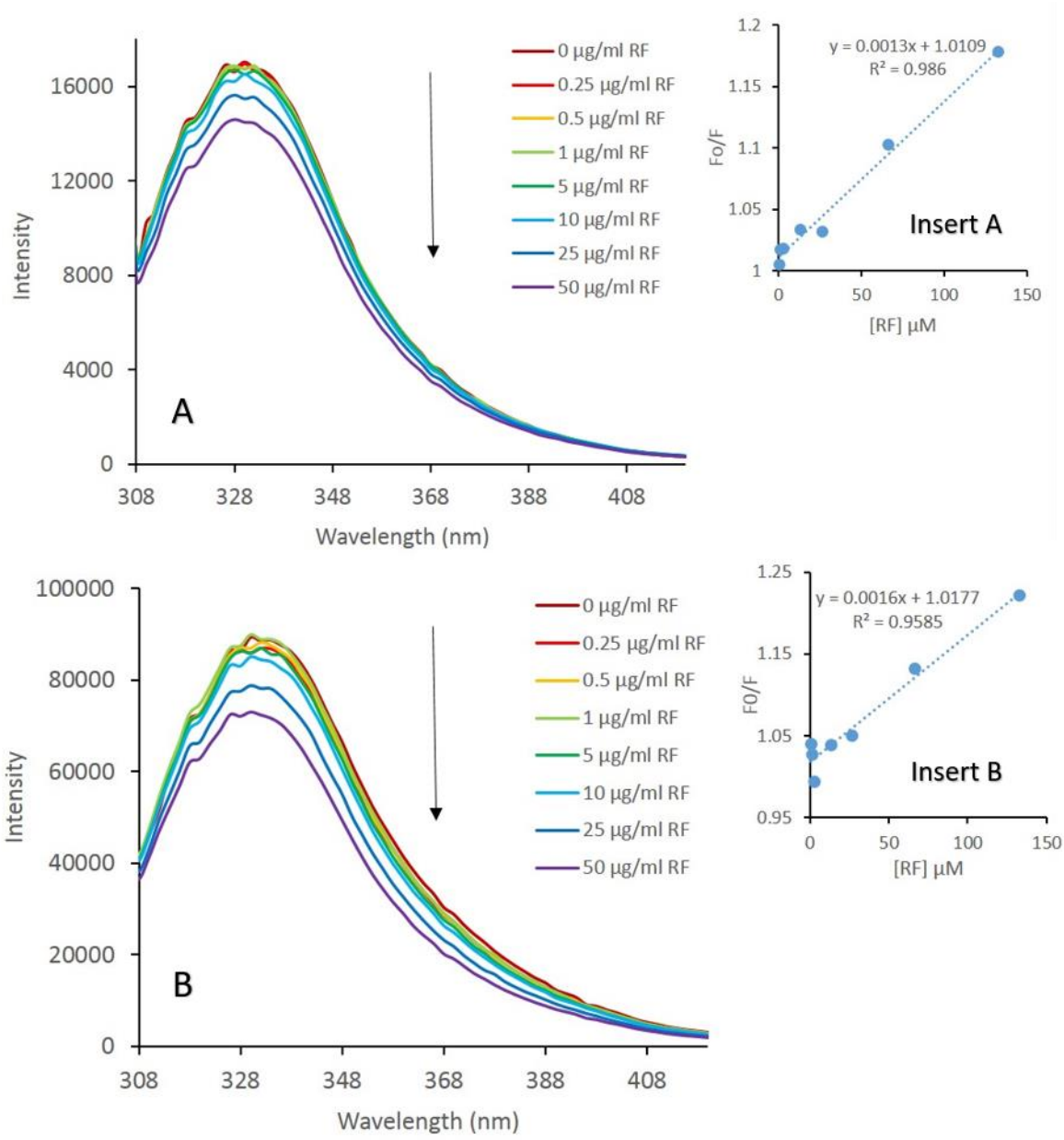

Fig. 3.3. Fluorescence emission spectra of WPI with the addition of riboflavin; (A) in Milli-Q water; (B) in 30% v/v ethanol system (Excitation wavelength: 280 nm, at 25°C). Inserts: Stern-Volmer plots for the WPI quenching by riboflavin; (A): in Milli-Q water; (B) in 30% v/v ethanol system.

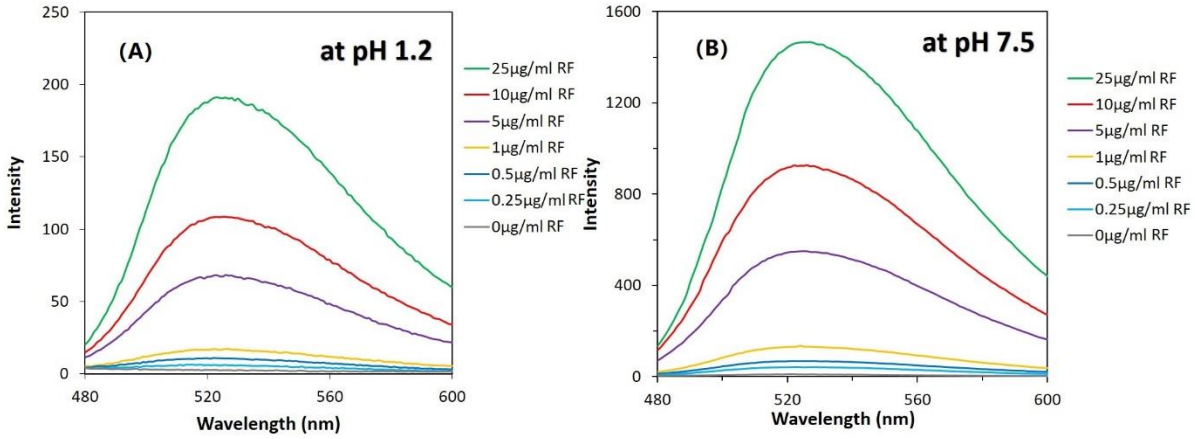

Fig. 3.4. Fluorescence emission spectra of riboflavin in WPI solutions; (A) in the SGF at pH 1.2; (B) in the SIF at pH 7.5 (Excitation wavelength: 370 nm, at 25°C; the concentration of WPI was fixed at 2.7 mg/ml).

Table 3.2: The dynamic quenching rate constant *Kq* and Stern-Volmer quenching constant K_{SV} of WPI with elevated temperatures, as per Eq. (3.4).

Ethanol ratio (v/v)	Temperature (°C)	Stern-Volmer equation	Correlation coefficient	K_{sv} (μM^{-1})	K_q (M^{-1} s^{-1})
0%	25	y=0.0013x+1.0109	0.986	0.0013	1.0×10^{12}
	35	y=0.0016x+0.9418	0.9855	0.0016	1.3×10^{12}
	42	y=0.0016x+0.9226	0.9893	0.0016	1.3×10^{12}
30%	25	y=0.0016x+1.0177	0.9585	0.0016	1.3×10^{12}
	35	y=0.0012x+1.0036	0.9548	0.0012	9.4×10^{11}
	42	y=0.0012x+1.0077	0.9378	0.0012	9.4×10^{11}

3.4.3 Functional properties of spray-dried WPI-riboflavin microparticles.

The size and size distribution of each sample are shown in **Table 3.1**. The SEM images of WPI-riboflavin microparticles produced *via* spray drying are shown in **Fig. 3.5**. The microparticles displayed potlike shapes (spherical, wrinkled, and hollow). The morphology of microparticles changed with the types of solvent used. By varying the composition of solvent from pure water to 30% v/v ethanol system, the microparticles tended to exhibit more wrinkled surfaces. It could be due to the change in boiling points and specific heat capacities of the various solvents (water > ethanol). This resulted in

the difference in latent heat of evaporation and drying rates. When the drying process is faster, the droplet undergoes faster heat and mass transfers. This more vigorous drying process caused more wrinkles and greater deformation on the microparticles shown in **Fig. 3.5** (2) and (4), compared to the samples in **Fig. 3.5** (1) and (3) (Maa et al., 1997; Walton, 2000).

With the incremental addition of calcium chloride powders from 0 to 2 mM, WPI-riboflavin complex microparticles obtained are shown in **Fig. 3.5** (4)-(8). WPI molecules crosslinked with higher [Ca^{2+}] exhibited stronger water-holding capacity (Hongsprabhas & Barbut, 1997a). This results in slower water diffusion and drying rate, allowing more time for microstructures to shrink, deform and collapse during drying process (Oakley, 1997). Therefore, there was a tendency to obtain microparticles having a higher degree of roughness and deformation with higher crosslinking extents.

The moisture contents of samples are displayed in **Table 3.1**. The moisture content comparison between WPI microparticles and WPI-riboflavin microparticles is quite interesting shown in **Fig. 3.6** (A). Note that when 180/80°C set as the inlet/outlet temperatures, no solid WPI microparticles could be produced from 3% w/v WPI solutions from both solvent systems using our microfluidic spray dryer, with only slurry being observed in the outlet. As the inlet/outlet temperatures were raised to 200/90°C, moisture content of WPI microparticles collected were 7.5±0.6% and 6.3±0.5% from water and 30% v/v ethanol solvent systems, respectively. With the addition of riboflavin (0.1 mg/ml) and formation of ground-state WPI-riboflavin complexes, the complex microparticles collected at lower inlet/outlet temperature (180/80°C) contained even lower moisture content of 5.5±0.2% from water solvent and 3.5±0.8% from 30% v/v ethanol solvent.

Theoretically, the boiling point is strongly influenced by intermolecular hydrogen bond, especially the bonding with water molecules. Hydrogen bond can be classified into intermolecular and intramolecular bond while the number of binding sites (*e.g.,* hydrogen, oxygen, and halogen) on a molecule (WPI in our case) is constant. When the number of intramolecular bonds increases, that of intermolecular bonds decreases, resulting in a reduction of boiling point. FTIR measurements were carried out to investigate the conformational effect of WPI-riboflavin complexes on their boiling point, shown in **Fig. 3.7**. It is observed that an increase in the ethanol and Ca^{2+} concentrations contributed to the increase of three peaks marked with dotted lines. In **Fig. 3.7**, the bands appearing at 1260 cm^{-1} were attributed to the C-N stretching for

aromatic amines from 1335-1250 cm^{-1}. If the impurity of WPI was ignored, there were only two possible sources of aromatic amines in the complexes *i.e.,* exposed tryptophan side chains on WPI and isoalloxazine rings of riboflavin. All these complex samples had the same WPI and riboflavin contents. Hence, the absorption enhancement at 1260 cm^{-1} indicates that more tryptophan residues exposed due to desolvation and crosslinking promoted the effect of conjugation and/or H-bond formation between N atoms of aromatic amines mentioned above and H atoms on the complexes. Moreover, the peaks representing out-of-plane N-H wagging vibration in WPI should have appeared at 817 cm^{-1} (Bagheri et al., 2013), but were observed at 799 cm^{-1}, presumably due to red shift caused by the formation of hydrogen bond. The peaks at 1042 cm^{-1} assigned to alkoxyl C-O stretching from 1000-1100 cm^{-1} increased with desolvation and crosslinking. This implies that the effect of conjugation and/or H-bond formation improved the bond polarity and thus its absorption. As one possibility, the generation of WPI-riboflavin complexes facilitated the electron delocalisation and H-bond formation in this conjugated system, causing less intermolecular H-bonds between WPI and water molecules, impairing the hydration layer, and thus yielding microparticles with lower moisture contents at lower inlet temperature upon spray drying. This will be further investigated in future by single droplet drying (Putranto et al., 2017).

As shown in **Fig. 3.6** (B), considering only complex microparticles obtained, it is not surprising that they displayed a lower moisture content after ethanol desolvation. The addition of calcium ions enhanced the water-holding capacity of WPI and thus led to a higher moisture content.

With respect to encapsulation efficiency of riboflavin, high values around 90% are observed in most of the samples except the microparticles produced from pure water solvent (**Table 3.1**). It could be explained by the stable coupling between riboflavin and WPI as a result of complex formation *via* ethanol desolvation, which efficiently avoided the loss of riboflavin during spray drying. Similar trend is found in the loading efficiency of riboflavin.

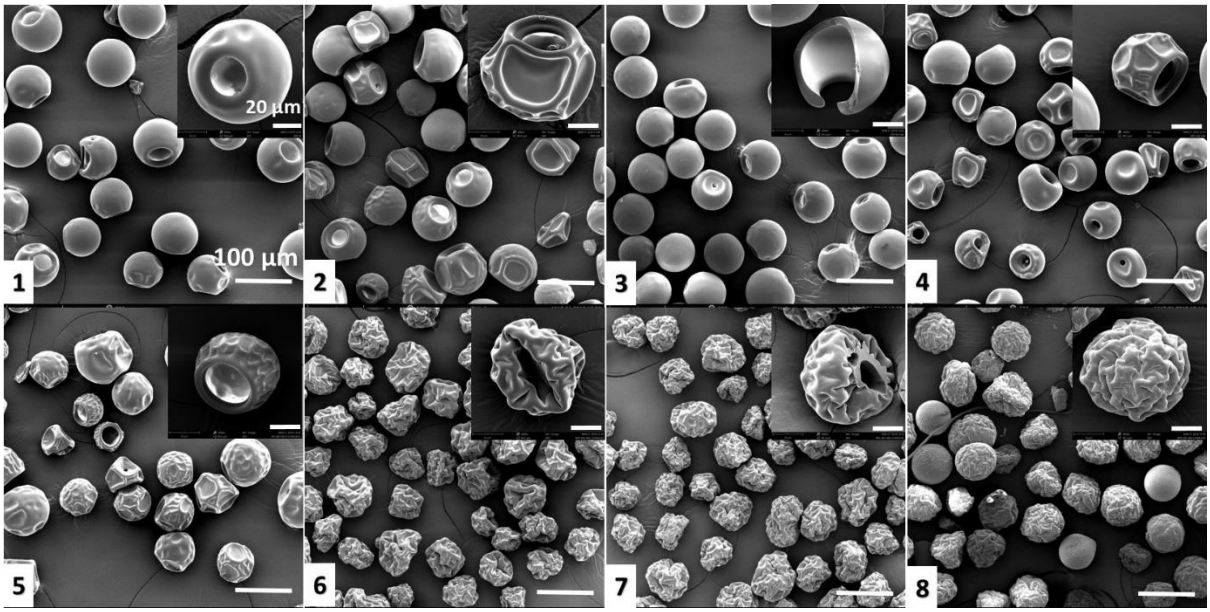

Fig. 3.5. SEM images of microparticles produced from (1) pure WPI in pure water system; (2) pure WPI in 30% v/v ethanol system; (3) WPI-riboflavin complexes in pure water system; WPI-riboflavin complexes in 30% v/v ethanol system at (4) [Ca^{2+}] = 0 mM; (5) [Ca^{2+}] = 0.5 mM; (6) [Ca^{2+}] = 1 mM; (7) [Ca^{2+}] = 2 mM; (8) WPI-riboflavin complexes in 50% v/v ethanol system at [Ca^{2+}] = 2 mM. (Scale bars: 20 µm in the inserts and 100 µm in the original images.)

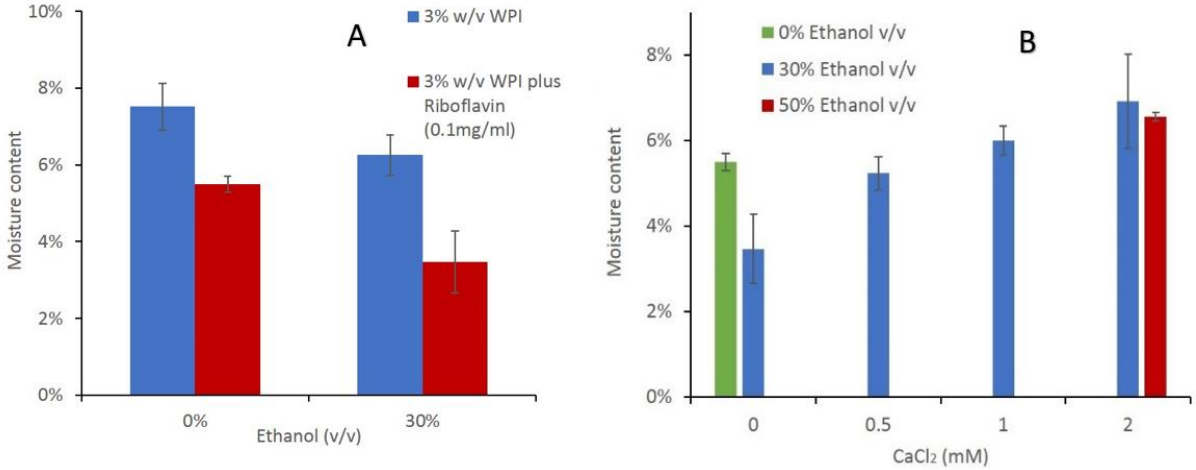

Fig. 3.6. Moisture content of (A) WPI microparticles as a function of riboflavin concentration and ethanol volume ratio (Inlet/outlet temperatures of WPI and WPI-riboflavin are 200/90°C and 180/80°C, respectively); (B) WPI-riboflavin microparticles as a function of calcium ion concentration and ethanol volume ratio. (Inlet/outlet temperatures: 180/80°C).

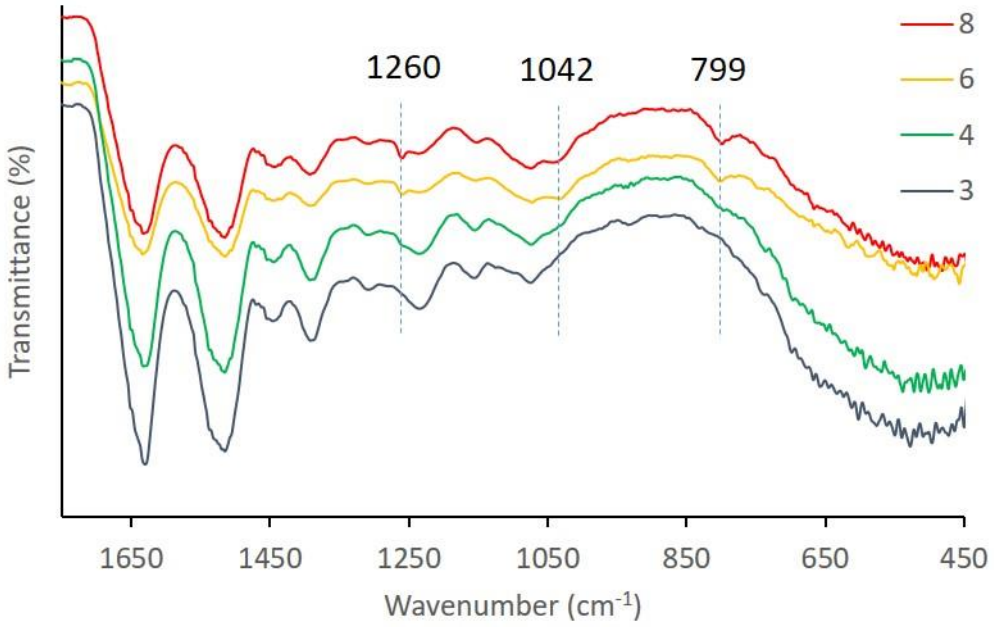

Fig. 3.7. FTIR absorbance spectra (1750-450 cm^{-1}) of the WPI-riboflavin microparticles prepared (3) from pure water solvent; from 30% v/v ethanol system at (4) $[Ca^{2+}]$ = 0 mM; (6) $[Ca^{2+}]$ = 1 mM; (8) in 50% v/v ethanol system at $[Ca^{2+}]$ = 2 mM.

3.4.4 *In vitro* release of riboflavin

The dissolution behaviours of the 8 samples summarised in **Table 3.1** were examined under 6-hour vigorous stirring and centrifuged in water without pepsin. It was observed that the spray-dried WPI particles *via* ethanol desolvation were insoluble in water. Only in the presence of pepsin, the desolvated and insoluble proteins were cleaved and converted into soluble peptides.

In general, gastric residence time is in the range of 5 min to 2 hours. **Fig. 3.8** (A) shows the release characteristics of riboflavin from WPI-riboflavin complex microparticles in the SGF environment. Initial burst release of riboflavin was observed in all samples, caused by the surface distribution of core materials in matrix-type microparticles. Riboflavin-WPI microparticles prepared in pure water solvent was labelled as sample 3 and used as control (light blue line). It had low encapsulation efficiency (about 70%) but suitable release characteristics. Ethanol desolvation can be used to improve the encapsulation efficiency. Sample 4 (red) which lacked calcium crosslinking with desolvation had high encapsulation efficiency of around 90%.

However, ethanol desolvation alone was insufficient. The release percentages of sample 4 was much higher than that of sample 3 at the same running time. This was caused by ethanol desolvation through the exposure of hydrophobic amino acids from WPI. Protein cleavage sites for pepsin are at the carboxyl side of apolar amino acid residues. Therefore, proteins *via* desolvation enabled more cleavage sites accessible for pepsin and became more digestible. The incremental addition of calcium ions was used to bring it back to the suitable release characteristics similar to the control run. Analogous rapid release profile was observed in sample 5 (grey) which was desolvated and crosslinked at 0.5 mM Ca^{2+}. In sample 6 (yellow) and 7 (blue) with 30% v/v ethanol solvent system, the WPI molecules were crosslinked at [Ca^{2+}] = 1 and 2 mM, respectively. Sample 6 and 7 released about 30% riboflavin within the first 2 hours, exhibiting a better gastric resistance than that of the control run. For sample 8 (green), further addition of ethanol to 50% v/v resulted in the decreasing resistance to pepsin even if its [Ca^{2+}] was up to 2 mM, indicating the effect of ethanol desolvation on protein digestibility. SEM images in **Fig. 3.9**, further verify the protein digestion profiles of sample 3 and 7 in the SGF. Both samples kept their structural integrity in 30-minute peptic digestion. Only microparticles with crosslinking at higher Ca^{2+} concentration *i.e.,* sample 7, were able to keep intact after 3-hour digestion.

Fig. 3.8 (B) displays the release profiles of riboflavin from microparticles in the SIF. The overall release trends were similar with those in the SGF and comparatively faster. Considering the intestinal transit time (36 to 48 hours) (Evans et al., 1992) is much longer than the gastric residence time (5 minutes to 2 hours), the core material, riboflavin, could be released slowly during digestion and absorption in the small intestine. Furthermore, it also demonstrates that the variation in protein configuration *via* desolvation and the resulting change in digestibility could be preserved in the dry state.

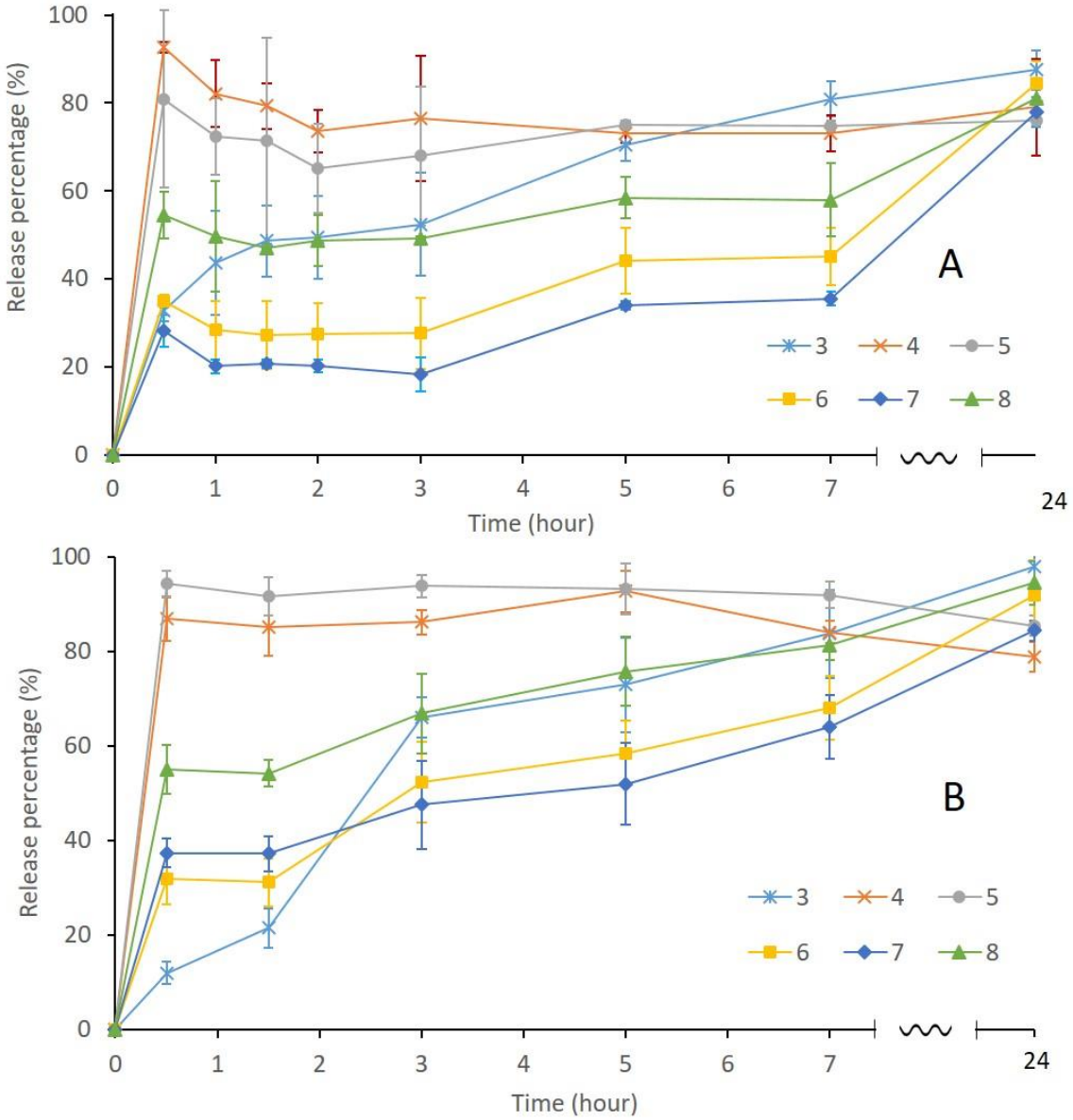

Fig. 3.8. Release characteristics of riboflavin from microparticles (A) in the SGF with pepsin; (B) in the SIF with trypsin; [(3) microparticles prepared from pure water solvent; from 30% v/v ethanol system at (4) [Ca^{2+}] = 0 mM; (5) [Ca^{2+}] = 0.5 mM; (6) [Ca^{2+}] = 1 mM; (7) [Ca^{2+}] = 2 mM; (8) in 50% v/v ethanol system at [Ca^{2+}] = 2 mM.]

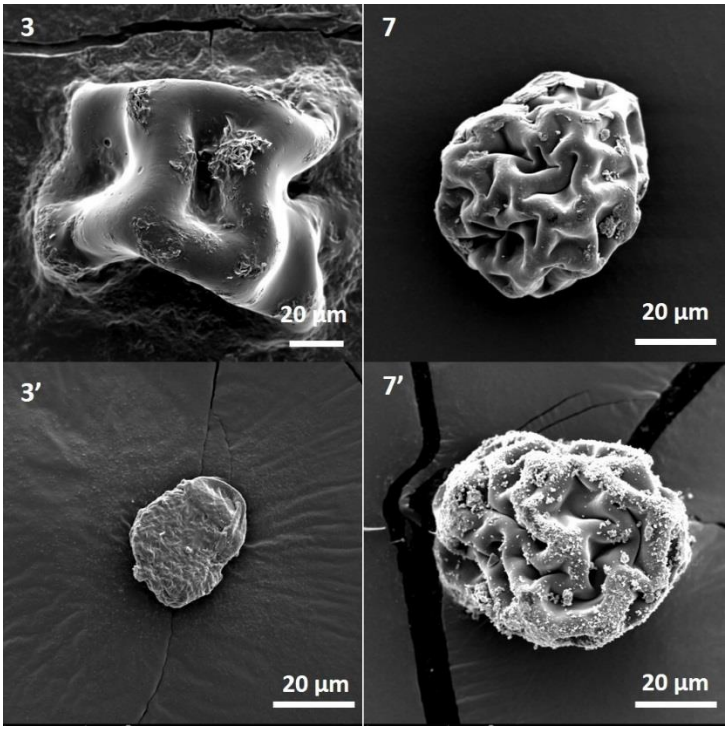

Fig. 3.9. SEM images of WPI-riboflavin microparticles produced from pure water system (3) after 30 minutes SGF digestion; (3') after 3 hours SGF digestion; microparticles prepared in 30% v/v ethanol system at [Ca^{2+}] = 2 mM (7) after 30 minutes SGF digestion; (7') after 3 hours SGF digestion (all the scale bars represent 20 µm).

3.5 Conclusion

The combination of ethanol desolvation and calcium ion bridging has allowed the production of crosslinked WPI-riboflavin microparticles using spray drying. Ethanol, as a desolvating agent in the system, has several basic functions *i.e.,* reducing drying temperature, increasing encapsulation efficiency, facilitating the formation of ground-state riboflavin-WPI complexes, and exposing WPI cleavage sites to pepsin. The modification of WPI conformation and accessibility to cleavage sites for pepsin *via* desolvation were successfully retained in the dry state using spray drying. The release characteristics and digestibility of WPI-riboflavin microparticles can be easily tuned by ethanol content and calcium ion concentration. Samples produced from 30% v/v ethanol at 1 and 2 mM Ca^{2+} showed good gastric resistance and sustained intestinal release. The coupling between desolvation and spray drying displays a great potential

for applications in the food industry as a versatile and low-cost approach to microencapsulation with proteins for targeted release.

3.6 References

Alawode, A. O. (2014). Quantification of protein fractions in aqueous phases of whey and emulsions.

Arbos, P., Arangoa, M., Campanero, M., & Irache, J. (2002). Quantification of the bioadhesive properties of protein-coated PVM/MA nanoparticles. *International journal of pharmaceutics, 242*(1-2), 129-136.

Bagheri, L., Madadlou, A., Yarmand, M., & Mousavi, M. E. (2013). Nanoencapsulation of date palm pit extract in whey protein particles generated via desolvation method. *Food research international, 51*(2), 866-871.

Bryant, C. M., & McClements, D. J. (1998). Molecular basis of protein functionality with special consideration of cold-set gels derived from heat-denatured whey. *Trends in Food Science & Technology, 9*(4), 143-151.

Dalgalarrondo, M., Dufour, E., Chobert, J.-M., Bertrand-Harb, C., & Haertlé, T. (1995, 1995/01/01/). Proteolysis of β-lactoglobulin and β-casein by pepsin in ethanolic media. *International dairy journal, 5*(1), 1-14.

Diarrassouba, F., Liang, L., Remondetto, G., & Subirade, M. (2013). Nanocomplex formation between riboflavin and β-lactoglobulin: Spectroscopic investigation and biological characterization. *Food research international, 52*(2), 557-567.

Duffy, R., Wiseman, H., & File, S. E. (2003). Improved cognitive function in postmenopausal women after 12 weeks of consumption of a soya extract containing isoflavones. *Pharmacology Biochemistry and Behavior, 75*(3), 721-729.

Dufour, E., & Haertlé, T. (1993). Temperature-induced folding changes of β-lactoglobulin in hydro-methanolic solutions. *International journal of biological macromolecules, 15*(5), 293-297.

Egger, L., Ménard, O., Delgado-Andrade, C., Alvito, P., Assunção, R., Balance, S., Barberá, R., Brodkorb, A., Cattenoz, T., & Clemente, A. (2016). The harmonized INFOGEST in vitro digestion method: From knowledge to action. *Food research international, 88*, 217-225.

Evans, R., Kamm, M., Hinton, J., & Lennard-Jones, J. (1992). The normal range and a simple diagram for recording whole gut transit time. *International journal of colorectal disease, 7*(1), 15-17.

Gülseren, İ., Fang, Y., & Corredig, M. (2012). Whey protein nanoparticles prepared with desolvation with ethanol: Characterization, thermal stability and interfacial behavior. *Food Hydrocolloids, 29*(2), 258-264.

Guo, X.-J., Sun, X.-D., & Xu, S.-K. (2009). Spectroscopic investigation of the interaction between riboflavin and bovine serum albumin. *Journal of Molecular Structure, 931*(1-3), 55-59.

Hirota-Nakaoka, N., & Goto, Y. (1999). Alcohol-induced denaturation of β-lactoglobulin: a close correlation to the alcohol-induced α-helix formation of melittin. *Bioorganic & medicinal chemistry, 7*(1), 67-73.

Hongsprabhas, P., & Barbut, S. (1997a). Protein and salt effects on Ca2+ ‐ induced cold gelation of whey protein isolate. *Journal of Food Science, 62*(2), 382-385.

Hongsprabhas, P., & Barbut, S. (1997b). Structure-forming processes in Ca2+-induced whey protein isolate cold gelation. *International dairy journal, 7*(12), 827-834.

Hongsprabhas, P., Barbut, S., & Marangoni, A. (1999). The structure of cold-set whey protein isolate gels prepared with Ca++. *LWT-Food Science and Technology, 32*(4), 196-202.

Jeyarajah, S., & Allen, J. C. (1994). Calcium binding and salt-induced structural changes of native and preheated. beta.-lactoglobulin. *Journal of Agricultural and Food Chemistry, 42*(1), 80-85.

Kitabatake, N., & Kinekawa, Y.-I. (1998). Digestibility of bovine milk whey protein and β-lactoglobulin in vitro and in vivo. *Journal of Agricultural and Food Chemistry, 46*(12), 4917-4923.

Lakowicz, J. (1999). Principles of fluorescence spectroscopy Kluwer Academic Plenum. *New York*.

Langer, K., Balthasar, S., Vogel, V., Dinauer, N., Von Briesen, H., & Schubert, D. (2003). Optimization of the preparation process for human serum albumin (HSA) nanoparticles. *International journal of pharmaceutics, 257*(1-2), 169-180.

Li, J., Wang, J., Gavalas, V. G., Atwood, D. A., & Bachas, L. G. (2003). Alumina− pepsin hybrid nanoparticles with orientation-specific enzyme coupling. *Nano Letters, 3*(1), 55-58.

Liang, L., Tajmir-Riahi, H., & Subirade, M. (2007). Interaction of β-lactoglobulin with resveratrol and its biological implications. *Biomacromolecules, 9*(1), 50-56.

Maa, Y.-F., Costantino, H. R., Nguyen, P.-A., & Hsu, C. C. (1997). The effect of operating and formulation variables on the morphology of spray-dried protein particles. *Pharmaceutical development and technology, 2*(3), 213-223.

Maltais, A., Remondetto, G. E., & Subirade, M. (2010). Tabletted soy protein cold-set hydrogels as carriers of nutraceutical substances. *Food hydrocolloids, 24*(5), 518-524.

Maynard, F., Weingand, A., Hau, J., & Jost, R. (1998, 1998/02/01/). Effect of High-pressure Treatment on the Tryptic Hydrolysis of Bovine β-Lactoglobulin AB. *International dairy journal, 8*(2), 125-133.

O'Neill, G. J., Jacquier, J. C., Mukhopadhya, A., Egan, T., O'Sullivan, M., Sweeney, T., & O'Riordan, E. D. (2015). In vitro and in vivo evaluation of whey protein hydrogels for oral delivery of riboflavin. *Journal of Functional Foods, 19*, 512-521.

Oakley, D. E. (1997). Produce uniform particles by spray-drying. *Chemical engineering progress, 93*(10), 48-54.

Pallarès, I., Vendrell, J., Avilés, F. X., & Ventura, S. (2004). Amyloid fibril formation by a partially structured intermediate state of α-chymotrypsin. *Journal of molecular biology, 342*(1), 321-331.

Pelegrine, D., & Gasparetto, C. (2005). Whey proteins solubility as function of temperature and pH. *LWT-Food Science and Technology, 38*(1), 77-80.

Piyakulawat, P., Praphairaksit, N., Chantarasiri, N., & Muangsin, N. (2007). Preparation and evaluation of chitosan/carrageenan beads for controlled release of sodium diclofenac. *Aaps PharmSciTech, 8*(4), 120.

Putranto, A., Foerster, M., Woo, M. W., Selomulya, C., & Chen, X. D. (2017). A continuum‐approach modeling of surface composition and ternary component distribution inside low fat milk emulsions during single droplet drying. *AIChE Journal, 63*(7), 2535-2545.

Schmidt, D., Meijer, R., Slangen, C., & Van Beresteijn, E. (1995). Raising the pH of the pepsin‐catalysed hydrolysis of bovine whey proteins increases the antigenicity of the hydrolysates. *Clinical & Experimental Allergy, 25*(10), 1007-1017.

Shu, X., & Zhu, K. (2002). Controlled drug release properties of ionically cross-linked chitosan beads: the influence of anion structure. *International journal of pharmaceutics, 233*(1-2), 217-225.

Soppimath, K. S., Aminabhavi, T. M., Kulkarni, A. R., & Rudzinski, W. E. (2001). Biodegradable polymeric nanoparticles as drug delivery devices. *Journal of controlled release, 70*(1-2), 1-20.

Tang, D., Li, H.-J., Li, P., Wen, X.-D., & Qian, Z.-M. (2008). Interaction of bioactive components caffeoylquinic acid derivatives in Chinese medicines with bovine serum albumin. *Chemical and Pharmaceutical Bulletin, 56*(3), 360-365.

Varma, M. V., Khandavilli, S., Ashokraj, Y., Jain, A., Dhanikula, A., Sood, A., Thomas, N. S., Pillai, O., Sharma, P., & Gandhi, R. (2004). Biopharmaceutic classification system: a scientific framework for pharmacokinetic optimization in drug research. *Current drug metabolism, 5*(5), 375-388.

Walton, D. (2000). The morphology of spray-dried particles a qualitative view. *Drying Technology, 18*(9), 1943-1986.

Wang, C., & Damodaran, S. (1991). Thermal gelation of globular proteins: influence of protein conformation on gel strength. *Journal of Agricultural and Food Chemistry, 39*(3), 433-438.

Wang, T., & Lucey, J. A. (2003, 2003/10/01/). Use of Multi-Angle Laser Light Scattering and Size-Exclusion Chromatography to Characterize the Molecular Weight and Types of Aggregates Present in Commercial Whey Protein Products. *Journal of dairy science, 86*(10), 3090-3101.

Zhang, Y., & Zhong, Q. (2012). Binding between bixin and whey protein at pH 7.4 studied by spectroscopy and isothermal titration calorimetry. *Journal of agricultural and food chemistry, 60*(7), 1880-1886.

Chapter 4

On improving bioaccessibility and targeted release of curcumin-whey protein complex microparticles in food

This chapter has been published as a peer reviewed research paper by Food Chemistry, (2020), 346, 128900-128900
https://doi.org/10.1016/j.foodchem.2020.128900

Based on the methodology established in chapter 3, the research aim of this project was to expand its applications to encapsulate the hydrophobic bioactive small molecules (*e.g.,* isoprenes, polyphenols, and phytosterols). This chapter was to propose a strategy in which food ingredients containing this kind of nutrients can be incorporated into a food matrix to improve bioaccessibility and targeted release, without affecting their sensory properties. Curcumin, a hydrophobic polyphenol, was selected as the model core material.

4.1 Abstract

Curcumin is a bioactive food component, with poor bioaccessibility due to low water solubility and stability. Spray drying retained and in fact enhanced curcumin-whey protein isolate (WPI) complexation *via* desolvation, lowering the amount of unbound curcumin to < 5% wt after drying, forming microparticles with better water solubility, stability, and bioaccessibility than raw curcumin. The desolvated microparticles encapsulated 3.47±0.05 mg/g curcumin, almost one order of magnitude higher than the un-desolvated sample 0.37±0.03 mg/g. After incorporation into yogurt, the rapid-release formula liberated 87% curcumin, whereas the targeted-release one discharged 44% before entering the simulated intestinal condition. Most of the yogurt sensory properties were not adversely affected, except for colour and curcumin flavour. This study proposed a strategy in which food ingredients containing hydrophobic bioactive small molecules can be incorporated into a food matrix to improve bioaccessibility and targeted release, without affecting their sensory properties.

Keywords: curcumin; complexation; bioaccessibility; food matrix; targeted release; sensory

4.2 Introduction

Curcumin is a hydrophobic polyphenol extracted from the rhizome of turmeric plant, reported to be around 3% by dry weight (Wang et al., 2008). Chemically, it is composed of two aryl rings with one hydroxyl and one methoxy substituents on individual moiety, connected with a seven-carbon chain in keto or enol form according to the medium pH. The keto/enol moiety and two phenolic groups of curcumin are considered as reactive functional groups, responsible for its pharmacological effects such as anti-inflammatory, antioxidant, anti-tumour, anti-proliferative, and anti-angiogenic activities (Khan et al., 2016). Several issues still limit the application of curcumin in food and pharmaceutical industry. These include a short shelf life from chemical instability, and low bioaccessibility due to poor aqueous solubility, low absorption, rapid metabolism, and elimination.

The technique of nano/microencapsulation is recognised as a feasible method to control release characteristics, and to increase solubility, stability, and resulting bioavailability of curcumin. It has been reported that curcumin entrapped within chitosan nanoparticles *via* ionic gelation exhibited sustained release and anti-proliferative activity (Khan et al., 2016). Curcumin coated within complexed biopolymers of zein and alginate/gelatin using electrostatic deposition and solvent evaporation, showed improved stability, bioaccessibility and antioxidant activity (Yao et al., 2018). However, most of these formulations were prepared in batch processes, which are challenging to scale up. Only a few cases were made in a continuous process of spray drying (Liu et al., 2016; Pan et al., 2013), which is extensively used in the food industry. These previous efforts focused on increasing solubility and dispersibility of curcumin, with little attention paid to incorporate curcumin-loaded microparticles into a food matrix, to investigate their targeted-release behaviour in food with improved bioaccessibility and without diminishing its sensory properties.

It has been extensively reported that polyphenols have a characteristic binding affinity for proteins, especially proline-rich proteins (*e.g.,* salivary proteins), resulting in the generation of polyphenol-protein complexes (Carnovale et al., 2015; Guo et al., 2020; Kaspchak et al., 2019). The extent of polyphenol-protein interaction depends on hydrophobic forces, hydrogen bonding, pH, polyphenol properties (*i.e.,* molecular size, chemical reactivity, solubility, and conformational flexibility), and others. Here whey

protein isolate (WPI) was selected as wall material to fabricate curcumin-WPI complex microparticles *via* spray drying. WPI is a by-product of the cheese-making process and regarded as a low-cost, safe, water-soluble, and nutritious complete protein, containing β-lactoglobulin, α-lactalbumin, bovine serum albumin and immunoglobulins (Bryant & McClements, 1998). Our previous study demonstrates that the shift of WPI conformation due to desolvation can be retained by spray drying (Ye et al., 2019). In the current study, we investigated whether the complexation between proteins and small hydrophobic molecules upon desolvation could also be retained in the microparticles after spray drying. If the complexation can be retained, another question would be how it affects the solubility, stability, release characteristics, and bioaccessibility of the curcumin. Finally, the microparticles were incorporated into a model food matrix (yogurt) to study the effects on targeted release, bioaccessibility, and sensory properties. The curcumin release profiles from microparticles with and without food matrix were compared to evaluate the impact of food matrix upon digestion. The organoleptic perception of the curcumin-enriched food was studied *via* sensory analysis. The outcomes from the study could provide a better strategy on the delivery system of water-insoluble bioactive food ingredients for human consumption.

4.3 Materials and methods

4.3.1 Materials

Whey protein isolate (WPI) containing ≥90% w/w whey protein was obtained from Premium Powders, Marayong, NSW, Australia. Non-food grade curcumin (≥94% curcuminoid content, ≥80% curcumin), pepsin from porcine gastric mucosa powder (≥400 units/mg protein), pancreatin from porcine pancreas (8 x USP specifications), bile salts, and phosphate-buffered saline (10 × concentrate) were from Sigma-Aldrich, St Louis, Mo, USA. Food-grade ethanol (≥95%) was purchased from Henan Xinheyang Alcohol Co., Ltd, Henan, China. Food-grade calcium chloride was obtained from Henan Wan Bang Industrial Co., Ltd, Henan, China. Food-grade curcumin 98% was from Xi'an Shengqing Biotechnology Co., Ltd, Xi'an, China. Low-fat yogurt was purchased from Beijing Hongda Dairy Co., Ltd, Beijing, China. Hydrochloric acid 32% and absolute ethanol 99.5% were obtained from Univar, Germany. Polysorbate 80 (Tween 80) from Fluka, Germany. Other chemicals used were from Merck, Germany.

Milli-Q water from a Millipore system (18.2 MΩ cm^{-1} at 25°C). All chemicals were used without further purification.

Simulated Gastric Fluid (SGF) and Simulated Intestinal Fluid (SIF) were prepared according to the standard INFOGEST protocol (Minekus et al., 2014). Electrolyte stock solutions containing KCl (0.5 mol L^{-1}), KH_2PO_4 (0.5 mol L^{-1}), $NaHCO_3$ (1 mol L^{-1}), NaCl (2 mol L^{-1}), $MgCl_2(H_2O)_6$ (0.15 mol L^{-1}), and $(NH_4)_2CO_3$ (0.5 mol L^{-1}) were prepared. The SGF (100 mL, acidified to pH=1.6 ± 0.1 with 6 M HCl) was made up of the electrolyte stock solutions of 80 ml, 0.3 M $CaCl_2$ of 0.05 ml, Milli-Q water of 19.95 ml, and porcine pepsin with a final enzyme activity of 2000 units/ml. The SIF (200 ml, adjusted to pH=7.0 ± 0.1 with 6 M HCl) contained 160 mL the electrolyte stock solutions, 0.4 ml 0.3 M $CaCl_2$, 39.6 ml Milli-Q water, 10 mM bile salts, and pancreatin with a trypsin activity of 100 units/ml. The activity of pepsin and trypsin in the SGF and SIF would be twice the values mentioned above, when they were diluted by yogurt in a ratio of 50 : 50 (v/v), to achieve the final enzyme activity as suggested by Minekus et al. (2014).

4.3.2 Preparation of WPI-curcumin complex microparticles

Non-food grade WPI-curcumin feed solutions was prepared following a modified method from our previous study (Ye et al., 2019). Briefly, 5% w/v WPI and 125 µg/ml curcumin were dispersed in Milli-Q water and stirred at 500 rpm overnight at room temperature. If ethanol was introduced, equivalent volumes of water would be deducted to reach the final WPI content of 5% w/v in the water-ethanol mixtures. 30% v/v ethanol was added to the WPI solutions to convert the protein molecules to sub-microparticle suspensions. The addition rate of ethanol was set at 2 ml/min with continuous stirring at room temperature. Anhydrous $CaCl_2$ fine powder was dispersed into the WPI suspensions after desolvation at 0, 1, 3, 5 and 10 mM. The suspensions were under magnetic stirring for 4 hours for complete crosslinking, followed by centrifugation at 269 x g for 10 min at room temperature to remove any undissolved curcumin and oversize WPI aggregates. The resulting six feed solutions were referred to as **CW-0mMCa** prepared from pure water system, crosslinked at $[Ca^{2+}]$= 0 mM; **CE-0mMCa** from 30% v/v ethanol system at $[Ca^{2+}]$= 0 mM; **CE-1mMCa** from the ethanol system at $[Ca^{2+}]$= 1 mM, **CE-3mMCa** from the ethanol system at $[Ca^{2+}]$=3 mM; **CE-**

5mMCa from the ethanol system at [Ca^{2+}]= 5 mM, and **CE-10mMCa** from the ethanol system at [Ca^{2+}]= 10 mM.

The monodisperse curcumin-WPI microparticles (non-food grade) with uniform drying history were produced by using a triple nozzles micro-fluidic-jet spray dryer (MFJSD) and a microfluidic aerosol nozzle with an orifice of 100 μm (Nantong Dong Concept New Material Technology Ltd., Nantong, China). The feed solutions were pumped into a feed tank and formed a jet from the nozzle. A 10 kHz sinusoidal pulse from a piezoelectric ceramic covering the nozzle tip broke up the jet into monodisperse droplets. The feed rate was tuned varying from 8 to 13 psi by dehumidified airflow according to the feed solution viscosity. The drying chamber was 3.2 m in height with a concurrent drying air supply. The inlet and outlet temperatures were set at 190 °C and 90 °C, respectively.

Food-grade WPI-curcumin feed solutions were prepared with the same method described above without centrifugation using food-grade ingredients (10% w/v WPI and 3 mg/ml curcumin). Food-grade curcumin-WPI complex microparticles for sensory analysis and colourimeter test were produced using a H-Spray Mini spray dryer (Anhui Holves Engineering Technology Co., Ltd, Anqing, China) with the same drying temperatures as above. The sample details were summarised in **Table 4.1**.

4.3.3 Characterisation of WPI-curcumin complex microparticles

The UV-vis spectra of 1 mg/ml in 30% v/v ethanol with various concentrations of curcumin were obtained using a plate reader (SpectraMax M2e, Molecular Devices, USA). The fluorescence spectra and Stern-Volmer analysis of curcumin-WPI feed solutions were evaluated based on the methodology in our previous study (Ye et al., 2019), recorded by using Infinite 200 PRO, Tecan. The Stern-Volmer equation is a useful method to evaluate dynamic quenching, the Eq. (4.1):

$$F_0/F = 1 + K_q\tau_0[CUR] = 1 + K_{SV}[CUR] \quad (4.1)$$

Where F_0 and F are WPI fluorescence intensity in the absence and presence of quencher, respectively. K_{SV} is the Stern-Volmer quenching constant, K_q the dynamic quenching rate constant of the biopolymer, and τ_0 the fluorophore lifetime without quencher. [CUR] is the curcumin concentration. τ_0 of tryptophan in β-lactoglobulin under neutral pH is 1.28×10^{-9} s (Liang et al., 2007).

The viscosity of curcumin-WPI feed solutions was acquired at room temperature using a DV1 Brookfield viscometer (Brookfield, USA). Spindle S61 providing a torque value more than 10%, at a motor speed of 100 rpm. The hydrodynamic diameter by volume (*i.e.,* D[4,3]) and polydispersity (PDI) of the curcumin-WPI complex feed solutions were evaluated using Nano ZS (Malvern, UK).

The solubility of curcumin in water was determined using a spectrophotometric method (Shin et al., 2016). An excess amount of curcumin was dispersed in Milli-Q water (pH 6.52-6.70) under magnetic stirring at room temperature in darkness for 24 hours, followed by centrifugation (10,000 x g for 30 min). The saturated amount of curcumin in the supernatant was evaluated using the microplate reader at 425 nm according to calibrations made with known amounts of curcumin dissolved in 0.05% wt Tween 80 aqueous solutions.

To determine the saturated content of curcumin in each feed solution, 100 µl the feed solutions were added into 900 µl absolute ethanol and incubated at room temperature in dark under vigorous shaking for 3 hours to fully extract curcumin into ethanol, from a modified method (Anitha et al., 2011). The 1 ml mixture was centrifuged at 9168 x g for 10 min. The concentration of curcumin was examined from the absorbance at 425 nm on the plate reader based on calibrations made with known amounts of curcumin dissolved in absolute ethanol.

A scanning electron microscopy (Phenom SEM XL) was applied to measure the morphology, average size, and the size distribution of the non-food grade microparticles by counting over 200 microparticles per sample. Powder X-ray diffraction (XRD) patterns of non-food grade curcumin, raw WPI, and non-food grade spray-dried WPI-curcumin complex microparticles were measured with a Rigaku Miniflex 600 X-ray diffractometer (Japan) with Ni-filtered Cu Kα radiation (λ = 1.5406 Å). The setting of amperage and voltage was 25 mA and at 40 kV. Each scanning was carried out from 5 to 35 °C in 2θ with a step size of 0.02 °C.

The curcumin content encapsulated in the non-food grade microparticles was determined following a modified method (Patel et al., 2010), by adding a precisely weighted amount of microparticles into 1 ml the SGF with pepsin containing 0.05% wt Tween 80 at 37 °C at 100 rpm overnight in darkness. Tween 80 was used as an emulsifier to fully dissolve the water-insoluble curcumin (Onoue et al., 2010). The mixtures were centrifuged for 5 min at 9168 x g. The curcumin content in the supernatant was examined on the microplate reader at 425 nm. The ethanol-

extractable curcumin content (*i.e.,* the curcumin unbound with WPI and extractable with ethanol) in the microparticles was determined by dispersing a precisely weighted amount of microparticles into 500 µl absolute ethanol at 37 °C at 100 rpm overnight in darkness, followed by the same centrifuge process and concentration calculation as mentioned above.

The loading efficiency (LE) and encapsulation efficiency (EE) of non-food grade curcumin were calculated from Eq. (4.2) and (4.3):

$$Loading\ efficiency\ (LE)(\%) = \frac{Amount\ of\ curcumin\ encapsulated}{Amount\ of\ microparticles} \times 100 \quad (4.2)$$

$$Encapsulation\ efficiency\ (EE)(\%) = \frac{Amount\ of\ curcumin\ encapsulated}{Amount\ of\ curcumin\ in\ feed\ solution} \times 100 \quad (4.3)$$

4.3.3.1 Stability measurements of spray-dried curcumin-WPI complex microparticles

The stability of non-food grade WPI-curcumin complex microparticles in the SGF of pH 1.2, SIF of pH 6.8, and phosphate-buffered saline buffer (PBS) of pH 7.3, was evaluated by recording the maximum absorbance at 425nm for 3 hours at 37°C (Tapal & Tiku, 2012). The stability of raw curcumin in the same media was also investigated for comparison. The SGF and SIF were prepared in the absence of enzyme.

4.3.3.2 DPPH radical scavenging activity of spray-dried curcumin-WPI microparticles

DPPH (2,2-diphenyl-1-picrylhydrazyl) radical scavenging activity was tested from a modified method (Tapal & Tiku, 2012). The measurements were conducted to evaluate the radical scavenging activity of curcumin after spray drying. Briefly, non-food grade samples were incubated in water or SIF with trypsin to obtain a concentration of 0-10 mg/ml. Then, 0.5 ml of the sample was added to 0.5 ml 0.2 mM DPPH ethanol solution, mixed vigorously, and incubated in darkness for 30min. After centrifugation at 5867 x g for 5 min, the absorbance of the resulting supernatant was recorded at 517 nm using the plate reader. The solution in the absence of any sample was regarded as the control. The solution without DPPH was used as the blank. The DPPH radical scavenging activity was determined according to Eq. (4.4):

$$\text{Radical scavenging activity}\ (\%) = \left(1 - \frac{OD\ of\ sample - OD\ of\ blank}{OD\ of\ control}\right) \times 100 \quad (4.4)$$

4.3.4 Incorporation of complex microparticles into food matrix

A plain low-fat yogurt purchased from local market was chosen as the model food matrix, containing cow milk ≥90%, whey protein powder, additives (acetylated distarch phosphate, gelatin, aspartame, phenylalanine, acesulfame potassium), *Streptococcus thermophilus*, *Lactobacillus bulgaricus*, and sucrose ≤0.5 g/100g. The nutrition information panel per 100 g yogurt shows energy 197 kJ, protein 3.0 g, fat 1.2 g, carbohydrate 6.0 g, sodium 60 mg, and calcium 100 mg. The complex microparticles or raw curcumin powders were mixed into the yogurt under homogenisation at 1000 rpm for 5 min (IKA, T18 digital ULTRA TURRAX, Germany), stirring at 600 rpm for 18 hours at 4°C, and storage at 4°C until analysis. The effect of microparticle addition, homogenization, and stirring treatment on the shear viscosity of the original yogurt was evaluated using a Malvern Kinexus pro+ rheometer (UK) shown in **Table 4.2**.

The homogenization plus stirring showed a negligible influence on the viscosity of the original yogurt, at $P < 0.05$ level. 8 mg/ml CE-0mMCa and CE-5mMCa were incorporated into the plain yogurt. The shear viscosities of the plain yogurt, yogurt+ CE-0mMCa, and yogurt+ CM-5mMCa had comparable results, at $P < 0.05$ level.

4.3.4.1 In vitro release studies of curcumin with and without food matrix

40 mg of non-food grade microparticles were weighted accurately and incubated in 5 ml the SGF with pepsin at 37 °C, adjusted to pH 3 with 6 M HCl, at 100 rpm (Incubator-Shaker, Thermoline Scientific, Australia). After 1-h digestion, the gastric digesta was mixed with 5 ml the SIF with trypsin, adjusted to pH 7 with 1 M NaOH, and was left for further 5-hour incubation at 37°C, 100 rpm. 250 µl of chyme was taken out at definite time intervals and centrifuged at 5867 x g for 5 min at 4°C. Meanwhile, 250 µl of the SGF with pepsin or SIF with trypsin was added to the mixture to ensure a constant final volume. Curcumin content was tested based on the fluorescence spectra of the supernatant of 200 µl, from excitation at 480 nm and emission at 520 nm (Onoue et al., 2010). As comparison, the SGF and SIF with enzyme containing 0.05% wt Tween 80 were also used in the release studies to evaluate the release profile of non-food grade curcumin in the ethanol-extractable form which cannot be detected in an aqueous system without emulsifier such as Tween 80.

To investigate the effects of food matrix on the *in vitro* release of curcumin from the complex microparticles according to the standard INFOGEST protocol (Minekus et al., 2014), 40 mg of non-food grade CE-0mMCa without crosslinking and 40 mg of CE-5mMCa with 5 mM Ca^{2+} crosslinking were each incorporated into the plain yogurt of 5 ml. After equilibration to room temperature, 5 ml of yogurt containing 40 mg of microparticles were added into 5 ml of SGF with pepsin, adjusted to pH 3 with 6 M HCl, incubated at 37°C, 100 rpm. After 1 h incubation, 10 ml of SIF with trypsin was mixed with the chyme, alkalised to pH 7 with 6M NaOH solution, for further 2 h intestinal digestion at 37°C, 100 rpm. 400 µl of the chyme was collected after 30 min, 60 min, 90 min, 120 min, and 180 min, centrifuged at 9168 x g for 20 min at 4°C. The curcumin content was examined using the same method above. The plain yogurt without complex microparticles was used as blank. The fluorescence value of the blank was subtracted from each measurement to eliminate the intrinsic influence of yogurt (Onoue et al., 2010). After each collection, 400 µl of SGF or SIF was added into the chyme to make sure the final volume unchanged. Raw curcumin of equal amount as those in 40 mg CE-0mMCa was added into the yogurt of 5 ml as a control. Its release experiment followed the same method mentioned above.

4.3.4.2 Sensory analysis of yogurt and yogurt containing complex microparticles

Forty untrained panellists between the ages of 21 and 33, twenty men and twenty women, participated in the sensory study. Three yogurt samples were chosen to avoid taste fatigue (Choi, 2014), including the plain yogurt, yogurt containing 8 mg/ml food-grade CE-0mMCa, and yogurt with 8 mg/ml food-grade CE-5mMCa. CE-0mMCa and CE-5mMCa were chosen to represent rapid and prolonged release characteristics from the microparticles, respectively.

Twelve characteristic traits of each sample, including colour, mouthfeel, creaminess, sliminess, foreign particle, off flavour, bitterness, sourness, sweetness, curcumin flavour, aftertaste, and smell, were rated by the panellists. A 9-point hedonic scale with 1 step, was designed with 1 being the most unfavourite and 9 being the most favourite expression. Hedonic sensory analysis has been applied widely in the evaluation of dairy products like yogurt (Rognlien et al., 2012). In this current study, the panellists were provided with 20 ml of sample in 50-ml odourless paper cups and

encouraged to drink some water as palate cleanser between applications. All samples were refrigerated at 4°C for storage and then equilibrated to room temperature prior to the sensory evaluation. Other personal opinions from the panellists were also recorded.

4.3.4.3 Colour determination of yogurt and yogurt containing complex microparticles

Three colour features (*L**, *a** and *b**) of the three food-grade samples, which are low-fat yogurt, low-fat yogurt containing 8 mg/ml food-grade CE-0mMCa, and low-fat yogurt with 8 mg/ml food-grade CE-5mMCa, were examined using a colourimeter (CHROMA METER CR-400, from Minolta Camera Co., Osaka, Japan). Calibration with a white tile standard was conducted prior to each measurement. *L** means the lightness component, ranging from 0 (blank) to 100 (white). *a** is *a* chromatic component, from red (positive) to green (negative). *b** is another chromatic component, representing from yellow (positive) to blue (negative). *ΔE** means the colour differences between the plain yogurt as control distinguished by the subscript '0' and the yogurt containing complex microparticles by the subscript '*n*', which can be calculated from the CIE (Commission Internationale de l'Eclairage) 1976 *L*a*b** colour-difference formula (de l'Eclairage, 1978), Eq. (4.5):

$$\Delta E^*_{n0} = \sqrt{(\mathrm{L}^*_n - L^*_0)^2 + (a^*_n - a^*_0)^2 + (b^*_n - b^*_0)^2} \quad (4.5)$$

4.3.5 Statistical analysis

Each sample measurement was conducted in triplicate. Mean and error bars (*i.e.,* standard deviations) were calculated from the statistical model using analysis of variance (ANOVA) with Microsoft Excel 2010. The statistical differences between the groups were analysed according to Duncan's multiple range test (Duncan, 1955), where $P = 0.05$.

	Components			Before spray drying (in the feed solution state)			After spray drying (in the dry state)				
Sample Number	WPI (w/v)	Ethanol (v/v)	$CaCl_2$ (mM)	Saturated curcumin (μg/ml)	D [4.3] (nm)	PDI	Viscosity * (cP)	Diameter (μm)	Total curcumin (mg/g particle)	Ethanol-extractable curcumin (%)	Loading Efficiency (%)	Encapsulation Efficiency (%)
CW-0mMCa	5%	0%	0	19.2±0.4	311	0.17	/	102±14	0.37±0.03^{e}	1.03±0.29^{c}	0.037±0.003^{e}	87.8±8.0^{b}
CE-0mMCa	5%	30%	0	68.3±4.1	600	0.30	6.0	82±15	1.97±0.07^{d}	0.27±0.15^{cd}	0.197±0.007^{c}	96.4±3.3^{ab}
CE-1mMCa	5%	30%	1	64.4±1.6	809	0.23	6.4	64±14	1.78±0.04^{c}	0.09±0.03^{d}	0.178±0.004^{d}	94.3±2.1^{ab}
CE-3mMCa	5%	30%	3	91.6±0.7	1231	0.46	11.5	64±10	3.22±0.17^{b}	0.89±0.43^{cd}	0.322±0.017^{b}	96.5±5.1^{ab}
CE-5mMCa	5%	30%	5	94.9±0.9	1005	1	12.3	68±9	3.47±0.05^{a}	4.01±1.09^{b}	0.347±0.005^{a}	98.1±1.4^{ab}
CE-10mMCa	5%	30%	10	87.9±3.7	1828	0.91	15.8	64±11	3.42±0.09^{a}	2.97±0.08^{a}	0.342±0.009^{a}	97.9±2.5^{a}

Table 4.1: Summary of composition and results of 6 samples. (When the torque value < 10%, the corresponding viscosity* values would be omitted. $^{a\text{-}e}$ represent that with the same letter, there is no statistical significances at $P < 0.05$, n=3.)

Table 4.2: Power law parameters for the steady shear viscosity of the yogurt with various treatments and microparticle addition. (There is no statistical difference at $P < 0.05$, n=3.)

Treatment	*K* (Pas^{n}s)	*n*	R^2
Original yogurt	1.457±0.076^a	0.410±0.004^b	0.982
1000 rpm + stirring	1.413±0.057^a	0.426±0.006^a	0.981
10000 rpm + stirring	1.188±0.060^b	0.409±0.010^b	0.983
Sample after 1000 rpm+ stirring	*K* (Pas^{n}s)	*n*	R^2
Original yogurt	1.413±0.057^a	0.426±0.006^a	0.981
Original yogurt+ CE-0mMCa	1.417±0.098^a	0.411±0.011^a	0.978
Original yogurt+ CE-5mMCa	1.414±0.012^a	0.413±0.007^a	0.982

4.4 Results and discussion

4.4.1 Increasing curcumin solubility in feed solutions.

Increasing curcumin solubility in feed solutions to spray drying enables more curcumin to be loaded onto the microparticles. The solubility of curcumin in the 5% w/v WPI aqueous solution was increased to 19.2±0.4 µg/ml from 0.11±0.01 µg/ml in Milli-Q water. The increase in solubility is because the central hydrophobic calyx on β-lactoglobulin surrounded with hydrophobic amino acids can bind with curcumin to form a complex (Sneharani et al., 2010). A combination of hydrophobic forces and hydrogen bonding is responsible for the interaction between β-lactoglobulin and various polyphenols *e.g.,* curcumin, catechin, epicatechin, epicatechin gallate, epigallocatechin gallate, and green tea infusions (Kanakis et al., 2011; Sneharani et al., 2010; Von Staszewski et al., 2011).

Curcumin is soluble in ethanol, up to 4 mg/ml (Aziz et al., 2007). With the addition of ethanol, the solubility of curcumin increased to 68.3±4.1 µg/ml in the 30% v/v ethanol system containing 5% w/v WPI. Ethanol worked not only as a solvent for curcumin but also as a desolvating agent for WPI in this case. Desolvation is known as the separation and coacervation of polymeric molecules in aqueous solutions caused by the addition of desolvating agents such as alcohols (Dalgalarrondo et al., 1995). The hydrophobic core on β-lactoglobulin could be exposed and solvated in a less polar environment with the addition of desolvating agent (Dalgalarrondo et al.,

1995). This implies that the binding sites for curcumin would become more accessible with the exposure of the hydrophobic core due to desolvation.

Therefore, UV-visible absorption spectroscopy was applied to study possible interactions between desolvated WPI and curcumin, shown in **Fig. 4.1**. A peak at 273 nm which is characteristic of the aromatic amino acids in proteins *i.e.,* tryptophan, tyrosine, and phenylalanine (Frederix et al., 2003) was blue-shifted to 268 nm with the addition of curcumin. The blue shift points to a polarity increase close to tryptophan residues and an extension of peptide strand of WPI, and thus a change in hydrophobicity in the presence of incremental curcumin (Liu et al., 2016).

Fluorescence spectroscopy and Stern-Volmer analysis were carried out to evaluate 5% w/v WPI with varying concentrations of curcumin in aqueous and 30% v/v ethanol systems, as shown in **Fig. 4.2** and **Table 4.3**. Analogous methodology and fluorescence quenching phenomenon were reported previously (Ye et al., 2019). Briefly, the ethanol-induced desolvation promoted the binding and complexation between curcumin and hydrophobic core on WPI in feed solutions.

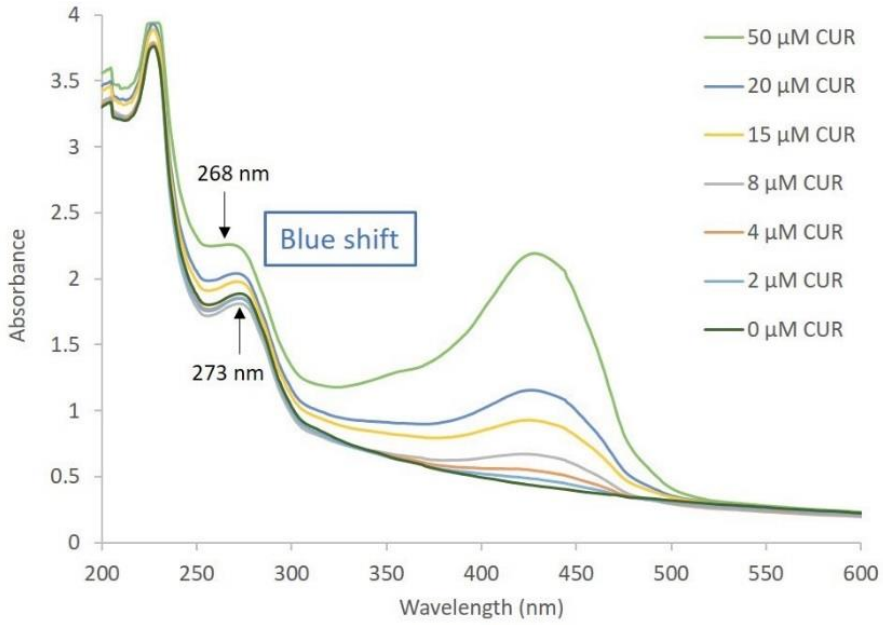

Fig. 4.1. UV-vis absorption spectra of WPI solutions 1 mg/ml in 30% ethanol v/v system with the addition of curcumin.

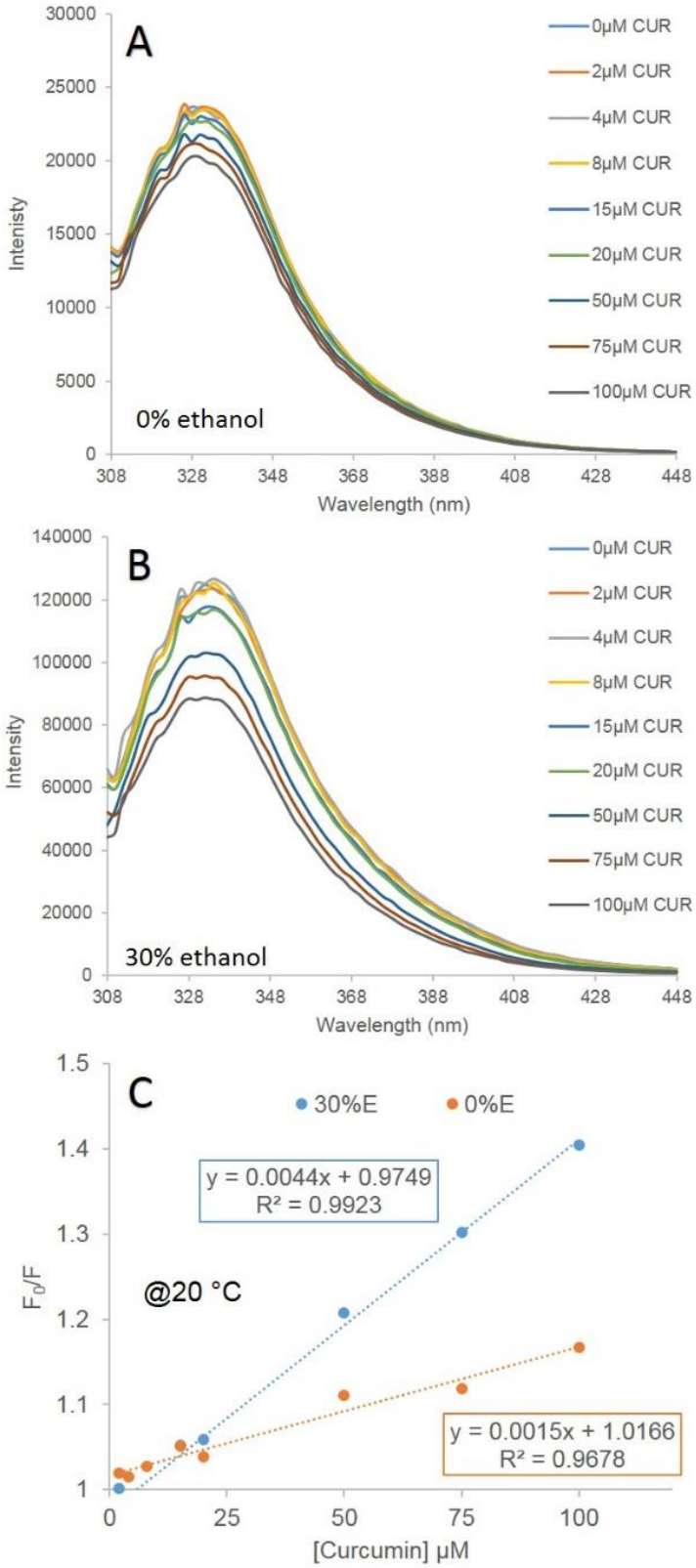

Fig. 4.2. Fluorescence emission spectra of WPI with the addition of curcumin; (A) in pure water (Excitation wavelength: 280 nm, at 20°C); (B) in 30% v/v ethanol system; (C) Stern-Volmer plots for the WPI quenching by curcumin.

Table 4.3: The dynamic quenching rate constant K_q and Stern-Volmer quenching constant K_{SV} of WPI with elevated temperatures.

Ethanol ratio (v/v)	Temperature (°C)	Stern-Volmer equation	Correlation coefficient	K_{sv} (μM^{-1})	K_q ($M^{-1}s^{-1}$)
0%	20	y=0.0015x+1.0166	0.9678	0.0015	1.2×10^{12}
	30	y=0.0020x+1.0018	0.9904	0.0020	1.6×10^{12}
	40	y=0.0024x+0.9799	0.9940	0.0024	1.9×10^{12}
30%	20	y=0.0044x+0.9749	0.9923	0.0044	3.4×10^{12}
	30	y=0.0029x+1.0184	0.9429	0.0029	2.3×10^{12}
	40	y=0.0022x+1.0333	0.8599	0.0022	1.7×10^{12}

4.4.2 Curcumin in ethanol-extractable form and in complex form.

The amounts of curcumin saturated in the feed solutions at varying calcium concentrations are summarised in **Table 4.1**. In this study, curcumin existed in two forms in the feed solution state: the complex form binding with proteins, and the ethanol-extractable form unbound with WPI but dissolved in the ethanol portion. Hence, the main form of curcumin existing in the feed solution state and in the spray-dried state were investigated.

Upon desolvation, $CaCl_2$ fine powders were dissolved into the WPI-curcumin feed solutions, leading to calcium ion-induced protein crosslinking (Bryant & McClements, 1998). The crosslinking is proven by the increase in viscosity and hydrodynamic diameter by volume (D [4,3]) of feed solutions, as shown in **Table 4.1**. The micro-scale D [4,3] observed in samples at $[Ca^{2+}] \geq 3$ mM may cause blockage during spray drying. Therefore, the samples were centrifuged to separate and discard oversized complex aggregates. The precipitates were oven-dried at 60°C overnight and weighed. Their weights were deducted from the total mass of each sample. Consequently, curcumin in the complex form with crosslinking at higher Ca^{2+} concentrations has a higher possibility to form oversized complex aggregates and to be discarded than those in the ethanol-extractable form or without/with crosslinking at lower $[Ca^{2+}]$. This is the main drawback of this technique which might cause less curcumin to be retained in the samples with higher crosslinking. However, the saturated curcumin in the centrifuged feed solutions crosslinked at $[Ca^{2+}] \geq 3$ mM were 88-92 µg/ml, higher than

those at [Ca^{2+}] < 3 mM (19-68 μg/ml), as shown in **Table 4.1**. This was explained in literatures as due to the effect of Ca^{2+} on polyphenol-protein interaction. It has been reported that with the addition of Ca^{2+}, the entropy values of protein-polyphenol interactions change from negative to positive and the resulting Gibbs free energy becomes more negative, presenting an increase in the binding affinity (Kaspchak et al., 2019). The role of Ca^{2+} on protein-polyphenol-Ca^{2+} complexes is described as withholding more polyphenol between protein molecules in the complexes and stabilising the large networks of complexes by electrostatic interactions *via* Ca^{2+} bridging (Carnovale et al., 2015). Guo et al. (2020) reported the complexation of curcumin, pea protein isolate, and high methoxyl pectin. Ca^{2+} could penetrate high methoxyl pectin molecular chains and form Ca^{2+} bridges by electrostatic interactions between pea protein isolate and high methoxyl pectin molecules, generating a compact structure to enhance curcumin stability in the complexes. In this study, more curcumin was presumably withheld in the complexes stabilised by increasing Ca^{2+}, instead of being centrifuged and discarded along with oversized aggregates. This accounted for the larger amounts of curcumin present in the centrifuged feed solutions at [Ca^{2+}]≥ 3 mM. Note that when the feed solutions were fully mixed with pure ethanol at a volume ratio of 1:9 and centrifuged, almost all of the curcumin was extracted into the ethanol-water supernatants, with negligible curcumin detected in the protein precipitates. This indicates that the curcumin in the ethanol-extractable form played a major role in the feed solution state, although Ca^{2+} could promote and stabilise the protein-curcumin-Ca^{2+} interaction.

After spray drying, the percentage of ethanol-extractable curcumin measured by immersing spray-dried particles in ethanol overnight, reduced to < 5% (**Table 4.1**). The curcumin in the complex form had a dominant role in the spray-dried state. The spray drying process promoted the complexation between curcumin and WPI, facilitating the production of water-soluble curcumin-WPI complexes. The phenomenon can be explained by the hydrophobic nature of curcumin. In the multicomponent evaporation of water-ethanol mixtures, due to the stronger evaporative nature of ethanol, it is well known that the mixture will experience a progressive enrichment of water throughout the evaporation process (Liu et al., 2008). In order to avoid the unfavourable interaction with water molecules, the ethanol-extractable curcumin previously existing in ethanol is driven by its hydrophobic forces, moving and inserting its phenyl moiety to the hydrophobic cores of WPI, which is an exothermic process (Sun et al., 2006).

The water molecules with high energy in the hydrophobic cores of proteins migrate to the bulk feed solution, also an exothermic process (Sun et al., 2005). The thermodynamic analysis of binding between curcumin and human serum albumin has been reported by Basu and Kumar (2014). Increasing negative values of the standard molar binding enthalpies from -3.73 $kJ \cdot mol^{-1}$ to -14.21 $kJ \cdot mol^{-1}$ were obtained with increasing temperature, indicating favourable exothermic interactions. Although the standard molar entropy decreased from 28.60 $kJ \cdot mol^{-1}$ to 16.29 $kJ \cdot mol^{-1}$, as the temperature increased, the compensation between the standard molar enthalpy and entropy renders the standard molar Gibbs free energy change negative and almost independent of temperature (Basu & Kumar, 2014). This binding phenomenon has been observed in many biomolecular processes (Paul & Kumar, 2013), indicating a significant hydrophobic contribution to the standard molar binding energies. Thus, the results confirmed that the complexation between WPI and curcumin by desolvation was retained and even enhanced by the drying process.

4.4.3 Functional properties of spray-dried complex microparticles

The size distribution and SEM images of each sample are present in **Table 4.1** and **Fig. 4.3**, respectively. Similar morphology and microstructure have been reported in our previous study (Ye et al., 2019). Generally, the microparticles exhibited spherical, wrinkled, and pot-like shape. The morphology of microparticles became more wrinkled once ethanol and calcium ions were introduced.

In the spray-dried state, the total curcumin contents of samples upon desolvation were up to 3.47 mg/g particle, approximately one order of magnitude higher than that of CW-0mMCa without desolvation (0.37 mg/g particle) (**Table 4.1**). Encapsulation efficiency increased from about 87% to 98% after desolvation. In **Fig. 4.4**, the desolvated CE-0mMCa without crosslinking exhibited good solubility in the SIF with trypsin within 15 min, indicating an improved bioaccessibility of the complex form compared with raw curcumin. CE-5mMCa with desolvation and crosslinking at $[Ca^{2+}]$ = 5 mM could be dispersed in the SIF, forming a curcumin-WPI complex suspension before digestion. After 3-hour incubation, curcumin was released to the SIF with trypsin in the form of soluble curcumin-protein complexes, generating a clear yellow

solution. The loading efficiency, encapsulation efficiency, solubility, and bioaccessibility of curcumin were largely enhanced in this study.

Note that after CE-0mMCa dissolved in the SIF in the complex form as shown in **Fig. 4.4**, the aqueous complexed curcumin still could be extracted into ethanol at a volume ratio of 1:9. This further implies the dominant role of the curcumin in the ethanol-extractable form in the binary system of water and ethanol.

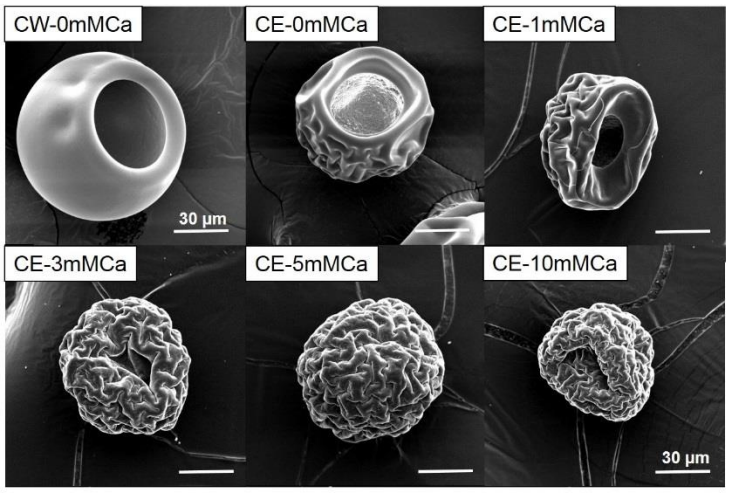

Fig. 4.3. SEM images of curcumin-WPI complex microparticles. CW-0mMCa prepared from pure water system and crosslinked at [Ca^{2+}] = 0 mM, CE-0mMCa from 30% v/v ethanol system at [Ca^{2+}] = 0 mM, CE-1mMCa from 30% v/v ethanol system at [Ca^{2+}] = 1 mM, CE-3mMCa from 30% v/v ethanol system at [Ca^{2+}] = 3 mM, CE-5mMCa from 30% v/v ethanol system at [Ca^{2+}] = 5 mM; CE-10mMCa from 30% v/v ethanol system [Ca^{2+}] = 10 mM (all the scale bars represent 30 µm).

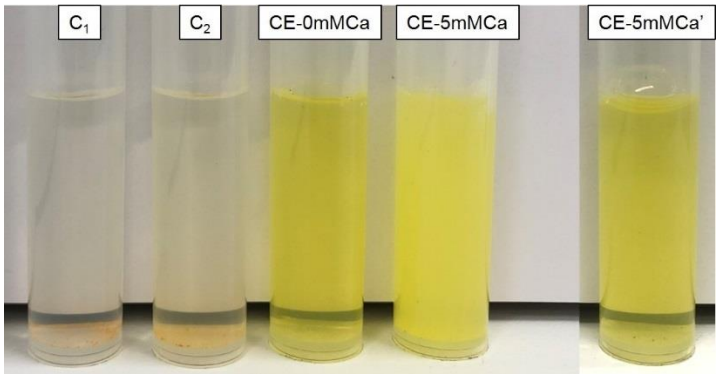

Fig. 4.4. Image of raw curcumin dispersed in water for 15 min (C_1), raw curcumin in the SIF with trypsin for 15 min (C_2), 10 mg/ml reconstituted CE-0mMCa in the SIF with trypsin for 15 min (CE-0mMCa), 10 mg/ml reconstituted CE-5mMCa in the SIF with

trypsin for 15 min (CE-5mMCa), 10 mg/ml reconstituted CE-5mMCa the SIF with trypsin after 3-hour digestion (CE-5mMCa').

4.4.4 Stability of spray-dried curcumin-WPI complex microparticles.

The maximum absorbance of curcumin occurs at a wavelength of 425 nm, designated as λ_{max}, due to the π-π* type excitation of the extended aromatic moiety (Wang et al., 2008). The relative intensity of the characteristic value λ_{max} as a function of time is used to investigate the stability of WPI-curcumin complexes and raw curcumin dispersed in various media separately at 37 °C. The media selected include the SGF at 1.2, SIF at 6.8, and PBS buffer at 7.3 without enzyme. **Fig. 4.5**(A) shows that raw curcumin was unstable at neutral and physiological pH values and degraded by over 60% within 30 min. Under acidic condition, the degradation percentage was also up to 20% after 30 min. By comparison, **Fig. 4.5**(B) shows that around 96%, 83%, 73% of curcumin was stable in the curcumin-WPI complex form in the SGF, SIF, and PBS buffer after 3 hours, respectively. This reveals that the generation of curcumin-WPI complexes effectively enhanced the stability of curcumin better than that of raw curcumin.

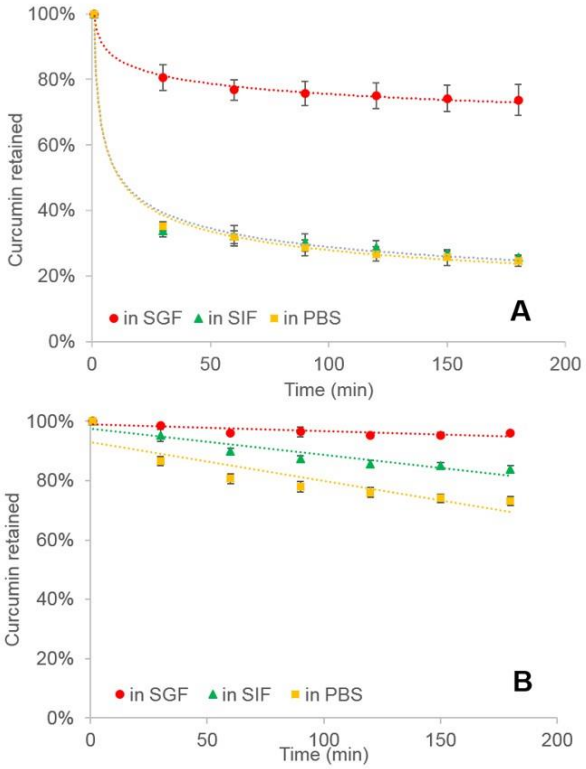

Fig. 4.5. Stability profile of (A) 8 µM raw curcumin and (B) 5 mg/ml CE-0mMCa prepared from 30% v/v ethanol at [Ca^{2+}] = 0 mM dispersed in different media as a function of time. (The SGF and SIF without enzyme)

4.4.5 DPPH scavenging activity of spray-dried curcumin-WPI microparticles.

The effect of spray drying on the properties of raw WPI and spray-dried curcumin-WPI complex microparticles was examined *via* DPPH radical scavenging assay (**Fig. 4.6**). The raw WPI alone was used as a control, exhibiting similar radical scavenging activity as previously reported (Liu et al., 2016). In order to reveal the effect of physiological condition and incubation time on curcumin degradation, the radical scavenging activities of samples were measured in various media. **Fig. 4.6**(A) demonstrates that the radical scavenging activity of the curcumin-WPI complexes in CE-0mMCa was retained after spray drying and was higher than raw WPI alone, due to the donation of hydrogen atoms from the curcumin loaded to radicals (Tapal & Tiku, 2012). A comparison of **Fig. 4.6**(A) and **Fig. 4.6**(B) reveals that when entering the small intestine and getting hydrolysed by trypsin, both raw WPI and the complex samples exhibited much higher DPPH radical scavenging activity than those in water

without enzymatic hydrolysis. This is presumably because some amino acid residues and N and C terminal extremities exposed during digestive proteolysis exhibit high DPPH scavenging effect (Laroque et al., 2008). The imidazole ring on histidine favours the DPPH radical scavenging activity, while tyrosine or tryptophan in N-terminal position exhibits stronger antioxidant activity (Laroque et al., 2008). In **Fig. 4.6**(B), the DPPH radical scavenging activity of raw WPI was approximately 4% higher than that of the complex samples. Similar inhibition of antioxidant activity was reported by Von Staszewski et al. (2011). Whey proteins have been shown to mask the DPPH radical scavenging activity of Argentinean green tea infusions. The extent of masking effect in each green tea variety was irrelevant to the total polyphenol content, but depended on the specific polyphenol composition of each variety (Von Staszewski et al., 2011), presumably due to covalent or non-covalent interactions between polyphenols and proteins (Ozdal et al., 2013). The DPPH radical scavenging activities of CE-0mMCa within short- and long-time incubation seemed to be unchanged in **Fig. 4.6**(B) and **4.6**(C). This might be due to the degradation products of curcumin at physiological conditions, identified as bicyclopentadiones, trans-6-(40-hydroxy-30-methoxyphenyl)-2,4-dioxo-5-hexenal, ferulic acid, feruloyl methane, ferulic aldehyde, vanillin, vanillic acid, *etc.* (Gordon & Schneider, 2012). Some of them such as vanillin and ferulic acid remain able to scavenge radicals (Gordon & Schneider, 2012), even though curcumin is degraded. Curcumin degradation resulting from long digestion time thus may have a minor influence on the DPPH scavenging activity of curcumin in the complex form. Even with similar amounts of curcumin (**Fig. 4.6**(C)), the radical scavenging activities of CE-5mMCa were lower than those of CE-0mMCa. This is possibly because curcumin was not fully released from CE-5mMCa within 3-hour digestion due to its strong crosslinking by calcium ions, which was confirmed by the results of *in vitro* release in the next section 4.4.6.

The SEM images and XRD analysis (**Fig. 4.7**) of raw curcumin indicate its high crystalline structure. Nevertheless, the characteristic peaks of curcumin could not be found in the complex microparticles in the dry state. The amorphous XRD pattern of these samples further demonstrates the generation of curcumin-WPI complexes upon spray drying. The amorphous structure of curcumin displays significant solubility and bioaccessibility advantages over its crystalline counterpart (Shin et al., 2016).

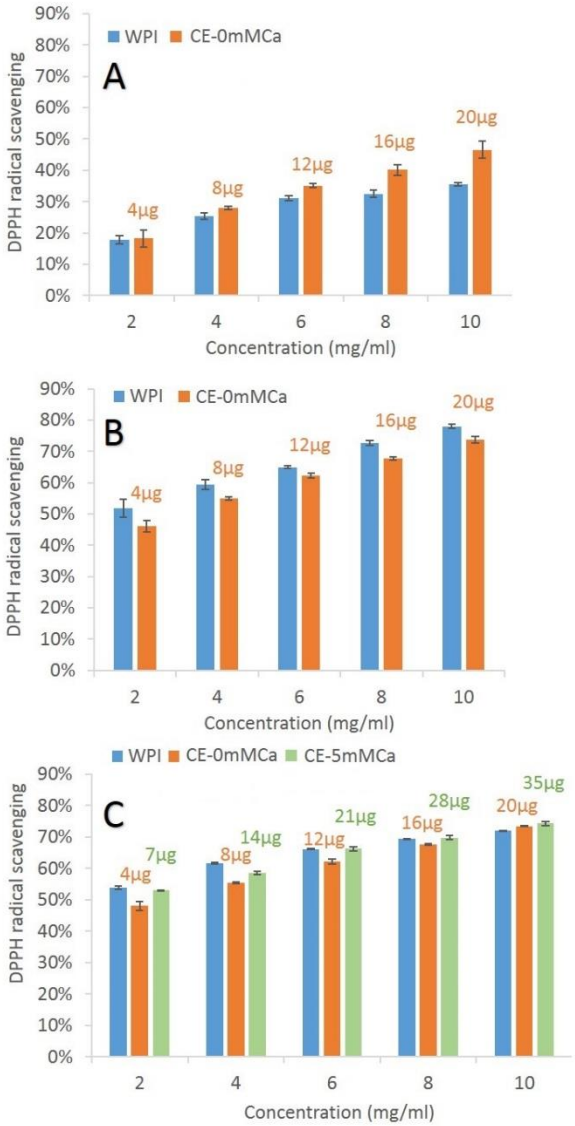

Fig. 4.6. DPPH free radical scavenging activity of WPI and spray-dried microparticles (CE-0mMCa or CE-5mMCa) at different concentrations, incubated (A) in water for 10 min; (B) in SIF with trypsin for 10 min; (C) in SIF with trypsin for 3 hours. (CE-0mMCa at $[Ca^{2+}]$ = 0 mM, CE-5mMCa at $[Ca^{2+}]$ = 5 mM from 30% v/v ethanol system; the numbers on top of each column represent the curcumin contents loaded in the samples at certain concentrations.)

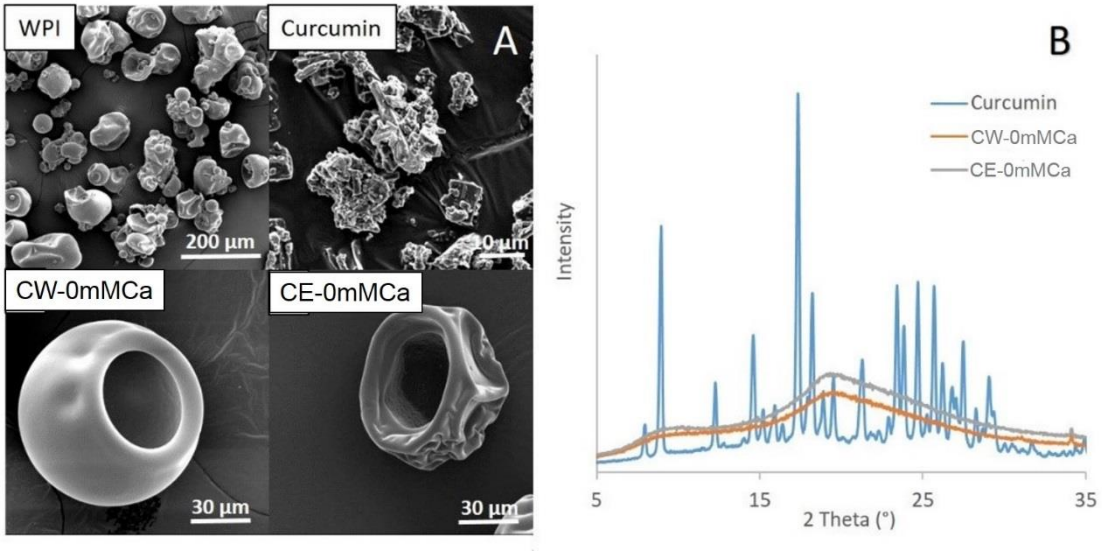

Fig. 4.7. (A) SEM images and (B) powder X-ray diffraction patterns of raw WPI powder, raw curcumin powder, CW-0mMCa produced from pure water system at [Ca^{2+}] = 0 mM, CE-0mMCa from 30% v/v ethanol system at [Ca^{2+}] = 0 mM.

4.4.6 *In vitro* release of curcumin with and without food matrix.

Fig. 4.8(A) displays the release profiles of curcumin from WPI-curcumin complex microparticles in the simulated GI tract without the effect of emulsifier or food matrix. The initial burst release of curcumin observed from CE-0mMCa to CE-10mMCa was from the fact that some of the core materials may be distributed to the surface of matrix-type microparticles (Bryant & McClements, 1998). CW-0mMCa without desolvation was not tested due to its extremely low loading efficiency of curcumin compared to other samples. In **Fig. 4.8**(A) (red line), over 60% of curcumin was released from CE-0mMCa in 15 min. This is because desolvation has been proven to improve the digestibility of WPI by shifting its secondary structure and exposing its cleavage sites for pepsin (Dalgalarrondo et al., 1995; Ye et al., 2019). With the increasing extent of calcium ion crosslinking, CE-3mMCa (yellow), CE-5mMCa (blue) and CE-10mMCa (green) showed prolonged and targeted release characteristics.

Sneharani et al. (2010) reported an exponential increase in the association constant of curcumin and β-lactoglobulin from 1.1×10^3 to 1.1×10^5 M^{-1}, when pH increased from 5.5 to 7.0 due to pH-dependent conformation change of protein molecules. Based on this observation, the WPI-curcumin complexes in this case should have a stronger binding affinity under the intestinal condition than that under the gastric condition. Only the curcumin complexed with WPI could be detected with

the fluorescence method in the *in vitro* release studies. The release percentages of curcumin in the soluble complex form, especially for CE-0mMCa and CE-1mMCa from 60 min to 120 min intestinal digestion, were reduced by more than 20% in **Fig. 4.8**(A). The stability test in section 4.4.4 shows that about 15% of the complexed curcumin degraded in the SIF after 2 hours. The reduction in the percentages of released curcumin was approximately 5% higher than expected. This indicates that in the absence of food matrix, the curcumin release was due to the predominant role of curcumin-WPI complex dissociation with protein structure breakdown by proteolysis as a function of time. The released curcumin should be in the ethanol-extractable form and thus water-insoluble, which could not be measured in an aqueous system without emulsifier such as Tween 80. Therefore, we conducted an additional study using a simulated GI fluid containing 0.05% wt Tween 80 to dissolve the curcumin released, as shown in **Fig. 4.8**(B). The general tendencies of release showed a similarity to those in the absence of Tween 80 although the corresponding curcumin contents released were comparatively larger. The release profile with Tween 80 was not a representative of *in vivo* digestion and release, but was used to demonstrate that the curcumin in the ethanol-extractable form was still being released from the complexed curcumin due to its dissociation during digestion.

We then incorporated the complex microparticles into a food matrix, yogurt in this case. Among these complex microparticles, CE-0mMCa representing rapid release and CE-5mMCa with targeted release were selected and mixed into a plain yogurt. The release profile of yogurt without complex microparticles was measured as a blank and subtracted from each measurement to eliminate the effect of yogurt. Raw curcumin of equal amount as entrapped in CE-0mMCa was incorporated into yogurt as control, in **Fig. 4.9**(C) (green line). Without the pre-complexation and pre-microencapsulation with WPI, only a trace amount of curcumin could be detected in the aqueous phase during gastric incubation even if emulsifiers and other dairy proteins were present in the yogurt. After 90 min, the percentage of curcumin measured slightly increased to 8%-9%, indicating the role of protein hydrolysates on complexation and dissolution of raw curcumin during digestion. This further suggests the importance of complexation between curcumin and WPI to enhance its bioaccessibility.

Fig. 4.9(A) and **4.9**(B) shows that in the absence of yogurt, more curcumin from the complex microparticles could be detected with the addition of Tween 80 as

emulsifier. Compared to them, **Fig. 4.9**(C) exhibits significantly lower release profiles of curcumin in early gastric digestion and higher release percentages in the intestinal condition, in the presence of yogurt. In the first half hour of gastric incubation, the curcumin released from CE-0mMCa decreased from about 61% (without emulsifier) and 78% (with emulsifier) to 30% (with yogurt). At the same time interval, the release reduction in CE-5mMCa was from around 18% (without emulsifier) and 25% (with emulsifier) to 9% (with yogurt). A possible reason is the exponential increase in association constant of β-lactoglobulin and curcumin with pH (Sneharani et al., 2010), causing more curcumin to be complexed, and thus soluble and detectable. Another reason is probably the proteins present in yogurt. The complex microparticles might be entrapped in the proteins of yogurt (3.0 g/ 100 g) so that protein digestion took place prior to the disintegration of microparticles (McClements et al., 2017). At the time slot of 60 min, **Fig. 4.9**(B) and **4.9**(C) display similar release percentages of curcumin. This indicates that the factors reducing curcumin release discussed above were overcome by the 1-hour gastric digestion. The bulk casein and whey protein hydrolysates in chyme after digestion may be able to bind to curcumin released, forming complexes (Pan et al., 2019; Sahu et al., 2008). In the intestinal condition, **Fig. 4.9**(C) exhibits relatively higher release percentages compared to **Fig. 4.9**(B). This could also be attributed to the emulsifiers and protein hydrolysates, which possibly accelerate microparticle disintegration and complex dissociation by generating competing binding with curcumin released. Overall, the incorporation of curcumin microparticles into yogurt did affect the release characteristics of curcumin. However, CE-0mMCa still showed its rapid release with approximately 87% curcumin discharged before entering the simulated intestinal condition, compared to 44% curcumin from CE-5mMCa with targeted-release formulation.

In future, the release characteristics of curcumin from complex microparticle-food matrix will be further studied using a near real dynamic *in vitro* human stomach system to look into the crucial microscopic processes in food digestion and nutrient release *e.g.,* gastric sieving, gastric emptying, and pH variation of digesta.

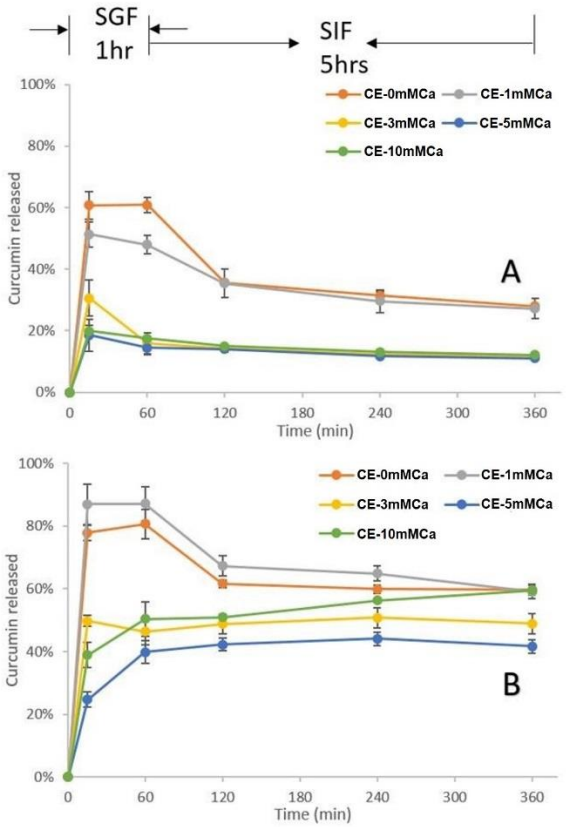

Fig. 4.8. Curcumin release profiles from the microparticles (A) without emulsifier; (B) with emulsifier, 0.05% wt Tween 80. (CE-0mMCa crosslinked at [Ca^{2+}] = 0 mM, CE-0mMCa at [Ca^{2+}] = 1 mM, CE-3mMCa at [Ca^{2+}] = 3 mM, CE-5mMCa at [Ca^{2+}] = 5 mM, and CE-10mMCa at [Ca^{2+}] = 10 mM prepared from 30% v/v ethanol system.)

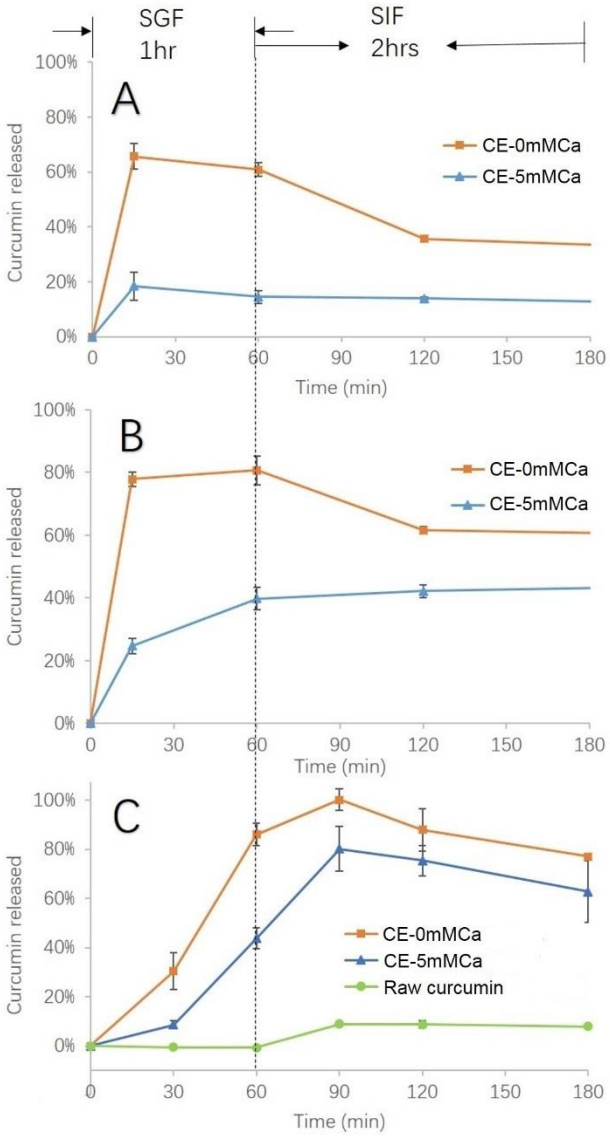

Fig. 4.9. Comparison of curcumin release profiles from the microparticles in simulated GI tract (A) without emulsifier; (B) with emulsifier, 0.05% wt Tween 80; (C) with food matrix *i.e.,* yogurt. (CE-0mMCa crosslinked at [Ca^{2+}] = 0 mM, and CE-5mMCa at [Ca^{2+}] = 5 mM from 30% v/v ethanol system.)

4.4.7 Sensory analysis and colour determination.

The sensory evaluation was conducted to investigate the effect of curcumin-WPI complex microparticles (food-grade CE-0mMCa and CE-5mMCa) on yogurt properties, including colour, mouthfeel, creaminess, sliminess, foreign particle, off flavour, bitterness, sourness, sweetness, curcumin flavour, after taste, and smell. The yogurt selected was a type of low-fat yogurt obtained from local market, whose ingredient list and nutrition information panel are present in section 4.3.4.

The change of appearance and hedonic sensory analysis are shown in **Fig. 4.10**. The detailed mean values of each characteristic trait of yogurts including statistical differences are summarised in **Table 4.4**. The appeal on colour was significantly higher for the white plain yogurt, compared to those of curcumin-enriched yogurts in light yellow, although yellow is generally considered to draw attention and activate the appetite for other types of food (Singh, 2006). Our panellists described the yellow colour as '*rare in yogurt*' and '*suspicious in yogurt*'. In the current market, the colour of mainstream yogurt products is white even for some products containing yellowish pulps such as passion fruit, banana, apricot, peach, and rhubarb. Thus, the overall yellow observed in our curcumin-enriched yogurts may be less acceptable. Additionally, the flavour of curcumin as a well-known spice was perceived and given a higher hedonic point in the two curcumin-enriched yogurts, no matter in the rapid release form (CE-0mMCa) or in the targeted release form (CE-5mMCa). This flavour presumably came from the surface distribution of curcumin in the matrix-type microparticles so that the Ca^{2+} crosslinking extent (rapid release in CE-0mMCa and prolonged release in CE-5mMCa) showed a minor influence on the characteristic trait. Another possible reason for the higher points was the cue of yellow colour of curcumin. Many studies have demonstrated people's belief on the relationship between colour and flavour on distinguishing food flavour (Spence et al., 2010). Therefore, the panellists might tend to give a higher point on curcumin flavour when seeing the yellow colour of the latter two yogurts. Furthermore, mouthfeel, foreign particle, bitterness, and sourness were scored slightly higher for the plain yogurt, but with no statistic significances between these three yogurt samples ($P < 0.05$), as shown in **Table 4.4**. The remaining six characteristic traits of yogurts received similar points with no statistical difference ($P < 0.05$). It reflected that the addition of curcumin-WPI complex microparticles only had a marginal impact on most of the yogurt properties, which could be due to the taste/smell masking effect of the wall material of WPI (Yang et al., 2012).

According to the results of colorimeter measurements as shown in **Table 4.5**, the lightness component from black to white (L^*) of three samples were close to each other. The negative shift of the a^* values indicates that the addition of CE-0mMCa and CE-5mMCa turned the yogurts slightly to green in the red-green dimension. The significantly positive shift of b^* values shows that the yogurts with complex microparticles appeared yellow in the yellow-blue dimension. The colour difference

which is visually detectable is referred to as perceptibility threshold, ranging from ΔE^* = 1.0 to 3.7 (Johnston & Kao, 1989; Kuehni & Marcus, 1979; Seghi et al., 1989). The colour difference forming an unacceptable alteration to aesthetics is known as acceptability threshold, from ΔE^* = 2.72 to 6.8 (Johnston & Kao, 1989; Ruyter et al., 1987). In this study, the colour differences between the plain yogurt and the curcumin-enriched yogurts were 10.90±0.01 (CE-0mMCa added) and 11.19±0.07 (CE-5mMCa added), much higher than the thresholds of perceptibility and acceptability. This indicates that the panellists enabled to distinguish the curcumin-enriched yogurt from the plain yogurt readily. Although there existed statistical differences in L^*, a^*, and b^* among the three yogurt samples ($P < 0.05$). The colour difference between the yogurt + CE-0mMCa and the yogurt + CE-5mMCa was 0.91±0.11, lower than the thresholds. It means that the panellists could hardly differentiate between two curcumin-enriched yogurts on colour. The results of colour difference perceptibility were consistent with the statistical differences observed on colour points scored in the sensory analysis, 7.6 ± 1.3^{a} (the plain yogurt), 5.5 ± 2.3^{b} (yogurt + CE-0mMCa), and 5.7 ± 2.4^{b} (yogurt + CE-5mMCa), in **Table 4.4**.

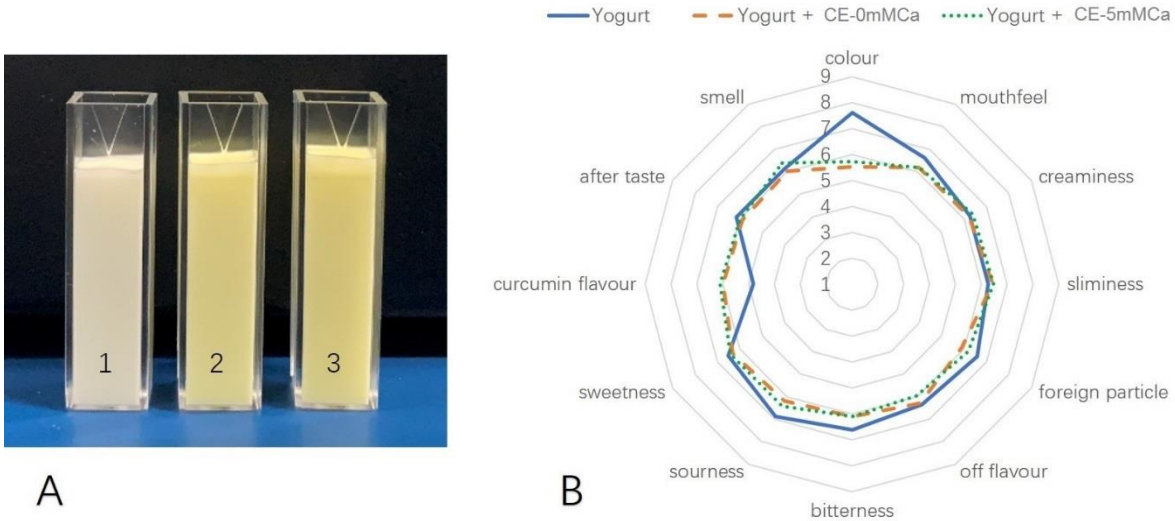

Fig. 4.10. (A) appearance change of (1) the plain yogurt, (2) the yogurt containing 8 mg/ml food-grade CE-0mMCa, and (3) the yogurt with 8 mg/ml food-grade CE-5mMCa; (B) hedonic sensory profile of three kinds of yogurts mentioned above. (The statistical differences and mean values of each sensory trait in **Fig. 4.10**(B) are summarised in **Table 4.4**.)

Table 4.4: Mean values of characteristic traits of three types of yogurts. [a-b] indicate that under the same letter, there exists no statistical significances calculated by Duncan's multiple range test ($P < 0.05$)

	Yogurt	Yogurt + CE-0mMCa	Yogurt + CE-5mMCa
Colour	7.6±1.3[a]	5.5±2.3[b]	5.7±2.4[b]
Mouthfeel	6.6±1.5[a]	6.2±1.7[a]	6.2±1.8[a]
Creaminess	6.3±1.8[a]	6.2±2.0[a]	6.4±1.8[a]
Sliminess	6.3±1.9[a]	6.4±1.7[a]	6.5±1.9[a]
Foreign particle	6.6±2.1[a]	5.9±1.9[a]	6.2±1.8[a]
Off flavour	6.4±2.0[a]	6.3±1.9[a]	6.0±2.1[a]
Bitterness	6.6±2.0[a]	6.1±1.9[a]	6.1±1.8[a]
Sourness	6.9±1.8[a]	6.2±1.8[a]	6.4±1.8[a]
Sweetness	6.5±2.0[a]	6.3±1.4[a]	6.4±1.6[a]
Curcumin flavour	4.8±2.3[b]	6.0±2.0[a]	6.1±1.5[a]
After Taste	6.2±1.7[a]	5.9±1.7[a]	6.0±1.4[a]
Smell	6.2±1.9[a]	6.0±1.6[a]	6.4±1.6[a]

Table 4.5: Colour parameters of the plain yogurt as control, the yogurt containing 8 mg/ml food-grade CE-0mMCa and the yogurt containing 8 mg/ml food-grade CE-5mMCa, under the same letter in the same row, there was no statistical significances at $P < 0.05$ (*ΔE*-1* and *ΔE*-2* represent the colour differences using the plain yogurt and the yogurt + CE-0mMCa as the control, respectively).

	Yogurt	Yogurt + CE-0mMCa	Yogurt + CE-5mMCa
*L**	64.52±0.07[c]	66.20±0.10[a]	65.39±0.06[b]
*a**	1.18±0.02[a]	-1.11±0.01[b]	-1.36±0.03[c]
*b**	0.59±0.01[c]	11.11±0.01[b]	11.45±0.08[a]
ΔE-1*	As control	10.90±0.01	11.19±0.07
ΔE-2*	/	As control	0.91±0.11

4.5 Conclusion

The complexation between WPI and curcumin upon desolvation was retained and enhanced *via* spray drying to produce microparticles. Upon desolvation, the maximum total curcumin content loaded was up to around 3.47 mg/g particle, almost one order

of magnitude higher that of the sample without desolvation. The spray-dried complex microparticles possessed better solubility and stability at physiological conditions compared to curcumin alone, enhancing the bioaccessibility. The radical scavenging property of curcumin was not affected by heat and was retained in the form of spray-dried complex microparticles. The incorporation of complex microparticles into yogurt influenced their release profiles. But to some extent, the microparticles still retained their respective release characteristics (rapid and targeted formulations). The addition of complex microparticles into yogurt had negligible effects on the sensory properties of yogurt, except for colour and curcumin flavour. This strategy has the potential to incorporate bioactive small molecule ingredients with hydrophobicity and low bioaccessibility into foods with negligible adverse effects on consumer acceptance.

4.6 Reference

Anitha, A., Deepagan, V. G., Divya Rani, V. V., Menon, D., Nair, S. V., & Jayakumar, R. (2011). Preparation, characterization, in vitro drug release and biological studies of curcumin loaded dextran sulphate–chitosan nanoparticles. *Carbohydrate polymers, 84*(3), 1158-1164.

Aziz, H. A., Peh, K. K., & Tan, Y. T. F. (2007). Solubility of core materials in aqueous polymeric solution effect on microencapsulation of curcumin. *Drug development and industrial pharmacy, 33*(11), 1263-1272.

Basu, A., & Kumar, G. S. (2014). Elucidating the energetics of the interaction of non-toxic dietary pigment curcumin with human serum albumin: A calorimetric study. *The Journal of Chemical Thermodynamics, 70*, 176-181.

Bryant, C. M., & McClements, D. J. (1998). Molecular basis of protein functionality with special consideration of cold-set gels derived from heat-denatured whey. *Trends in Food Science & Technology, 9*(4), 143-151.

Carnovale, V., Britten, M., Couillard, C., & Bazinet, L. (2015). Impact of calcium on the interactions between epigallocatechin-3-gallate and β-lactoglobulin. *Food research international, 77*(P3), 565-571.

Dalgalarrondo, M., Dufour, E., Chobert, J.-M., Bertrand-Harb, C., & Haertlé, T. (1995, 1995/01/01/). Proteolysis of β-lactoglobulin and β-casein by pepsin in ethanolic media. *International dairy journal, 5*(1), 1-14.

de l'Eclairage, C. I. (1978). Recommendations on uniform color spaces, color-difference equations, psychometric color terms. *Paris: CIE*.

Duncan, D. B. (1955). Multiple Range and Multiple F Tests. *Biometrics, 11*(1), 1-42.

Frederix, F., Friedt, J.-M., Choi, K.-H., Laureyn, W., Campitelli, A., Mondelaers, D., Maes, G., & Borghs, G. (2003). Biosensing based on light absorption of nanoscaled gold and silver particles. *Analytical Chemistry, 75*(24), 6894-6900.

Gordon, O. N., & Schneider, C. (2012). Vanillin and ferulic acid: not the major degradation products of curcumin. *Trends in molecular medicine, 18*(7), 361-363.

Guo, Q., Su, J., Xie, W., Tu, X., Yuan, F., Mao, L., & Gao, Y. (2020). Curcumin-loaded pea protein isolate-high methoxyl pectin complexes induced by calcium ions: Characterization, stability and in vitro digestibility. *Food hydrocolloids, 98*.

Johnston, W., & Kao, E. (1989). Assessment of appearance match by visual observation and clinical colorimetry. *Journal of dental research, 68*(5), 819-822.

Kanakis, C. D., Hasni, I., Bourassa, P., Tarantilis, P. A., Polissiou, M. G., & Tajmir-Riahi, H.-A. (2011). Milk β-lactoglobulin complexes with tea polyphenols. *Food chemistry, 127*(3), 1046-1055.

Kaspchak, E., Goedert, A. C., Igarashi-Mafra, L., & Mafra, M. R. (2019). Effect of divalent cations on bovine serum albumin (BSA) and tannic acid interaction and its influence on turbidity and in vitro protein digestibility. *International journal of biological macromolecules, 136*, 486-492.

Khan, M. A., Zafaryab, M., Mehdi, S. H., Ahmad, I., & Rizvi, M. M. A. (2016). Characterization and anti-proliferative activity of curcumin loaded chitosan nanoparticles in cervical cancer. *International journal of biological macromolecules, 93*, 242-253.

Kuehni, R. G., & Marcus, R. T. (1979). An Experiment in Visual Scaling of Small Color Differences*. *Color Research & Application, 4*(2), 83-91.

Laroque, D., Chabeaud, & Guérard, F. (2008). Antioxidant capacity of marine protein hydrolysates. In (pp. 147-162).

Liang, L., Tajmir-Riahi, H., & Subirade, M. (2007). Interaction of β-lactoglobulin with resveratrol and its biological implications. *Biomacromolecules, 9*(1), 50-56.

Liu, C., Bonaccurso, E., & Butt, H.-J. (2008). Evaporation of sessile water/ethanol drops in a controlled environment. *Physical Chemistry Chemical Physics, 10*(47), 7150-7157.

Liu, W., Chen, X. D., Cheng, Z., & Selomulya, C. (2016). On enhancing the solubility of curcumin by microencapsulation in whey protein isolate via spray drying. *Journal of Food Engineering, 169*, 189-195.

McClements, D. J., Xiao, H., & Demokritou, P. (2017). Physicochemical and colloidal aspects of food matrix effects on gastrointestinal fate of ingested inorganic nanoparticles. *Advances in Colloid and Interface Science, 246*, 165-180.

Minekus, M., Alminger, M., Alvito, P., Ballance, S., Bohn, T., Bourlieu, C., Carrire, F., Boutrou, R., Corredig, M., Dupont, D., Dufour, C., Egger, L., Golding, M., Karakaya, S., Kirkhus, B., Le Feunteun, S., Lesmes, U., Macierzanka, A., Mackie, A., Marze, S., McClements, D. J., Mnard, O., Recio, I., Santos, C. N., Singh, R. P., Vegarud, G. E., Wickham, M. S. J., Weitschies, W., & Brodkorb, A. (2014). A standardised static in vitro digestion method suitable for food an international consensus. *Food Funct., 5*(6), 1113-1124.

Onoue, S., Takahashi, H., Kawabata, Y., Seto, Y., Hatanaka, J., Timmermann, B., & Yamada, S. (2010). Formulation design and photochemical studies on nanocrystal solid dispersion of curcumin with improved oral bioavailability. *Journal of pharmaceutical sciences, 99*(4), 1871-1881.

Ozdal, T., Capanoglu, E., & Altay, F. (2013). A review on protein–phenolic interactions and associated changes. *Food research international, 51*(2), 954-970.

Pan, K., Zhong, Q., & Baek, S. J. (2013, 2013/06/26). Enhanced Dispersibility and Bioactivity of Curcumin by Encapsulation in Casein Nanocapsules. *Journal of Agricultural and Food Chemistry, 61*(25), 6036-6043.

Pan, Y., Xie, Q.-T., Zhu, J., Li, X.-M., Meng, R., Zhang, B., Chen, H.-Q., & Jin, Z.-Y. (2019). Study on the fabrication and in vitro digestion behavior of curcumin-loaded emulsions stabilized by succinylated whey protein hydrolysates. *Food chemistry, 287*, 76-84.

Patel, A., Hu, Y., Tiwari, J. K., & Velikov, K. P. (2010). Synthesis and characterisation of zein–curcumin colloidal particles. *Soft Matter, 6*(24), 6192-6199.

Paul, P., & Kumar, G. S. (2013). Thermodynamics of the DNA binding of phenothiazinium dyes toluidine blue O, azure A and azure B. *The Journal of Chemical Thermodynamics, 64*, 50-57.

Rognlien, M., Duncan, S., O'Keefe, S., & Eigel, W. (2012). Consumer perception and sensory effect of oxidation in savory-flavored yogurt enriched with n-3 lipids. *Journal of dairy science, 95*(4), 1690-1698.

Ruyter, I. E., Nilner, K., & Möller, B. (1987). Color stability of dental composite resin materials for crown and bridge veneers. *Dental Materials, 3*(5), 246-251.

Sahu, A., Kasoju, N., & Bora, U. (2008, 2008/10/13). Fluorescence Study of the Curcumin−Casein Micelle Complexation and Its Application as a Drug Nanocarrier to Cancer Cells. *Biomacromolecules, 9*(10), 2905-2912.

Seghi, R. R., Hewlett, E., & Kim, J. (1989). Visual and instrumental colorimetric assessments of small color differences on translucent dental porcelain. *Journal of dental research, 68*(12), 1760-1764.

Shin, G. H., Li, J., Cho, J. H., Kim, J. T., & Park, H. J. (2016). Enhancement of Curcumin Solubility by Phase Change from Crystalline to Amorphous in Cur‐TPGS Nanosuspension. *Journal of food science, 81*(2), N494-N501.

Singh, S. (2006). Impact of color on marketing. *Management decision*.

Sneharani, A. H., Karakkat, J. V., Singh, S. A., & Rao, A. A. (2010). Interaction of curcumin with β-lactoglobulin stability, spectroscopic analysis, and molecular modeling of the complex. *Journal of Agricultural and Food Chemistry, 58*(20), 11130-11139.

Spence, C., Levitan, C., Shankar, M., & Zampini, M. (2010). Does Food Color Influence Taste and Flavor Perception in Humans? *Chemosensory Perception, 3*(1), 68-84.

Sun, D.-Z., Li, L., Qiu, X.-M., Liu, F., & Yin, B.-L. (2006). Isothermal titration calorimetry and 1H NMR studies on host–guest interaction of paeonol and two of its isomers with β-cyclodextrin. *International journal of pharmaceutics, 316*(1-2), 7-13.

Sun, D.-Z., Wang, S.-B., Song, M.-Z., Wei, X.-L., & Yin, B.-L. (2005). A microcalorimetric study of host–guest complexes of α-cyclodextrin with alkyl trimethyl ammonium bromides in aqueous solutions. *Journal of solution chemistry, 34*(6), 701-712.

Tapal, A., & Tiku, P. K. (2012). Complexation of curcumin with soy protein isolate and its implications on solubility and stability of curcumin. *Food chemistry, 130*(4), 960-965.

Von Staszewski, M., Pilosof, A. M. R., & Jagus, R. J. (2011). Antioxidant and antimicrobial performance of different Argentinean green tea varieties as affected by whey proteins. *Food chemistry, 125*(1), 186-192.

Wang, X., Jiang, Y., Wang, Y.-W., Huang, M.-T., Ho, C.-T., & Huang, Q. (2008). Enhancing anti-inflammation activity of curcumin through O/W nanoemulsions. *Food chemistry, 108*(2), 419-424.

Yang, S., Mao, X.-Y., Li, F.-F., Zhang, D., Leng, X.-J., Ren, F.-Z., & Teng, G.-X. (2012). The improving effect of spray-drying encapsulation process on the bitter taste and stability of whey protein hydrolysate. *European Food Research and Technology, 235*(1), 91-97.

Yao, K., Chen, W., Song, F., McClements, D. J., & Hu, K. (2018). Tailoring zein nanoparticle functionality using biopolymer coatings: Impact on curcumin bioaccessibility and antioxidant capacity under simulated gastrointestinal conditions. *Food hydrocolloids, 79*, 262-272.

Ye, Q., Woo, M. W., & Selomulya, C. (2019). Modification of molecular conformation of spray-dried whey protein microparticles improving digestibility and release characteristics. *Food Chemistry, 280*, 255-261.

Chapter 5

Digestion of curcumin-fortified yogurt in before/after-meal states: A study using a near-real dynamic *in vitro* human stomach

The previous chapter has demonstrated that after incorporating curcumin-whey protein isolate microparticles with targeted-release formula in yogurt, 80% of curcumin was released at 90 min using the INFOGEST static protocol. However, upon yogurt ingestion, *in vivo* gastric emptying and secretion are largely dependent on ingestion pattern. Therefore, in this chapter, a near-real dynamic *in vitro* human stomach (DIVHS), simulating the anatomical structures, peristalsis, and biochemical environments of a human stomach, was applied to reproduce the *in vivo* gastric and duodenal conditions in before/after-meal states. This project aimed to study the possible mechanisms for controlling the release of curcumin from yogurt, by utilising the dynamic *in vitro* digestion system that closely mimics the behaviour *in vivo*.

5.1 Abstract

A dynamic *in vitro* human stomach (DIVHS), simulating the anatomical structures, peristalsis, and biochemical environments of a real stomach as practically as possible, was applied to mimic the gastric processes (emptying and pH changes) during yogurt digestion in before/after-meal states. The influences of peristalsis, dilution, and proteolysis on digesta viscosity were quantified respectively, indicating the dominant role of proteolysis and dilution. After incorporating curcumin-whey protein microparticles with targeted-release formula in yogurt, the curcumin release during intestinal digestion reached a maximum of 43% at 120 min in the before-meal state and 16% at 180 min in the after-meal state. The change in the maximum curcumin release was dependent on the different gastric emptying kinetics in the two states. This emptying-kinetics dependence was reflected by the slower microparticle disintegration and proteolysis in the after-meal state. The dynamic reproduction of realistic gastric conditions using DIVHS is helpful in understanding controlled release from foods.

Keywords: yogurt; gastric emptying; ingestion pattern; *in vitro* gastric model; digesta rheology; release characteristics

5.2 Introduction

Curcumin is a lipid-soluble bioactive ingredient with low aqueous solubility, chemical instability, and poor bioavailability. Previously we have reported the preparation of curcumin-whey protein isolate (WPI) complex microparticles with improved water solubility, stability, bioaccessibility and adjustable release profiles (Ye et al., 2020). After incorporating these microparticles into a food matrix (yogurt), the yogurt fortified with rapid-release curcumin-WPI microparticles discharged approximately 87% curcumin, while the targeted-release formula only liberated 44% curcumin in 1-hour simulated gastric digestion, using the standard INFOGEST protocol (Minekus et al., 2014). This standardised method allows consistent laboratory-to-laboratory comparisons. However, gastric secretion rate is constantly changing and depends on digestion time, ingestion patterns (before/with/after-meal), food properties (*e.g.,* pH, osmolality, nutrient density, buffering capacity, and solid-liquid or homogenised meal) and others (Keszthelyi et al., 2013; Malagelada et al., 1979). Hence, instead of a constant pH 3 during gastric incubation as used in the protocol, the stomach pH varies from <2 up to 6 with foodstuffs entering the stomach and leaving for the duodenum (Malagelada et al., 1979). A gastric transit time of two hours is predominantly employed by *in vitro* digestion methods. In the case of yogurt, its gastric emptying half-time varies from 15 min to 86 min in humans, depending on the intake volume, viscosity, nutrient density, and ingestion patterns (Berrada et al., 1991; Keszthelyi et al., 2013; Porkka et al., 1988). The *in vivo* study of the effect of gastric emptying on food/drug disintegration and active ingredient release is challenging on human subjects due to the application of invasive procedures like feeding tube insertion (Berrada et al., 1991) or by using sophisticated tracer techniques like scintigraphy monitored using a gamma camera (Porkka et al., 1988). Using a dynamic gastric model before any *in vivo* studies will be beneficial to first evaluate this physiological process. The dynamic stomach should be able to accurately reproduce the *in vivo* digestive parameters (*e.g.,* gastric secretion, emptying, and peristalsis) of different food/drug matrices in various ingestion patterns.

To achieve this case-by-case simulation, numerous dynamic human digestion models have been created. Some of them concentrate on mimicking the chemical environments and physical behaviours present in the GI tract, including the TNO's GI

model (TIM-1) (Minekus et al., 1995), the dynamic gastric model (DGM) (Mercuri et al., 2008), the human gastric simulator (HGS) (Kong & Singh, 2010), and the human gastric digestion simulator (GDS) (Kozu et al., 2014). Besides the simulation of these physicochemical conditions, several dynamic digestion models further imitate the anatomical and inner wrinkled structures of the human stomach, such as the rope-driven *in vitro* human stomach (RD-IV-HSM) (Chen et al., 2016), and the near real dynamic *in vitro* human stomach (DIVHS) (Wang et al., 2019). The DIVHS in particular can simulate the peristaltic waves moving chyme toward the pylorus and small intestine using a separate roller-eccentric wheel subsystem. When beef stew mixed with orange juice was consumed, the DIVHS could reproduce the actual gastric pH variation, emptying and sieving effect, and particle disintegration (Wang et al., 2019).

In this study, the DIVHS was firstly applied to match the gastric emptying and pH changes of yogurt in before- and after-meal states present *in vivo* (Jerry et al., 2002; Keszthelyi et al., 2013). The effects of gastric peristalsis, digestive juice dilution, and acid and enzymatic hydrolysis on digesta were evaluated by monitoring the rheological properties in different ingestion patterns (before and after meal) and digestion phases (gastric and duodenal phases). The yogurts fortified with the WPI-curcumin microparticles mentioned above in different release formulae were consumed in before- and after-meal states under respective physiological conditions reproduced by the DIVHS. By comparing the curcumin release profiles obtained in the DIVHS with those in the INFOGEST protocol, the release process is thought to be dependent on gastric emptying. The chyme morphology, microparticle disintegration, and curcumin distribution in both states were evaluated by optical, fluorescence, and scanning electron microscopy (SEM). The proteolysis pattern and hydrolysis degree were monitored using sodium dodecyl sulphate–polyacrylamide gel electrophoresis (SDS-PAGE). The aim of this study was to explore the mechanisms for controlling the release of curcumin from yogurt, by utilising the dynamic *in vitro* digestion system that closely mimics the behaviour *in vivo*. This helps revealing more realistically the mechanisms of the release process.

5.3 Materials and methods

5.3.1 Materials

5.3.1.1 Chemicals

Whey protein isolate (WPI) (≥ 90% w/w whey protein) was purchased from Premium Powders, Marayong, Australia. Curcumin (≥ 94% curcuminoid content, ≥ 80% curcumin) was from Sigma-Aldrich, St Louis, USA. Absolute ethanol 99.5% was obtained from Univar, Germany. Calcium chloride was from Merck, Germany. Milli-Q water was collected from a Millipore system (18.2 MΩ cm^{-1} at 25°C).

The standard INFOGEST protocol followed for the preparation of Simulated Gastric Fluid (SGF) and Simulated Intestinal Fluid (SIF) was as described by Minekus et al. (2014). Electrolyte stock solutions were made up of $MgCl_2(H_2O)_6$ (0.15 mol/l), $(NH_4)_2CO_3$ (0.5 mol/l), $NaHCO_3$ (1 mol/l), NaCl (2 mol/l), KCl (0.5 mol/l), and KH_2PO_4 (0.5 mol/l). The SGF was prepared with the electrolyte stock solutions (160 ml), 0.3 M $CaCl_2$ (0.1 ml), Milli-Q water (39.9 ml), and pepsin with a final enzyme activity of 4000 units/ml (from porcine gastric mucosa powder, ≥ 400 units/mg protein), with a pH of 1.6 ± 0.1 acidified using 6 M HCl. The SIF contained the electrolyte stock solutions (320 ml), 0.3 M $CaCl_2$ (0.8 ml), Milli-Q water (79.2 ml), bile salts (10 mM), and pancreatin with a trypsin activity of 200 units/ml (from porcine pancreas, 8 x USP specifications), with pH of 7.0 ± 0.1 adjusted with 6 M HCl. The activities of pepsin and trypsin in the SGF and SIF prepared were twice of the values suggested by the standard INFOGEST protocol (Minekus et al., 2014), since they would be roughly diluted with yogurt in a ratio of 50: 50 (v/v) during digestion. Bile salts, pepsin, and pancreatin mentioned above were from Sigma-Aldrich, St Louis, USA.

5.3.1.2 Preparation of two types of WPI-curcumin complex microparticles

The fabrication and properties of the WPI-curcumin complex microparticles were reported in our previous study (Ye et al., 2020). The complex microparticles were prepared from a 30% v/v ethanol aqueous feed solution containing 5% w/v WPI and 125 µg/ml curcumin at 0 mM Ca^{2+} or 5 mM Ca^{2+}, centrifuged at 269 x g for 10 min to discard any deposited curcumin and WPI aggregates. A triple nozzle micro-fluidic-jet spray dryer (MFJSD) from Nantong Dong Concept New Material Technology Ltd.,

Nantong, China, was applied to prepare the microparticles. The inlet and outlet temperatures were maintained at 190 °C and 90 °C, respectively. Without food matrix incorporation, the complex microparticles without crosslinking could release fourfold more curcumin (~61%) than those crosslinked at 5 mM Ca^{2+} (~15%) after 1-hour *in vitro* gastric digestion (Ye et al., 2020). Hence, the former was referred to as the rapid-release microparticles and the latter one was the targeted-release formula.

5.3.2 The DIVHS development

In **Fig. 5.1**, the DIVHS is a new type of GI model, which can simulate the anatomical features, peristalsis, and biochemical conditions present in the real human stomach and duodenum (Wang et al., 2019). A J-shaped stomach model with analogous dimension, morphology, and inner wrinkled structures to the *in vivo* observations (Chen et al., 2016; DeSesso & Jacobson, 2001) is fabricated with silicone material (Dragon Skin® 10 FAST, Smooth-on, USA) aided by 3D-printing technology. This endows the stomach with water insolubility, resistance to acid and base, high elasticity, tensile strength, and non-stickiness. A silicone duodenum model is connected to the pylorus on the stomach, with a length of approximately 25 cm and an inner diameter of 20 cm as reported *in vivo* (DeSesso & Jacobson, 2001). A combination of eccentric wheels and rollers, pyloric extrusion plates, motors, belts, and pulley systems makes up the electromechanical driving instrument. The eccentric wheels and rollers roll down periodically, providing peristaltic contractions to the proximal stomach (gastric body) and the distal part of the stomach (gastric antrum). The latter one would undergo a higher contractive force in the range of 5134 to 67292 $N \cdot m^2$ (Wang et al., 2019) to simulate the *in vivo* “antral contraction”, which is crucial for gastric disintegration of foods by grinding, rubbing, and emulsification with digestive juices (Schulze, 2006). The antral contraction is accompanied by an open pylorus aperture, which is reproduced in the DIVHS by varying the gap between the fixed support plate and the pylorus extrusion plate periodically. During this partial opening of pylorus, food particles of > 2 mm in size would be retained in the stomach for further digestion and the smaller chyme can enter the duodenum, known as the “sieving effect” (Schulze, 2006). Apart from the gastroduodenal pressure generated by the peristaltic contractions, an auxiliary emptying device is installed to regulate the gastric emptying by tuning its tilting angle ranging from −45° to +45° (“−” and “+” mean anticlockwise

and clockwise rotation, respectively). The clockwise rotation can cause chyme stasis throughout the stomach model with gravity, whereas the anticlockwise rotation accelerates the gastric emptying by redistributing the digesta to the distal part of the stomach close to the pylorus.

Additionally, a transparent acrylic plate is anchored onto the fixed plate to steady the stomach model during run time. The SGF and SIF are kept at 37 °C in a water bath and then pumped into the stomach and duodenum model at controlled rates using two peristaltic pumps (YZ2515X, Baoding Longer, China), separately. An acrylic box heated with an electric lamp is used to keep the inner temperature around 37 °C. This isothermal process is achieved using a thermocouple combined with an intelligent temperature controller.

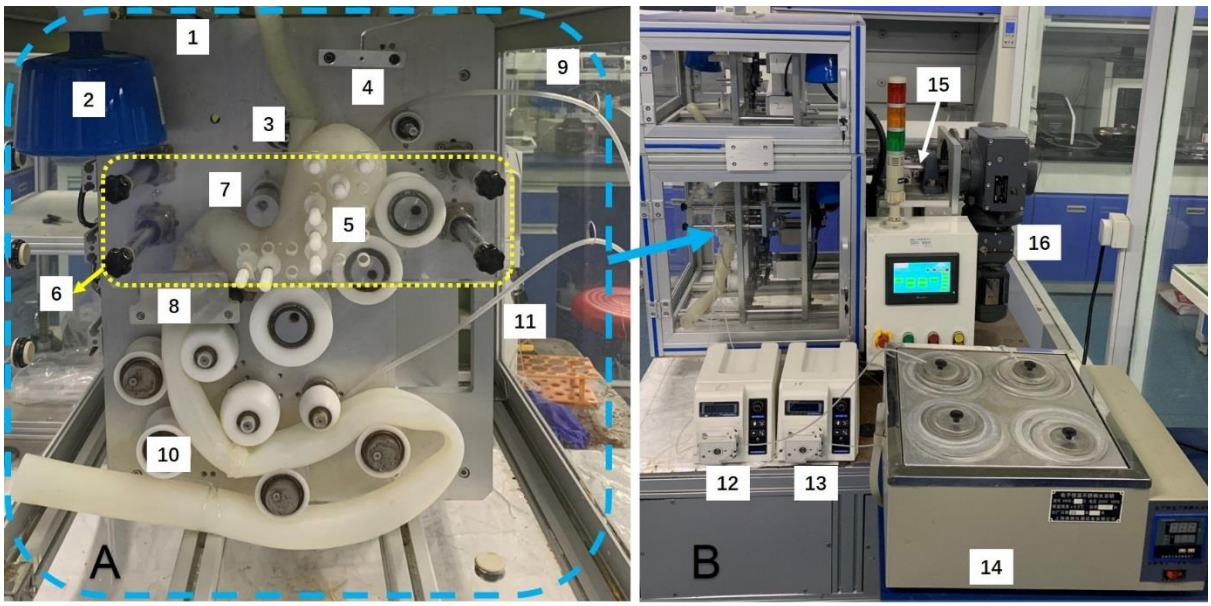

Fig. 5.1. Image of the DIVHS. (A) 1: fixed plate; 2: heat preservation lamp; 3: oesophagus model; 4: thermal sensor; 5: 3D-printed soft-elastic human stomach model; 6: transparent acrylic plate (yellow dashed box); 7: roller/eccentric wheel; 8: pylorus extrusion plate; 9: SGF secretion tube; 10: duodenum model; 11: SIF secretion tube. (B): the whole stomach system in the blue dashed box in (A) is installed in the metal/glass box in (B) as indicated by the blue arrow; (12) peristalsis pump used for pumping the SGF; (13) peristalsis pump for the SIF; (14) water bath for warming the simulated digestive fluids; (15) auxiliary emptying device; (16) motor.

5.3.3 *In vitro* digestion of yogurt in the DIVHS

5.3.3.1 Gastric emptying in before- and after-meal states in the DIVHS

Keszthelyi et al. (2013) has reported the gastric emptying characteristics of a plant sterol–containing yogurt drink (100 ml, 52 kcal, labelled with 1000 mg acetaminophen) consumed by 12 healthy male subjects, at 45 min before (test condition A), and 45 min after (test condition B) ingestion of a 500 g macaroni meal. The test condition A and B were called “in the before-meal state” and “in the after-meal state”, respectively. The *in vivo* gastric emptying of yogurt was derived from plasma acetaminophen concentrations by collecting venous blood (Keszthelyi et al., 2013). However, the macaroni meal was not labelled, causing a lack of *in vivo* gastric emptying data of the meal and that no solid foods were loaded into the DIVHS in this study. The macaroni meal had a minor effect of on the gastric emptying of the yogurt in the before-meal state since over 80% of yogurt had passed into the duodenum before 45 min (Keszthelyi et al., 2013). Marciani et al. (2013) reported that a 560 g rice pudding meal containing around 2250 kJ was consumed by human volunteers. More than 80% of chyme remained in the stomach after 45-min digestion, suggesting the potential influence of the residual gastric contents from the macaroni meal on the yogurt emptying at that time point. Hence, in the absence of solid meal ingested, the emptying process of yogurt in the after-meal state was achieved with the peristalsis and pyloric valve.

Gastric emptying is controlled by the nutrient density (total kcal / total grams or millilitres) of ingested foodstuffs entering the duodenum (Hunt & Stubbs, 1975). Therefore, the nutrient density of the yogurt we selected in this study was 47 kcal/100 ml, similar to the one used in the *in vivo* digestion (52 kcal/100ml). It was a plain low-fat yogurt from Beijing Hongda Dairy Co., Ltd (China), containing cow milk ≥90%, whey protein powder, additives (gelatin, aspartame, acetylated distarch phosphate, phenylalanine, acesulfame potassium), *Streptococcus thermophilus*, *Lactobacillus bulgaricus*, and sucrose ≤ 0.5 g/100g. The nutrition facts indicate that there are 197 kJ of energy, 3.0 g of protein, 6.0 g of carbohydrate, 1.2 g of fat, 60 mg of sodium, and 100 mg of calcium per 100 g of yogurt. The fabrication of microparticles has been presented in section 5.3.1.2 The curcumin-fortified yogurts were prepared by incorporating the complex microparticles into the original yogurt, under magnetic

stirring at 600 rpm overnight at 4°C, and storage at 4°C. The resulting two yogurts were referred to as RR-yogurt with 8 mg/ml rapid-release microparticles without crosslinking and TR-yogurt with 4.5 mg/ml targeted-release samples crosslinked at [Ca^{2+}]= 5 mM. Both of them contained 1.6 mg curcumin per 100 ml yogurt. These two types of yogurts were considered to have almost the same nutrient density as the original one, due to the low doses of microparticles added. Consequently, the original yogurt, RR-yogurt, and TR-yogurt should theoretically possess the analogous gastric emptying.

According to Keszthelyi et al. (2013), the 100 ml yogurt showed a steep *in vivo* emptying curve and a short half-time about 15 min in the fasting state. The emptying became remarkably slower in the postprandial state, leading to a half-time up to 42± 25 min. In this study, the *in vitro* digestion of our original yogurt, RR-yogurt, and TR-yogurt was conducted using the DIVHS to reproduce the *in vivo* gastric emptying data mentioned above. Simulated saliva fluids were not introduced since not much lubrication and mastication are required in drinking yogurt. Then, 100 ml of the yogurts (103 g) were delivered into the silicone stomach model in 1.5 min, equivalent to a drinking rate around 67 ml/min to simulate the yogurt ingestion by humans (Porkka et al., 1988). Note that our human stomach model was downscaled with a maximal internal volume of 400 ml, smaller than a full adult stomach dilating up to 1500 ml due to the limited expansion property of the silicone rubber used. Therefore, the volume of SGF pumped into the empty stomach was reduced to 10 ml in the before-meal state (Camilleri, 2006), whereas no SGF was injected before the yogurt loading in the after-meal state. The total volume of SGF which would be injected during the gastric digestion equalled to that of the yogurt *i.e.,* 100 ml, as suggested by the INFOGEST protocol (Minekus et al., 2014). The overall tendency of the secretion patterns in the two state was derived from the *in vivo* study by Malagelada et al. (1979). Sauter et al. (2012) have reported that the food emptied could induce about 61% of the release of gastric secretion by volume. Therefore, the differences in the secretion patterns between the two states were set according to the *in vivo* gastric emptying curves of the yogurt in each state (Keszthelyi et al., 2013), with an average value of 1.1 ml/min in the before-meal state and 0.7 ml/min in the after-meal state (**Fig. 5.2**). After the 100 ml of yogurt ingested, the electromechanical instrument was controlled to bring three contractions per minute to the stomach model according to the *in vivo* data (Schulze,

2006). The secretion rates of SGF were adjusted using the peristaltic pump. In both states, the pylorus extrusion plate moved at a steady speed of 2 mm/s, transmitting three compressions per minute to the pylorus model, allowing chyme of a size from 0 to 10 mm to pass through the pylorus as a function of time. Besides the pylorus, the auxiliary emptying device was also used to regulate the emptying of yogurt digesta by tuning the tilting angle. The angle was kept at -37.5° from 0 to 4 min, -22.5° during 4 to 9 min, -15° in the next 5 min (9 to 14 min), -7.5° from 14 to 19 min, and +7.5° during 19 to 85 min, to reappear the human gastric emptying characteristics in the before-meal state (Keszthelyi et al., 2013). In the after-meal state, the tilting angle was at -37.5° during 0 to12 min, -18.75° in the next 15 min (12 to 27 min), -0.5° during 27 to 64 min, +6.5° from 64 to 80 min, and +13.5° till the end of digestion (180 min). In the before-meal state, this gastric digesta were collected at seven time points (5, 10, 15, 20, 40, 60, and 85 min) with a maximum gastric endpoint of 85 min. In the after-meal state, the digesta were taken at 15, 30, 42, 52, 70, 85, 120, and 145 min with a gastric endpoint of 145 min. The samples were examined for pH, volume, and weight immediately, and then under storage at -70°C until rheological measurements.

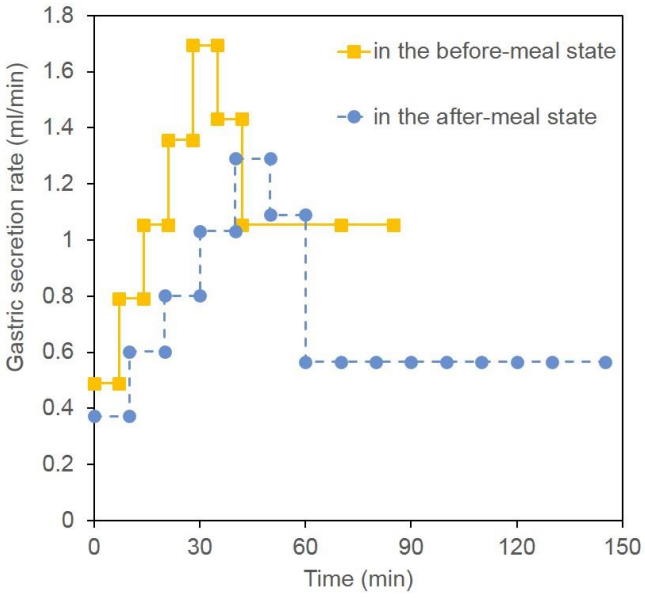

Fig. 5.2. SGF secretion flow (ml/min) in the DIVHS calculated from the human gastric secretion rate after a homogenised meal ingested (Keszthelyi et al., 2013; Malagelada et al., 1979; Sauter et al., 2012).

5.3.3.2 Small intestinal digestion in before- and after-meal states in the DIVHS

As the emptying process mentioned above repeated without gastric digesta collection, the SIF was simultaneously injected into the duodenum model using the peristaltic pump. A constant SIF secretion flow of 2.22 ml/min with a maximal intestinal endpoint of 90 min in the before-meal state and a constant rate of 1.11 ml/min with an intestinal endpoint of 180 min in the after-meal state were modified from the study by Minekus et al. (1995). The rollers and eccentric wheels were set to produce eleven contractions per minute to the duodenum model as described *in vivo* (Ehrlein & Schemann, 2005). In this case, the chyme left from the pylorus for the position around 25 cm away from the pylorus aperture (*i.e.,* the length of human duodenum), accompanied by mixing with the SIF injected. The chyme obtained here were regarded as the duodenal digesta. The sample collection occurred at 5, 10, 15, 20, 40, 60, and 85 min in the before-meal state, and at 15, 30, 42, 52, 70, 85, 120, and 145 min in the after-meal state. The digesta were evaluated for pH, volume, and weight immediately, and were kept at -70°C until rheological measurements.

The human jejunum and ileum are too long making it difficult to be simulated accurately. Hence, with the gastric emptying and duodenal digestion reproduced without sample collection, the chyme flowing from the duodenum model was incubated in a flask in a 37°C water bath under magnetic stirring at 100 rpm to mimic small intestinal digestion modified from the INFOGEST protocol (Minekus et al., 2014). In both states, the weight and volume of the intestinal digesta in the flask were monitored at the designated digestion time (15, 30, 60, 90, 120, and 180 min). Simultaneously, 400 µl of the intestinal digesta were collected at each digestion time point and stored in an Eppendorf microtube at -70°C until curcumin release test, microstructural characterisation, and SDS-PAGE analysis.

5.3.4 Characterisation

5.3.4.1 Rheological measurements of yogurt digesta.

The incorporation of complex microparticles into yogurt at a low dose of 8 mg/ml has been demonstrated to have a negligible influence on the rheological properties of the original yogurt, at $P < 0.05$ level (Ye et al., 2020). Thus, only the original yogurt, its gastric and duodenal digesta collected at 10, 20, and 40 min in the before-meal state,

and two digesta at 15, 30, 70 min in the after-meal state were selected for the rheological measurements in this section. The intestinal digesta was too dilute to be examined. To investigate the effect of SGF dilution and acid hydrolysis on the digesta rheology, the DIVHS digestion was repeated using the original yogurt without pepsin, following the same emptying curves. A similar "digestion" experiment in the absence of SGF and pepsin was conducted in the DIVHS to elucidate the influence of gastric peristalsis. The test yogurt was also "digested" without pepsin and SGF, following the same emptying kinetics by manual, under a condition of magnetic stirring at 100 rpm, 37°C. This condition is widely used in traditional static digestion methods (Minekus et al., 2014). Flow behaviours of these "digesta" were measured to compare the effects of the DIVHS peristalsis and the traditionally used stirring method on yogurt rheology.

The steady shear and oscillatory measurements were carried out using a Kinexus pro+ rotational rheometer at 37°C (Malvern Instruments Ltd. Worchestershire, UK), using a CP 4/40 cone-plate geometry (40 mm in diameter; 4° angle; 0.15 mm gap). A strain sweep was performed to determine the linear viscoelastic regime of 1.1 ml sample, followed by dynamic oscillatory measurements over a frequency domain from 0.1 to 100 rad/s with a fixed strain value of 1%. The shear stress and viscosity were evaluated at shear rates ranging from 0.1 to 100 s^{-1}.

The power law model is fitted to the data from the samples showing non-Newtonian flow behaviours under the steady shear measurements (Holdsworth, 1971), Eq. (5.1):

$$\eta = K \times \dot{\gamma}^{n-1} \quad (5.1)$$

where η and K represent the steady shear viscosity (Pa·s) and the consistency constant (Pa·s^n), respectively. $\dot{\gamma}$ is the shear rate (s^{-1}) and n is the flow behaviour index.

5.3.4.2 In vitro release of curcumin from complex microparticles with yogurt.

The amounts of curcumin present in the intestinal digesta as a function of time were expressed as the *in vitro* release profiles, because the intestine is the organ where absorption of curcumin occurs *in vivo* (Ravindranath & Chandrasekhara, 1981). Based on the digestion procedure in the section 5.3.3.2, 400 µl of the intestinal digesta of RR- and TR- yogurt were collected in the before- and after-meal states at 15, 30, 60, 90, 120, and 180 min, followed by centrifugation at 9168 x g for 20 min at 4°C. The

curcumin contents in the supernatant of 200 µl were determined by a microplate reader (SpectraMax M5, Molecular Devices, USA), using a fluorescence emission peak of curcumin at 520 nm upon excitation at 480 nm (Ye et al., 2020). A calibration curve was fitted with known amounts of curcumin in a solution containing milli-Q water, SGF, and SIF at a ratio of 1:1:2 without enzymes at 0.05% wt Tween 80, alkalised to pH 7 using 6 M NaOH. This solution was prepared to mimic the biochemical conditions of intestinal digesta. Tween 80 was added as an emulsifier to completely dissolve curcumin with hydrophobicity (Onoue et al., 2010). The original yogurt was subjected to digestion and used as blank, whose fluorescence emission values at 520 nm were subtracted from the measurements to remove the intrinsic effect of yogurt.

5.3.4.3 Morphology and fluorescence characterisation of yogurt digesta.

SEM (Hitachi SU1510, Hitachi Co. Ltd., Tokyo, Japan) was applied to characterise the morphology of the intestinal digesta of the original yogurt, RR-yogurt, and TR-yogurt in both states at the sampling time of 0, 30, and 180 min. Optical and fluorescence microimages of the digesta were taken with a Leica digital camera (DFC450) mounted on a Leica Z16 APOA MacroFluo microscope, using a LAS 4.4 multi-stacking imaging system (Leica, Wetzlar, Germany).

5.3.4.4 Sodium dodecyl sulfate-polyacrylamide gel electrophoresis (SDS-PAGE) analysis of yogurt digesta.

The intestinal digesta of the original yogurt, RR-yogurt, and TR-yogurt in both states at 0, 30, 180 min were subjected to the SDS-PAGE analysis (NuPAGE™ 4 to 12%, Bis-Tris, 1.0 mm, Mini Protein Gel, 12-well). The intestinal digesta at 0 min, 30 min, and 180 min were diluted with milli-Q water at a volume ratio of 7:123, 3:23, and 1:4, respectively. The digesta at 180 min was also used without dilution. Samples were prepared by mixing these above digesta 13:5:2 with NuPAGE™ LDS Sample Buffer (4x) and NuPAGE™ Sample Reducing Agent (10x), separately, followed by heating at 70°C for 10 min. Then, 10 µl of the mixtures were loaded to each lane of the gel, to achieve 10 µg proteins plus hydrolysates per lane for the optimal load. 20 µl of the mixtures containing the undiluted digesta at 180 min were also deposited with a protein load up to 100 µg per lane. 5µl of PageRuler™ Plus Prestained Protein Ladder (10 to

250 kDa) were applied on a separate strip. The gel electrophoresis was performed at 200 V for 50 min with a Tris-MES-SDS running buffer (1x) (Adamas-beta, Shanghai, China). The Tris-MES-SDS running buffer in the cathode buffer chamber also contained 0.25% v/v NuPAGE™ Antioxidant. A staining solution was made of 0.1% wt Coomassie brilliant blue R-250 (Solarbio, Beijing, China), 10% v/v acetic acid, and 40% v/v ethanol. A destaining solution was prepared with 10% v/v ethanol and 7.5% v/v acetic acid. All NuPage™ and PageRuler™ chemicals were purchased from Thermo Fisher Scientific, Somerset, NJ, USA.

5.3.5 Statistical analysis

Means and error bars (*i.e.,* standard deviations) were acquired from the statistical model with analysis of variance (ANOVA) in the GLM procedure of the SAS system. The statistical differences between the groups were set at a probability level of 0.05. All sample collections and measurements were performed in triplicate.

5.4 Results and discussion

5.4.1 Reproduction of gastric emptying kinetics and pH.

The gastric emptying kinetics of the test yogurt were simulated using the DIVHS based on the *in vivo* data reported (Keszthelyi et al., 2013). To compare the emptying *in vivo* to those in the DIVHS quantitatively, a modified Elashoff's power-exponential function was applied (Siegel et al., 1988), Eq. (5.2):

$$y(t) = 1 - (1 - e^{-kt})^{\beta} \quad (5.2)$$

where t and y(t) mean the digestion time in minutes and the fractional gastric retention at time *t*, respectively. *k* is the gastric emptying rate (minute^{-1}). β represents the extrapolated y-intercept from the terminal portion of the curve. The values of *k* and β were computed by nonlinear least squares regression with Microsoft Excel 2010.

The half-time ($t_{1/2}$) defined as the time required for half of the test meal emptied from the stomach into the small intestine, can be determined from Eq. (5.3) using y(t) = 0.5:

$$t_{1/2} = -\frac{1}{k} \times \ln\left(1 - 0.5^{\frac{1}{\beta}}\right) \quad (5.3)$$

The lag phase time (t_{lag}) reflecting the time taken to reach maximum emptying velocity was calculated assuming $\frac{d^2y(t)}{dt^2} = 0$, Eq. (5.4):

$$t_{lag} = \frac{\ln \beta}{k} \quad (5.4)$$

As shown in **Fig. 5.3**, all curves provided a good fit with the correlation coefficients (R^2) close to one (**Table 5.1**). The reproduction was proven by the agreement between the values of the gastric emptying rate (k), the extrapolated y-intercept from the terminal portion of the curve (β), half-time ($t_{1/2}$), and lag phase time (t_{lag}) from the *in vitro* and *in vivo* systems (**Table 5.1**).

In the before-meal state, the gastric digesta in the DIVHS and *in vivo* were both emptied in an exponential manner without an initial lag phase. The lag period is defined as the time required for the distal stomach to grind the solid chyme into smaller particles to flow through the pyloric sphincter (Siegel et al., 1988). The factor determining the length of the lag period is the chemical compositions and physical properties of the food ingested, including the caloric content, meal volume, particle size, and viscosity (Kong & Singh, 2008). In this study, the test yogurt as a low-calorie semi-solid food was much smaller than 2 mm in particle size as shown in the optical micro-images in **Fig. 5.4**, and the WPI-curcumin complex microparticles incorporated were ≤ 100 μm in diameter reported in our previous study (Ye et al., 2020). This indicates that the particle size of the test yogurt was not large enough to trigger the sieving effect of pylorus (Schulze, 2006). Therefore, the digestion of the test yogurt on an empty stomach caused a simple process in which the chyme could enter the duodenum directly without lag phases. It has been reported that the emptying rate has a positive correlation with the residual gastric volume (Kong & Singh, 2008), leading to the gradually slow emptying from 20 min to the gastric endpoint of 85 min with the decreased volumes of the gastric contents. Physiologically, gastric emptying mainly relies on the gastroduodenal pressure gradient and is driven by the tonic contraction of the proximal stomach and by the peristaltic contractions of the gastric antrum (Janssen et al., 2011). The gastric emptying of a liquid meal (*i.e.,* the case in the before-meal state) is governed by the pressure from the proximal stomach and by the opening/closure of the pylorus (Indireshkumar et al., 2000). This implies that the successful reproduction of gastric emptying of yogurt in the before-meal state resulted from the accurate mimicry of pyloric compressions and peristalsis to the proximal

stomach, which are based on the near-real gastric dimension, morphology, and inner wrinkled microstructures of the DIVHS.

According to Siegel et al. (1988), a value of $\beta < 1$ manifests an initial rapid gastric emptying for liquid meals, which was observed in the before-meal state (*in vivo* β=0.96; *in vitro* β=0.95±0.06), whereas $\beta > 1$ represents an initial delay in emptying for solid foods, noticed in the after-meal state (*in vivo* β=1.30; *in vitro* β=1.41±0.12) (Keszthelyi et al., 2013). The emptying in the after-meal state was prolonged with a lag period of 12.1 min *in vivo* and of 14.8±2.2 min in the DIVHS, ascribed to the residual gastric contents from a 500 g macaroni meal consumed 45 min before the yogurt intake (Keszthelyi et al., 2013). The peristalsis of the gastric antrum is crucial for the gastric emptying of solid foods (the case in the after-meal state) (Indireshkumar et al., 2000). Since no solid foods were loaded in the study, the gastric kinetics in the after-meal state were reproduced by the simulation of the peristalsis, the near-real anatomical structure of human stomach, and the aid of the pyloric valve and auxiliary emptying device.

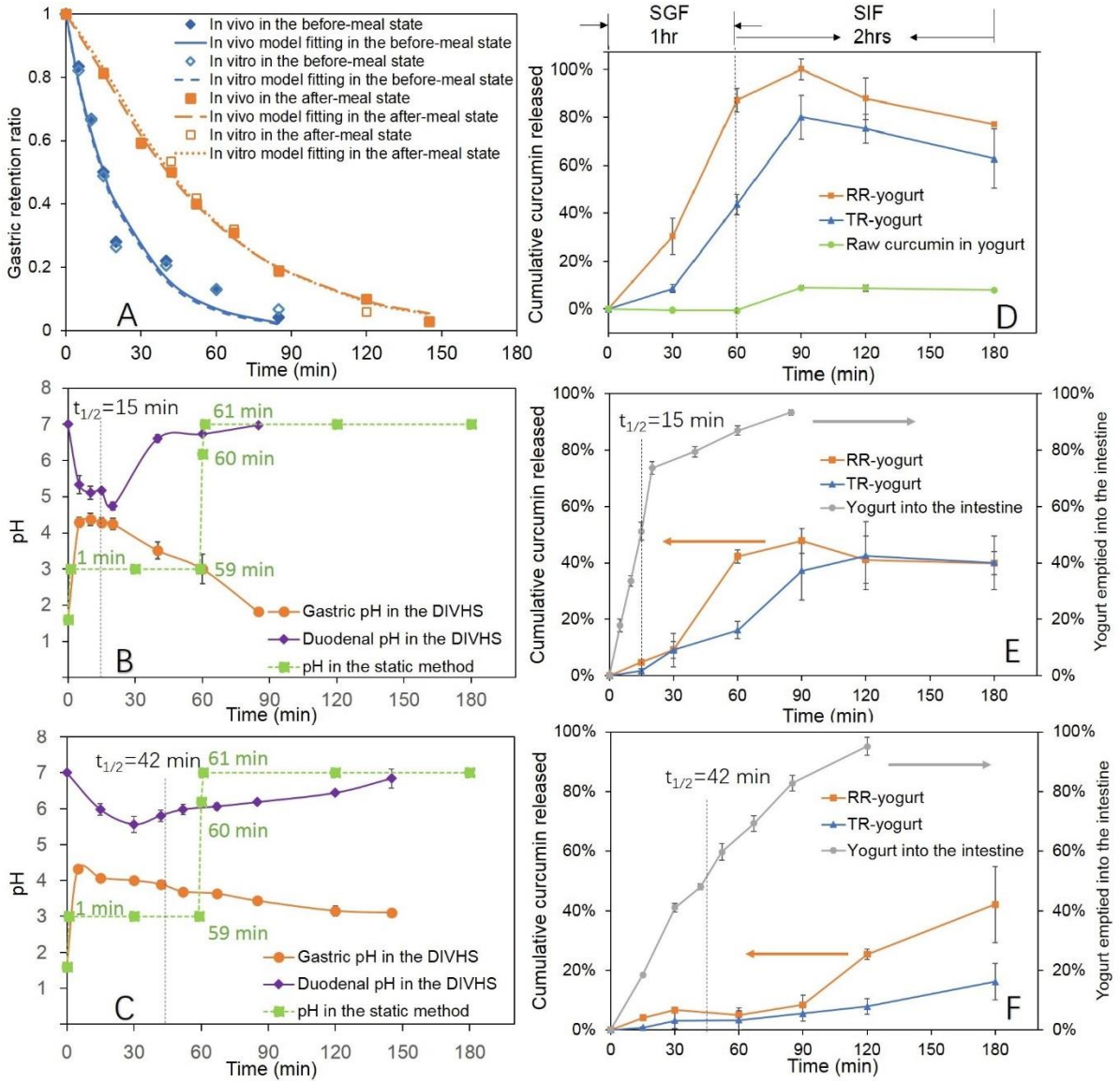

Fig. 5.3. (A): Gastric emptying curves (retention ratio in stomach) of the yogurt digesta in the before- and after-meal states observed in humans and the DIVHS, fitted with the modified Elashoff's power exponential function, the *in vivo* results are reported by Keszthelyi et al. (2013); pH profiles of the gastric and duodenal digesta of the test yogurt during digestion in the DIVHS (B) in the before-meal state and (C) in the after-meal state; curcumin release characteristics from the RR-yogurt and TR-yogurt (D) using the standard INFOGEST protocol as a control, reported previously (Ye et al., 2020); in the DIVHS (E) in the before-meal state; (F) in the after-meal state.

Table. 5.1: Modified Elashoff's function parameters of the gastric emptying of the yogurt digesta in the before- and after-meal states obtained in the DIVHS and *in vivo*

(Keszthelyi et al., 2013). (For the *in vivo* data, no standard deviations are presented since only average values of the emptying curves are provided.)

	Consumption pattern	k	β	$t_{1/2}$	t_{lag}	R^2
In vivo	In the before-meal state	0.0438	0.96	15.2	0	0.965
	In the after-meal state	0.0217	1.30	42.0	12.1	0.998
In vitro	In the before-meal state	0.0448±0.0043	0.95±0.06	14.7±1.1	0	0.960
	In the after-meal state	0.0233±0.0020	1.41±0.12	42.2±1.5	14.8±2.2	0.991

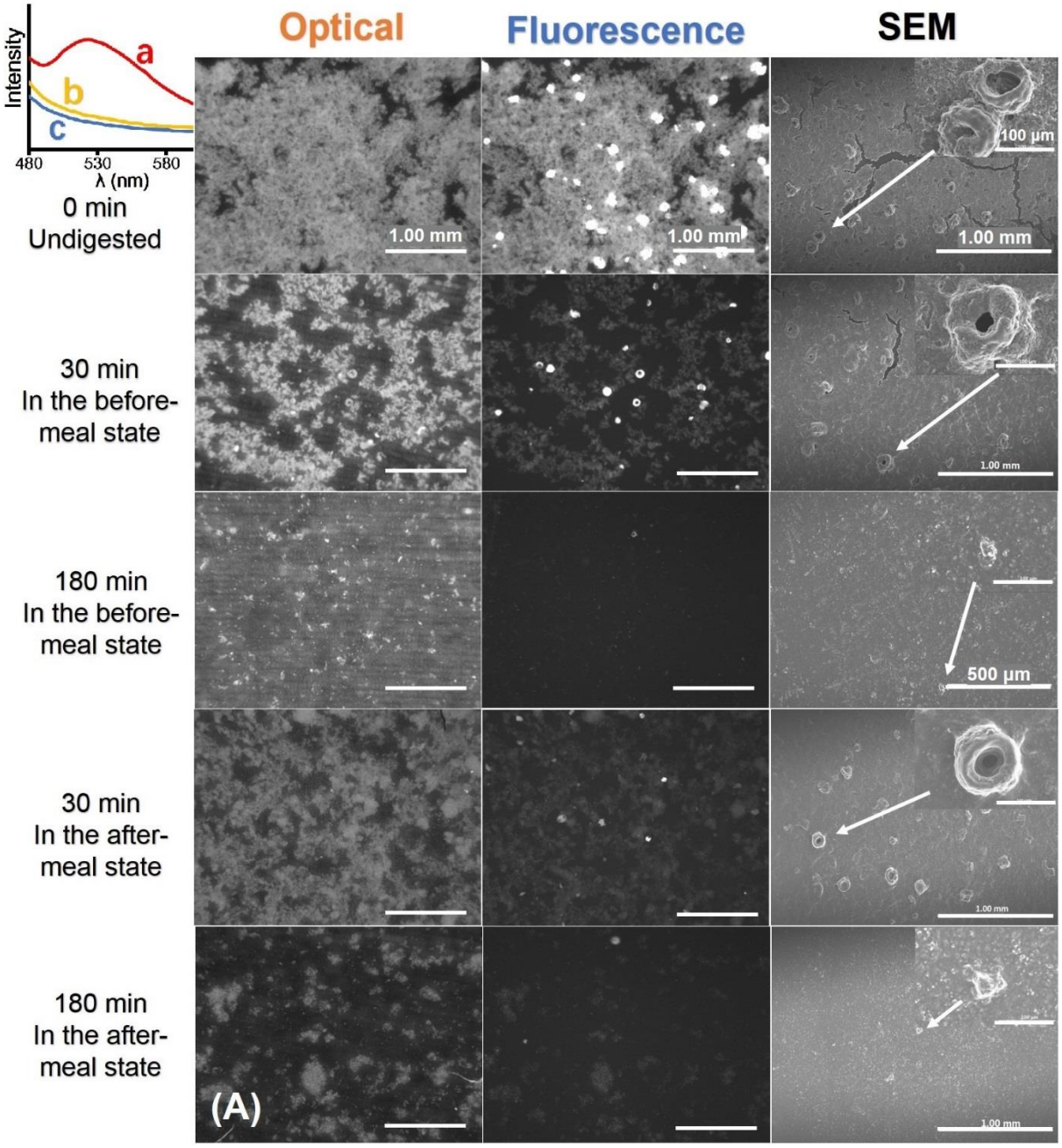

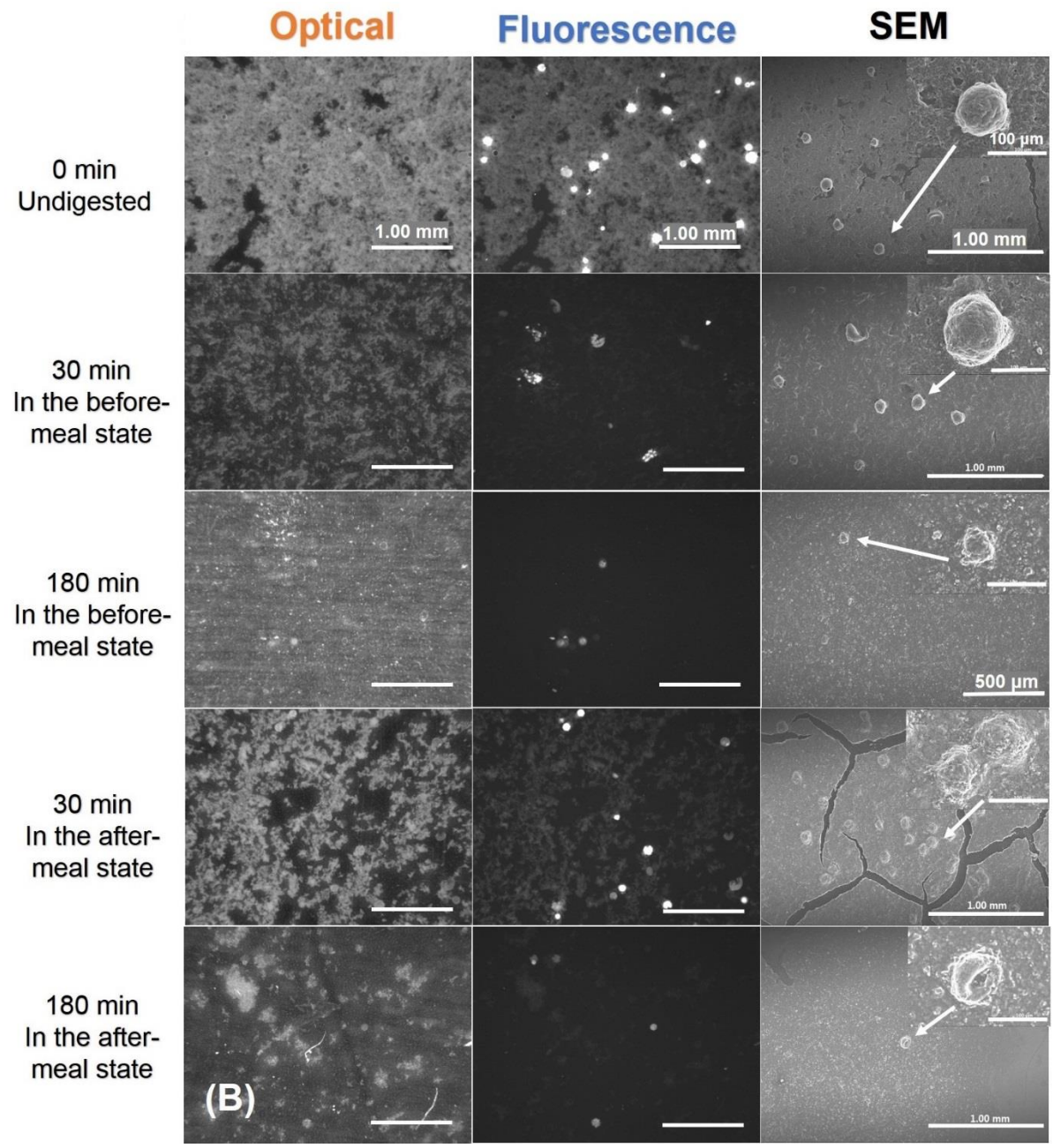

Fig. 5.4. Comparison of the intestinal digesta of RR-yogurt (A) and TR-yogurt (B) in the before- and after-meal states using optical, fluorescence, and SEM microscopy. (The inset in the upper-left corner displays the fluorescence spectra of (a) curcumin-WPI complex in water in red line, (b) curcumin in water in yellow line, and (c) water in blue upon excitation at 420 nm. Scale bars: 100 µm in the inserts and 1 mm in the original images.)

5.4.2 pH of the gastric and duodenal digesta.

Fig. 5.3(B) and (C) exhibit the pH profiles of the gastric and duodenal digesta in the before- and after-meal states. Note that no macaroni meals were fed before the yogurt ingestion in the after-meal state, hence, the buffering effect of the macaroni residuals was ignored and the initial values of pH in the gastric and duodenal phases were those of the SGF and SIF, respectively. After the yogurt intake, the values of pH in the stomach elevated rapidly from 1.6 to 4.29 in the before-meal state and to 4.32 in the after-meal state, caused by the meal diluting effect and the acid hydrolysis. Then, with the gastric secretion and emptying, the pH reduced to 1.8 at the gastric endpoint of 85 min in the before-meal state, and to a value of 3.1 at 145 min in the after-meal state. The gastric pH profiles observed in the DIVHS agree well with the *in vivo* results reported by Jerry et al. (2002). The pH values of duodenal digesta varied in reverse, with a slight decrease at an initial period called duodenal acidification due to the gastric chyme passing into the duodenum, followed by an increase in pH known as duodenal alkalinisation (McCloy et al., 1984; Worning et al., 1967). Compared to the pH profiles in the after-meal state, those in the before-meal state showed more rapid changes in two digesta. This is presumably due to a stimulating effect of the volume of the emptied food on the gastric secretion, *i.e.,* the food emptied could prompt the release of about 61% of its volume as gastric secretion (Sauter et al., 2012). The faster gastric emptying in the before-meal state, the more gastric juices secreted, and thus the steeper pH changes in the gastric phase. On the other hand, acidic chyme emptied from the pylorus stimulates the secretion of secretin, leading to bicarbonate production for neutralisation in human duodenum (Rumsey, 2005). This explains the faster pH changes of the duodenal digesta in the before-meal state. The green dashed lines represent the pH evolution suggested by the standard INFOGEST protocol, as a control (Minekus et al., 2014). The agreement in pH variations to those described from *in vivo* data further demonstrates the effective reproduction of gastroduodenal digestion using the DIVHS. An accurate dynamic simulation of real pH profiles is an essential prerequisite for simulating *in vivo* digestion and release. In terms of the digestive enzymes commonly used, porcine pepsin can hydrolyse over 50% of 0.08 mg/100 ml α-lactalbumin (a major component of WPI) at pH 3.5 in 20 min, whereas the degree of proteolysis drops to about 10% at pH 4.0 (Miranda et al., 1989). Due to the sensitivity of digestive enzymes to pH, the prolonged and unfavourable pH

conditions observed in the after-meal state may slow down yogurt digestion and microparticle disintegration, consequently delaying the release of curcumin, which will be discussed in the following sections.

5.4.3 Rheological measurements of the gastric and duodenal digesta.

Fig. 5.5 displays the storage modulus (*G'*) and loss modulus (*G''*) of the gastric and duodenal digesta in the before- and after-meal states, following a power-law behaviour (**Table 5.2**). The original yogurt and gastric digesta in both states had the elasticity *G'* greater than the viscous property *G''* with moduli nearly parallel to each other, behaving as weak gels. The undigested yogurt was less frequently dependent than the others, due to its relatively high solid content facilitating the stabilisation of the temporary networks of macromolecules (Xu et al., 2008). Gastric digestion was not enough to break down the weak-gel structure of yogurt. Physiologically, the small particle size of yogurt could not induce the sieving effect of pylorus (Schulze, 2006). Protein hydrolysates in the duodenum dose-dependently release cholecystokinin from enteroendocrine cells to inhibit gastric emptying (Liou et al., 2011). The former was achieved by controlling pyloric aperture diameter in the model and the pyloric extrusion plate. The latter mechanism is essential for protein digestion. However, it is inevitably simplified in the DIVHS by adjusting the pyloric valve and the tilting angle of the auxiliary emptying device to regulate emptying.

In the duodenal phase, the digesta in the before-meal state existed in an entanglement system or concentrated solution, where the curves of *G''* and *G'* intersected somewhere in the frequency domain studied and a viscoelastic fluid-like behaviour (*G'* > *G''*) merely appeared at higher frequencies (Ross-Murphy et al., 1983). Whereas the duodenal digesta in the after-meal state had the *G''* larger than *G'* over the whole frequency range and their moduli approached at higher frequencies, indicating a dilute-solution or liquid-like behaviour (Xu et al., 2008), even for the samples collected at a short digestion time of 15 min. The larger viscous property *G''* than *G'* in the duodenal phase presumably resulted from the proteolysis and dilution effect of SIF. The different flow behaviours of duodenal digesta in two states were caused by the different solid contents emptied from the stomach, determined by gastric emptying, which was strongly influenced by the ingestion pattern in this study.

No macaroni fed in the after-meal state may cause underestimation of the elasticity *G'* of the digesta. However, the meal intake will further stimulate the secretion of digestive fluids, followed by dilution, and enzymatic and acid hydrolysis. Therefore, the results here can be seen as the rheology of the yogurt portion in the digesta.

Fig. 5.6 shows that the steady shear viscosity of the gastric and duodenal digesta in both states reduced with the increasing shear rate, implying a shear-thinning non-Newtonian behaviour (Ross-Murphy et al., 1983). In **Table 5.3**, the values of *n* (flow behaviour index) of Power Law parameters for the steady shear viscosity were all between 0 and 1, in a pseudoplastic fluid range. Most of the *n* values fluctuated in a limited range of 0.301 to 0.516, except those of the duodenal digesta at 40 min in the before-meal state (n=0.833±0.209, close to the Newtonian flow range), and the digesta at 70 min in the after-meal state (0.614±0.050 in the gastric phase and 0.775±0.089 in the duodenal phase). For these long-time digestions, their *K* values (consistency coefficient) dropped in two-three orders of magnitude in both states, attributed to peristaltic contraction, liquid dilution, and acid and enzymatic hydrolysis. Thus, the DIVHS was employed to evaluate the weights of these factors contributing to the viscosity variations in the gastric phase (**Fig. 5.7**). When the dilution and acid hydrolysis of SGF without pepsin was introduced into the DIVHS, the *n* values of the test yogurt fluctuated in a small range from 0.325 to 0.451, whereas the *K* values fell in one order of magnitude in two states (**Table 5.4**). When only peristalsis from the DIVHS was applied to the test yogurt without the SGF or enzymes, the *n* values of gastric digesta were statistically similar at $P < 0.05$ level, while *K* values were reduced by over 60 % in the before-meal state and by 34% in the after-meal state. By contrast, when the same emptying kinetics were applied without SGF or pepsin, the *K* values only decreased by around 7% in both states under stirring at 100 rpm, which is widely used in the static digestion. This indicates that the peristalsis from the DIVHS was relatively effective in grinding foodstuffs, which may promote the extent and rate of hydrolysis due to its better hydrodynamic conditions during digestion (Huart et al., 2020). The viscosity of gastric digesta was affected by the combined effect of gastric peristalsis, dilution, and acid and enzymatic hydrolysis. Among them, enzymatic hydrolysis and dilution effect played a dominant role in the rheological properties of digesta in the gastric phase.

It is worth mentioning that the *K* values of the duodenal digesta obtained at a specific time (*e.g.,* 40 min) in the before-meal state were statistically similar with those

at a slightly longer time (70 min in this case) in the after-meal state, $P < 0.05$ (**Table 5.3**). The more rapid reduction of viscosity in the before-meal state was caused by the faster gastric emptying, more digestive fluids secreted, and more favourable pH conditions for enzymatic hydrolysis. Lower viscosity facilitated the intensive mixing of the simulated digestive fluids and the yogurt containing the WPI-curcumin microparticles, probably promoting the proteolysis and curcumin release in the before-meal state, which will be discussed below.

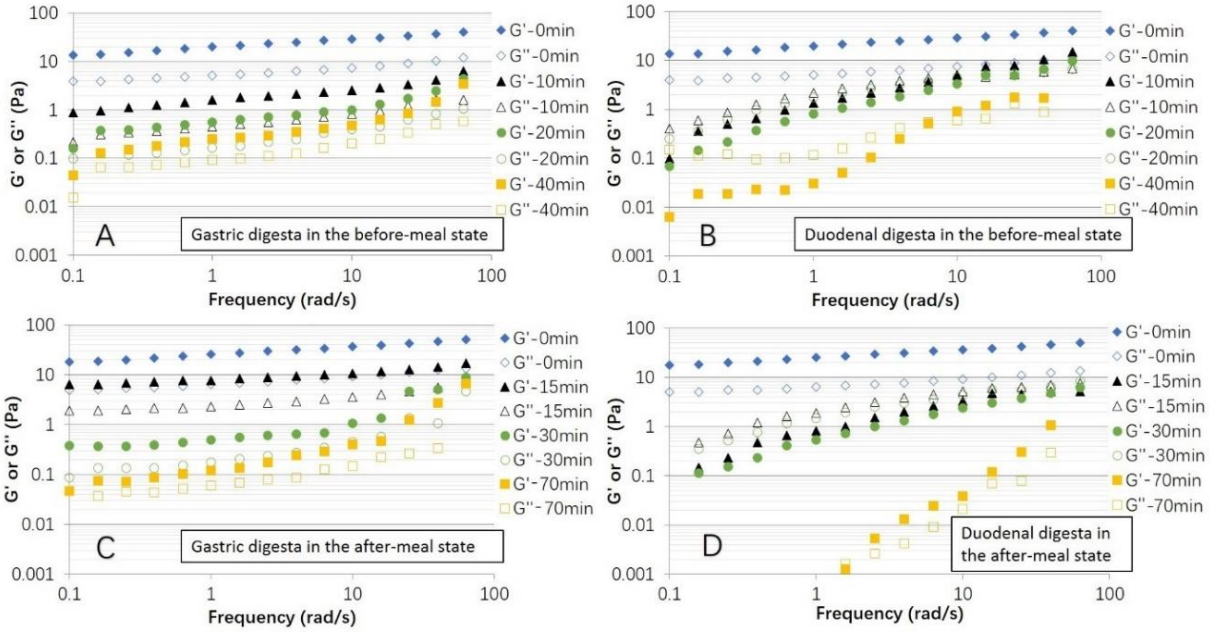

Fig. 5.5. Storage modulus (*G'*) and loss modulus (*G''*) of (A) the gastric digesta in the before-meal state, (B) the duodenal digesta in the before-meal state, (C) the gastric digesta in the after-meal state, and (D) the duodenal digesta in the after-meal state in the DIVHS at various sampling time points.

Table 5.2: Power law parameters of the storage modulus (*G'*) and loss modulus (*G''*) of the gastric and duodenal digesta of the test yogurt in the before- and after-meal states in the DIVHS. (The same parameters in one column with the same superscript are statistically insignificant, $P < 0.05$, n=3)

		Gastric digesta			Duodenal digesta		
	Time	*K* (Pa·s)	*n*	R^2	*K* (Pa·s)	*n*	R^2
G' In the before-meal state	0 min	22.483±2.867^{a}	0.165±0.004^{cd}	0.997	22.483±2.867^{a}	0.165±0.004^{d}	0.997
	10 min	1.375±0.172^{c}	0.237±0.027^{cd}	0.976	0.991±0.069^{b}	0.644±0.037^{c}	0.972
	20 min	0.568±0.007^{c}	0.269±0.043^{bc}	0.973	0.631±0.027^{b}	0.689±0.044^{c}	0.972
	40 min	0.277±0.050^{c}	0.346±0.030^{b}	0.955	0.042±0.027^{b}	1.298±0.439^{b}	0.970
G' In the after-meal state	0 min	22.483±2.867^{a}	0.165±0.004^{cd}	0.997	22.483±2.867^{a}	0.165±0.004^{d}	0.997
	15 min	9.879±2.056^{b}	0.145±0.008^{d}	0.978	0.715±0.129^{b}	0.545±0.085^{c}	0.962
	30 min	0.367±0.112^{c}	0.179±0.020^{cd}	0.955	0.447±0.022^{b}	0.758±0.126^{c}	0.971
	70 min	0.151±0.060^{c}	0.537±0.134^{a}	0.935	0.001±0.000^{b}	1.700±0.238^{a}	0.951
G'' In the before-meal state	0 min	5.896±0.673^{a}	0.162±0.006^{c}	0.974	5.896±0.673^{a}	0.162±0.006^{d}	0.974
	10 min	0.406±0.048^{c}	0.347±0.028^{a}	0.964	1.532±0.247^{b}	0.414±0.014^{c}	0.921
	20 min	0.195±0.017^{c}	0.268±0.025^{b}	0.962	1.428±0.152^{b}	0.465±0.020^{c}	0.939
	40 min	0.115±0.016^{c}	0.336±0.032^{ab}	0.948	0.076±0.057^{c}	0.858±0.199^{b}	0.977
G'' In the after-meal state	0 min	5.896±0.673^{a}	0.162±0.006^{c}	0.974	5.896±0.673^{a}	0.162±0.006^{d}	0.974
	15 min	2.834±0.520^{b}	0.172±0.012^{c}	0.953	1.344±0.341^{b}	0.389±0.142^{c}	0.956
	30 min	0.144±0.036^{c}	0.402±0.082^{a}	0.968	1.153±0.333^{b}	0.499±0.083^{c}	0.951
	70 min	0.069±0.020^{c}	0.351±0.056^{a}	0.943	0.001±0.000^{c}	1.292±0.086^{a}	0.915

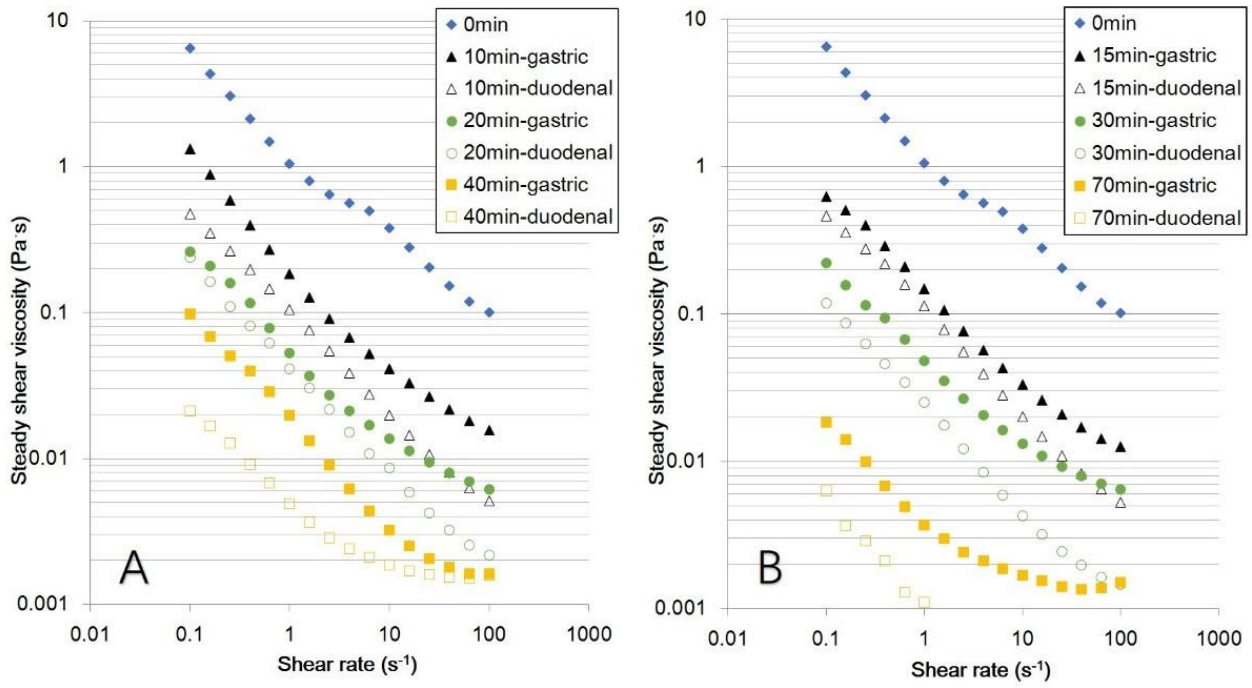

Fig. 5.6. Steady shear viscosity of the gastric and duodenal digesta of the test yogurt in the before- (A) and after-meal states (B) in the DIVHS at various sampling timepoints.

Table 5.3: Parameters from the power law relation for the steady shear viscosity of the gastric and duodenal digesta of the test yogurt in the before- and after-meal states. ($^{a\text{-}d}$ indicate that under the same letter, the parameter values in the same column are statistically insignificant at $P < 0.05$, n=3.)

		Gastric digesta			Duodenal digesta		
	Time	*K* (Pa·s)	*n*	R^2	*K* (Pa·s)	*n*	R^2
In the before-meal state	0 min	1.351±0.104^{a}	0.413±0.013^{b}	0.976	1.351±0.104^{a}	0.413±0.013^{bc}	0.976
	10 min	0.144±0.029^{b}	0.345±0.016^{cd}	0.919	0.106±0.004^{b}	0.320±0.004^{c}	0.993
	20 min	0.060±0.002^{c}	0.425±0.005^{b}	0.951	0.056±0.012^{bc}	0.301±0.006^{c}	0.978
	40 min	0.014±0.004^{c}	0.391±0.036^{bc}	0.942	0.003±0.002^{c}	0.833±0.209^{a}	0.970
In the after-meal state	0 min	1.351±0.104^{a}	0.413±0.013^{b}	0.976	1.351±0.104^{a}	0.413±0.013^{bc}	0.976
	15 min	0.147±0.005^{b}	0.432±0.031^{b}	0.987	0.100±0.011^{b}	0.315±0.011^{c}	0.991
	30 min	0.053±0.026^{c}	0.305±0.021^{d}	0.989	0.047±0.008^{bc}	0.516±0.039^{b}	0.983
	70 min	0.005±0.001^{c}	0.614±0.050^{a}	0.957	0.002±0.001^{c}	0.775±0.089^{a}	0.967

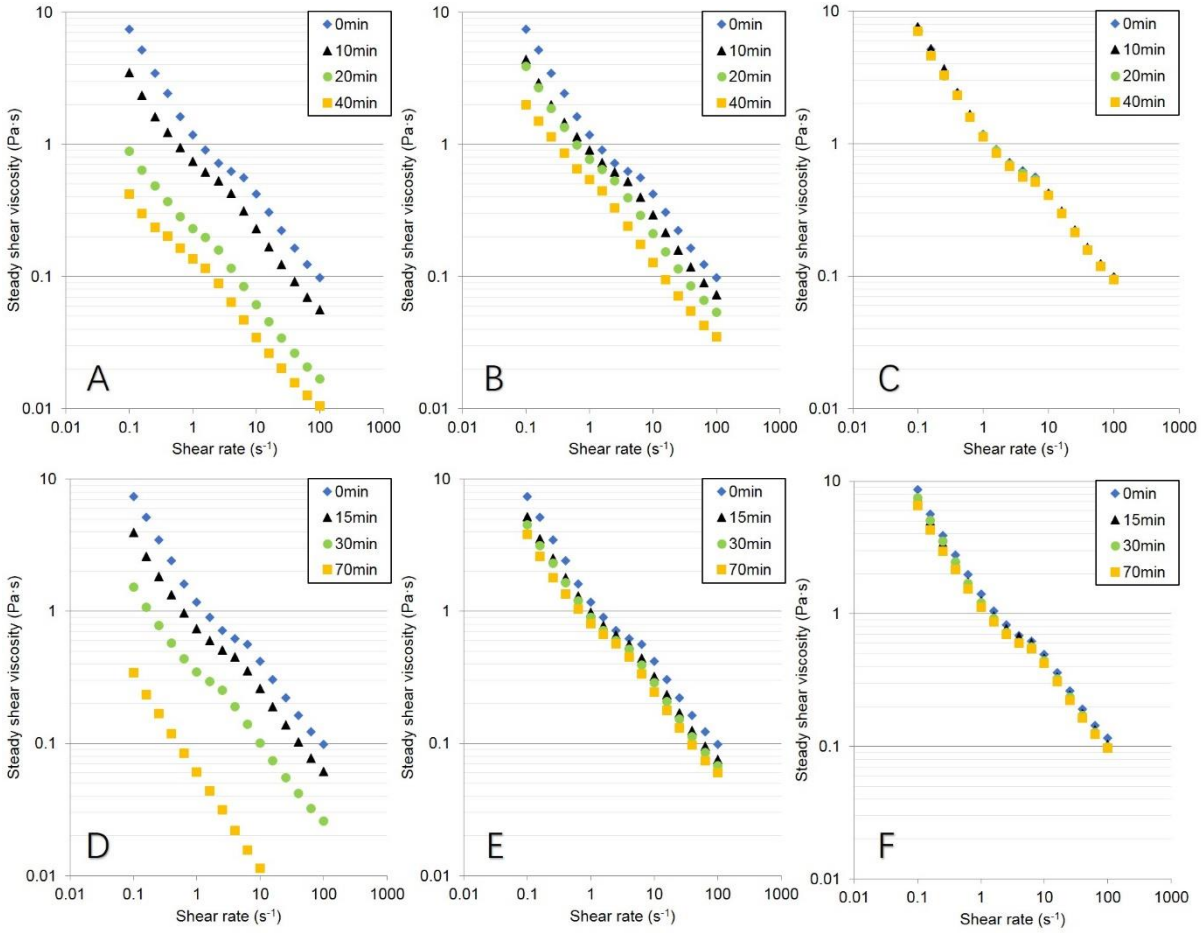

Fig. 5.7. Steady shear viscosity of the gastric digesta of the test yogurt (A) with SGF without pepsin in the DIVHS in the before-meal state; (B) without SGF or pepsin in the DIVHS in the before-meal state; (C) without SGF or pepsin under stirring in the before-meal state; (D) with SGF without pepsin in the DIVHS in the after-meal state; (E) without SGF or pepsin in the DIVHS in the after-meal state; (F) without SGF or pepsin under stirring in the after-meal state.

Gastric digesta	Time	With SGF without pepsin in the DIVHS			Without SGF or pepsin in the DIVHS			Without SGF or pepsin under stirring		
		K (Pas·s)	*n*	R^2	*K* (Pas·s)	*n*	R^2	*K* (Pas·s)	*n*	R^2
In the before-meal state	0min	1.351±0.104^{a}	0.413±0.013^{c}	0.976	1.351±0.104^{a}	0.413±0.013^{a}	0.976	1.526±0.147^{a}	0.410±0.005^{a}	0.979
	10min	0.818±0.075^{b}	0.421±0.004^{bc}	0.991	1.011±0.042^{b}	0.418±0.014^{a}	0.991	1.474±0.004^{a}	0.410±0.018^{a}	0.975
	20min	0.246±0.021^{d}	0.434±0.009^{b}	0.993	0.817±0.085^{c}	0.399±0.008^{a}	0.994	1.439±0.059^{a}	0.410±0.008^{a}	0.980
	40min	0.135±0.010^{e}	0.451±0.009^{a}	0.994	0.530±0.038^{d}	0.420±0.021^{a}	0.993	1.418±0.080^{a}	0.415±0.011^{a}	0.980
In the after-meal state	0min	1.351±0.104^{a}	0.413±0.013^{c}	0.976	1.351±0.104^{a}	0.413±0.013^{a}	0.976	1.526±0.147^{a}	0.410±0.005^{a}	0.979
	15min	0.856±0.087^{b}	0.425±0.003^{bc}	0.986	1.100±0.055^{b}	0.412±0.011^{a}	0.988	1.460±0.097^{a}	0.412±0.004^{a}	0.979
	30min	0.382±0.022^{c}	0.423±0.010^{bc}	0.992	1.015±0.037^{b}	0.411±0.007^{a}	0.991	1.446±0.096^{a}	0.408±0.005^{a}	0.976
	70min	0.062±0.001^{e}	0.325±0.015^{d}	0.982	0.885±0.027^{c}	0.414±0.004^{a}	0.991	1.386±0.060^{a}	0.424±0.003^{a}	0.980

Table 5.4: Power law parameters for the steady shear viscosity of the gastric digesta of the test yogurt in the before- and after-meal states under different conditions. (The parameter values with the same superscript in the same column have no statistical significances at $P < 0.05$, n=3.)

5.4.4 *In vitro* release of curcumin using the DIVHS.

Fig. 5.3(E) and (F) display the release profiles of curcumin from the fortified yogurt in the before- and after-meal states, respectively. The RR-yogurt was enriched with the rapid-release WPI-curcumin complex microparticles without crosslinking and the TR-yogurt with the targeted-release samples crosslinked at [Ca^{2+}]= 5 mM. The release experiments following the standard INFOGEST protocol (Minekus et al., 2014) have been reported in our previous study, as shown in **Fig. 5.3**(D) as a control (Ye et al., 2020). In comparison, the release curves in the DIVHS were more gradual to varying degrees, which could be attributed to three factors: the intrinsic disintegration features of the carriers of curcumin, the gastric emptying kinetics, and the GI secretion. The breakdown features of the rapid- and targeted-release microparticles were controlled by the addition of ethanol and Ca^{2+} in the feed solutions before spray drying. In the case of rapid-release formula, the ethanol-induced desolvation exposed the cleavage sites of β-lactoglobulin for pepsin, improving the digestibility of WPI and thus accelerating the release of curcumin (Dalgalarrondo et al., 1995). The desolvation also improved the complexation between curcumin and WPI, facilitating the production of water-soluble WPI-curcumin complexes (Ye et al., 2020). On the basis of desolvation, the feed solution for the targeted-release samples was crosslinked at [Ca^{2+}]= 5 mM to enhance the gastric resistance of WPI. The different disintegration features of carriers led to the faster release of curcumin observed in the RR-yogurt than that in the TR-yogurt in all three digestion conditions.

Secondly, the absorption of curcumin takes place in the small intestine (Ravindranath & Chandrasekhara, 1981), whereas curcumin is unstable at neutral and physiological pH over there. To obtain the release profiles as realistic as possible, the digesta collection only occurred in the intestinal phase in the DIVHS, instead of the sampling method in the INFOGEST protocol, in which the chyme obtained in the first one hour had to be from the gastric phase as shown in **Fig. 5.3**(D). The amount of curcumin released equals the concentration detected times the volume of digesta in the intestinal phase. The grey lines show the volume percentages of yogurt digesta cumulated in the small intestine with time. The relatively rapid emptying in the before-meal state caused the accumulation of digesta containing curcumin in the small intestine in a short time. When all digesta flew into the intestine in 85 min in the before-meal state, the peak release of 48% in the RR-yogurt and 43% in the TR-yogurt

appeared at 90 min and 120 min, respectively. In the after-meal state with the gastric-emptying endpoint of 120 min, the maximal percentages of release were 42% in the RR-yogurt and only 16% in the TR-yogurt both at 180 min. This indicates that the curcumin release profiles were dependent on the gastric emptying. The quicker emptying, the faster accumulation and release of curcumin in the intestinal phase.

Additionally, these two ingestion patterns caused different GI secretion. The volume of digesta emptied from the stomach can proportionally induce the secretion of gastric juices (Sauter et al., 2012). The acidic protein hydrolysates flowing into the duodenum stimulate the dose-dependent release of secretin and cholecystokinin, responsible for the secretion of bicarbonate and pancreatic digestive enzymes, respectively (Liou et al., 2011; Rumsey, 2005). This suggests a faster secretion pattern in the before-meal state, which was achieved by adjusting the flow rate of the secreting system in the DIVHS described in section 5.3.3.1 and 5.3.3.2. The INFOGEST protocol can be considered to push the digestion conditions to the limit, where the secretion of an equal volume of gastric juices to the food ingested is completed instantly with an optimised pH of 3. This may explain the larger peak releases observed in the INFOGEST protocol in **Fig. 5.3**(D), up to 100% in the RR-yogurt and 80% in the TR-yogurt.

The digesta of RR-yogurt and TR-yogurt showed a release plateau starting from 120 min till the intestinal endpoint in the before-meal state, in **Fig. 5.3**(E). This probably resulted from the WPI-curcumin complex dissociation with protein hydrolysis. According to the molecular docking studies by Sneharani et al. (2010), the binding sites of WPI for curcumin are possibly located at the hydrophobic amino acids on the central hydrophobic calyx of β-lactoglobulin (the primary component of WPI). The Ile, Leu, Val, and Met on the calyx wall are lined with curcumin. The hydrophobic residues of Pro 38 and Phe105 may be involved in an interaction with curcumin's hydroxyl group and phenolic ring, respectively. Lys60 is adjacent to the methoxy group of curcumin (Sneharani et al., 2010). However, the positions of cleavage sites of β-lactoglobulin for pepsin generated with Expasy PeptideCutter include most of the Ile, Leu, Val, Pro38, Lys60, and Phe105. Despite the high resistance of β-lactoglobulin to pepsin due to its stable globular conformation, Lys60 and Phe105 still can be cleaved by trypsin. This means that the majority of the binding conformations and orientations for curcumin would be gradually destroyed, as the microparticles reached the site of curcumin absorption *i.e.,* the small intestine. Most of the carriers made of proteins,

digestible polysaccharides, phospholipids, and fatty acids break down when they arrive at the small intestine. Then, the microvilli in the small intestine would be responsible for absorbing core materials like curcumin, which cannot be simulated using the DIVHS. Without the absorption process, the complex dissociation and curcumin precipitation occurred as a result of its poor aqueous solubility. The curcumin precipitate could not be detected with the fluorescence method used in this study, consequently appearing as the termination of curcumin release. There presumably existed a dynamic process including complex release, complex dissociation, and curcumin precipitation. The plateau and reduction shown in **Fig. 5.3**(E) and (D) represented the equilibrium phase and the consequent dissociation phase, respectively.

Overall, the microparticle disintegration and complex dissociation belong to the specific features of the wall and core materials selected, respectively. While the effect of gastric emptying and secretion on release characteristics is a universal phenomenon in the process of *in vivo* digestion. The fast gastric emptying can trigger the rapid secretion of digestive fluids, followed by a quick decrease in viscosity beneficial to thorough mixing and reaction, as well as a favourable pH environment for enzymatic hydrolysis, which were proven in the rheological and pH measurements, as shown in **Fig. 5.6** and **Fig. 5.3**(B)&(C), separately. A combination of these factors accounted for a higher peak release in a shorter time observed in the before-meal state. The digesta viscosity and pH profile can be seen as two indices of release extent.

5.4.5 Morphology and fluorescence characterisation.

The optical, fluorescence, and SEM images of the intestinal digesta of RR-yogurt in **Fig. 5.4**(A) and TR-yogurt in **Fig. 5.4**(B) were taken to evaluate the digesta appearance, curcumin distribution, particle morphology, and disintegration in both states. The optical micro-images of the undigested samples show the micro-scale protein clusters with the characteristic gel matrix of yogurts. The WPI-curcumin complex microparticles provided the yogurt with curcumin fluorescence which is weak and featureless from 480 nm to 650 nm in water but has a characteristic emission peak at 520 nm upon excitation at 420 nm after complexation with WPI, shown in the inset in the upper-left corner of **Fig. 5.4**(A). The bright spots in the fluorescence images at 0 min indicated the stability of complex microparticles with yogurt after overnight

stirring and storage at 4°C. The fluorescent bright protein clusters at 0 min may be due to the complexation between the bulk caseins and curcumin during the incorporation and storage (Sahu et al., 2008). The similar bright spots, protein clusters, and intact particle microstructures were observed at 30 min, irrelative to ingestion pattern or sample formula, due to the insufficient digestion after the short period. At the intestinal endpoint of 180 min, the digesta of RR-yogurt became very dilute but visible in the optical micro-images, whereas they lost the fluorescence and particle integrity in both states, caused by the high digestibility of the rapid-release microparticles. By contrast, a few fluorescent bright spots and large fragments of particles could be seen in the TR-yogurt digesta at 180 min. The presence of the targeted-release microparticles with nearly intact structures in the after-meal state at 180 min further explained its release percentage as low as 16% in the *in vitro* release section. Additionally, the fluorescent bright protein clusters were hardly captured under all conditions after 180-min digestion. This is due to the dilution effect of digestive juices, and the generation of unbound curcumin with extremely weak fluorescence, caused by the complex dissociation explained above.

5.4.6 SDS-PAGE analysis.

The SDS-PAGE technique was applied to evaluate the digestion patterns of the yogurt proteins in the before- and after-meal states, under reducing conditions. To investigate whether the curcumin complexation discussed above would affect the proteolysis pattern of caseins and whey proteins in yogurts, the intestinal digesta of the original yogurt, RR-yogurt, and TR-yogurt were examined parallelly. As shown in **Fig. 5.8**, the undigested yogurts contained a high amount of αs-casein (αs-CN), β-casein (β-CN), β-lactoglobulin (β-Lg), and α-lactalbumin (α-La), as well as a low level of lactoferrin (LF), bovine serum albumin (BSA), and immunoglobulin (Ig). The hydrolysis patterns in the before- and after-meal states exhibited their trends as a function of time, but had minimal differences among these three yogurts under a particular condition. This negligible effect of curcumin on the digestion of proteins in food matrix was possibly attributed to the low dose of curcumin used in this study (1.6 mg per 100 ml yogurt) and the rapid breakdown of yogurt proteins.

Due to the changes of solid contents during the *in vitro* dynamic digestion, the digesta were diluted with water at different ratios according to the gastric emptying

curves and secretion rates, to reach a final load of 10 µg proteins plus hydrolysates per lane. The intensity of each band was quantified based on the band volume using Gel Doc XR+ and Image Lab. The degree of hydrolysis was expressed as a percentage of the disappearance of the protein fraction bands compared to native protein fractions at 0 min, presented as the mean ± SD of the three yogurts (Meinlschmidt et al., 2016). After the first 30 min, the bands of BSA, LF, and Lg could not be observed in both states. Meanwhile, αs-CN and β-CN bands completely lost their intensities in the before-meal state, indicating the enzyme sensitivity of caseins due to the flexible and open structures. While the casein bands remained visible in the after-meal state at 30 min, showing a hydrolysis degree of (88.0±5.6)% for αs-CN and (87.4±6.0)% for β-CN. With αs- and β-CN largely hydrolysed in the after-meal state, the band of κ-casein (κ-CN, ~19 kDa) became identifiable with low intensity at 30 min. So did the band of γ-casein (γ-CN, ~16.0 kDa) as a proteolytic product of β-CN. In comparison to casein, β-Lg had a relatively low degree of hydrolysis, (80.0±4.6)% in the before-meal state, and (53.8±9.2)% in the after-meal state. The intensity of α-La band (~14 kDa) kept almost unchanged at 30 min in the before-meal state and even increased in the after-meal state superficially. This is presumably because of the enzyme resistance of native α-La (Nguyen et al., 2015) and the generation of polypeptides by enzymatic hydrolysis with a similar molecular weight. The intensive bands at the bottom of each lane represented the presence of proteolytic products with smaller molecular weights (<11 kDa) in both states at 30 min. All the bands disappeared in the electropherograms at 180 min with the only remaining band of ~58 kDa belonging to the heated pancreatin (Shen et al., 2013), observed in all digested samples with very low intensity. This means a high degree of protein hydrolysis, which was verified by increasing the final load of protein hydrolysates from 10 µg per lane to 100 µg per lane. Apart from the band of heated pancreatin, the six bands from 20-55 kDa were attributed to proteases (23.8 kDa), trypsin (~24 kDa), pepsin (34.5 kDa), lipase (~38 kDa), and amylase (~45 kDa, and 50-57 kDa) from the simulated digestive fluids. The fainter bands of polypeptides (~17.8 kDa) only appeared in the after-meal states. The bands of the peptides (3-15 kDa) in the after-meal state displayed higher intensities than those in the before-meal state. Both of them imply a slower digestion in the after-meal state, which was also observed in the digestion patterns at 30 min, caused by the slower emptying, secretion, higher viscosity, and the resulting more

unfavourable pH in the after-meal state. From the perspective of tenfold high load, the intensity of these peptide bands remained very low, indicating that the majority of the proteins were broken down to undetectable peptides less than 3 kDa *i.e.,* a high degree of protein hydrolysis at 180 min in both states.

The protein compositions of yogurt digesta were affected by the gastric emptying kinetics, secretion rate, and pH profiles. The proteolysis patterns were in turn considered as one of the dominant factors in the digesta viscosity (the other was dilution effect). In macroscopic view, the higher degree of hydrolysis implied the faster reduction in viscosity, and the quicker microparticle disintegration and curcumin release.

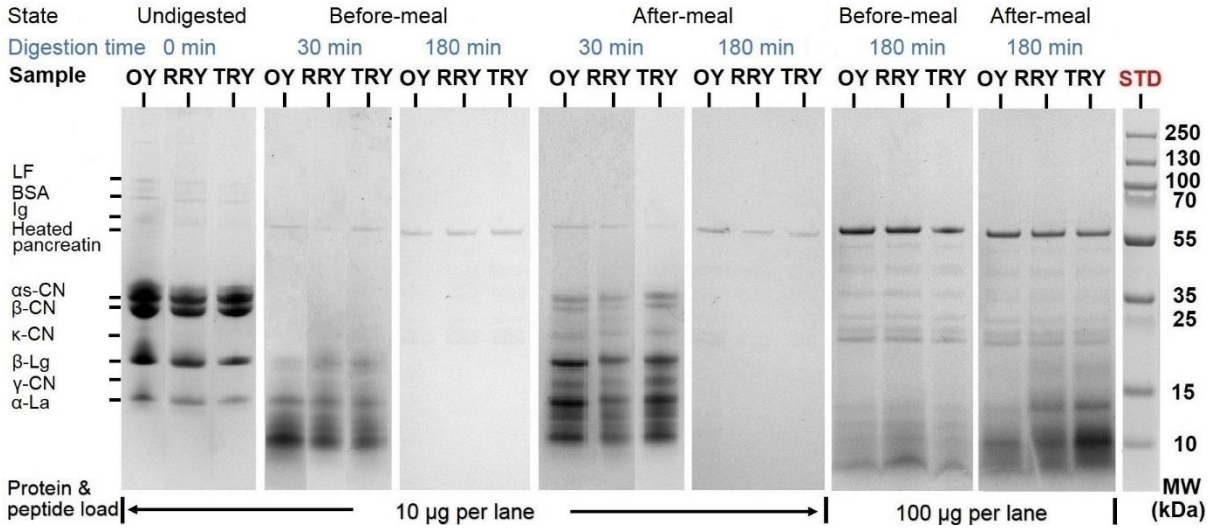

Fig. 5.8. SDS-PAGE profile of the intestinal digesta of the original yogurt (abbreviated to OY), RR-yogurt (RRY), and TR-yogurt (TRY) in the before- and after-meal states.

5.5 Conclusion

The DIVHS can be used to obtain more easily the digestion data comparing with the *in vivo* procedures which clearly have many limitations. The *in vitro* tests are useful for investigating digestion from various perspectives with high reproducibility. In this study, after yogurt intake, the *in vivo* gastric emptying and pH profiles in the before- and after-meal states were successfully reproduced using the DIVHS. The effects of enzymatic hydrolysis and dilution were found to play a predominant role in reducing the viscosity of the gastric digesta. The slower gastric emptying kinetics in the after-meal state caused the delay of curcumin release and proteolysis in both RR-yogurt

and TR-yogurt. A low-dose semi-solid food is unable to effectively trigger the sieving effect and cholecystokinin release to delay its gastric emptying. Therefore, the ingestion pattern largely affected the viscosity of gastric and duodenal digesta, intestinal release of active ingredients, structure disintegration, and proteolysis pattern, which was hardly observed using normal *in vitro* digestion methods.

5.6 Reference

Berrada, N., Lemeland, J.-F., Laroche, G., Thouvenot, P., & Piaia, M. (1991). Bifidobacterium from Fermented Milks: Survival During Gastric Transit. *Journal of dairy science, 74*(2), 409-413.

Camilleri, M. (2006). Integrated Upper Gastrointestinal Response to Food Intake. *Gastroenterology, 131*(2), 640-658.

Chen, L., Xu, Y., Fan, T., Liao, Z., Wu, P., Wu, X., & Chen, X. D. (2016, 2016/08/01/). Gastric emptying and morphology of a 'near real' in vitro human stomach model (RD-IV-HSM). *Journal of Food Engineering, 183*, 1-8.

Dalgalarrondo, M., Dufour, E., Chobert, J.-M., Bertrand-Harb, C., & Haertlé, T. (1995, 1995/01/01/). Proteolysis of β-lactoglobulin and β-casein by pepsin in ethanolic media. *International dairy journal, 5*(1), 1-14.

DeSesso, J. M., & Jacobson, C. F. (2001, 2001/03/01/). Anatomical and physiological parameters affecting gastrointestinal absorption in humans and rats. *Food and Chemical Toxicology, 39*(3), 209-228.

Ehrlein, H., & Schemann, M. (2005). Gastrointestinal motility. *Technische Universität München: Munich*, 1-26.

Holdsworth, S. D. (1971). APPLICABILITY OF RHEOLOGICAL MODELS TO THE INTERPRETATION OF FLOW AND PROCESSING BEHAVIOUR OF FLUID FOOD PRODUCTS. *J Texture Stud, 2*(4), 393-418.

Huart, F., Peclers, N., Béra, F., Beckers, Y., & Malumba, P. (2020, 2020/02/01/). The effect of hydrodynamic conditions on the monogastric-like in vitro digestion of maize flours dried at different temperatures. *LWT, 120*, 108917.

Hunt, J. N., & Stubbs, D. F. (1975). The volume and energy content of meals as determinants of gastric emptying. *The Journal of physiology, 245*(1), 209.

Indireshkumar, K., James, G. B., Henryk, F., Geoffrey, S. H., Patrik, K., John, D., Christine, F., Meijng, L., Peter, B., Michael, F., & Werner, S. (2000). Relative contributions of "pressure pump" and "peristaltic pump" to gastric emptying. *Am J Physiol Gastrointest Liver Physiol, 278*(4), 604-616.

Janssen, P., Vanden Berghe, P., Verschueren, S., Lehmann, A., Depoortere, I., & Tack, J. (2011). Review article: the role of gastric motility in the control of food intake. *Aliment Pharmacol Ther, 33*(8), 880-894.

Jerry, D. G., Arthur, A. C., & Malcolm, R. (2002). Measurement of meal-stimulated gastric acid secretion by in vivo gastric autotitration. *J Appl Physiol (1985), 92*(2), 427-434.

Keszthelyi, D., Knol, D., Troost, F., Avesaat, M., Foltz, M., & Masclee, A. (2013). Time of ingestion relative to meal intake determines gastrointestinal responses to a plant sterol–containing yoghurt drink. *European Journal of Nutrition, 52*(4), 1417-1420.

Kong, F., & Singh, R. P. (2008, Jun). Disintegration of solid foods in human stomach. *J Food Sci, 73*(5), R67-80.

Kong, F., & Singh, R. P. (2010, Nov-Dec). A human gastric simulator (HGS) to study food digestion in human stomach. *J Food Sci, 75*(9), E627-635.

Kozu, H., Nakata, Y., Nakajima, M., Neves, M. A., Uemura, K., Sato, S., Kobayashi, I., & Ichikawa, S. (2014). Development of a Human Gastric Digestion Simulator Equipped with Peristalsis Function for the Direct Observation and Analysis of the Food Digestion Process. *Food Science and Technology Research, 20*(2), 225-233.

Liou, A. P., Chavez, D. I., Espero, E., Hao, S., Wank, S. A., & Raybould, H. E. (2011). Protein hydrolysate-induced cholecystokinin secretion from enteroendocrine cells is indirectly mediated by the intestinal oligopeptide transporter PepT1. *Am J Physiol Gastrointest Liver Physiol, 300*(5), G895-G902.

Malagelada, J.-R., Go, V., & Summerskill, W. (1979). Different gastric, pancreatic, and biliary responses to solid-liquid or homogenized meals. *Digestive Diseases and Sciences, 24*(2), 101-110.

Marciani, L., Pritchard, S. E., Hellier-Woods, C., Costigan, C., Hoad, C. L., Gowland, P. A., & Spiller, R. C. (2013). Delayed gastric emptying and reduced postprandial small bowel water content of equicaloric whole meal bread versus rice meals in healthy subjects: novel MRI insights. *Eur J Clin Nutr, 67*(7), 754-758.

McCloy, R. F., Greenberg, G. R., & Baron, J. H. (1984). Duodenal pH in health and duodenal ulcer disease: effect of a meal, Coca-Cola, smoking, and cimetidine. *Gut, 25*(4), 386-392.

Meinlschmidt, P., Schweiggert-Weisz, U., Brode, V., & Eisner, P. (2016). Enzyme assisted degradation of potential soy protein allergens with special emphasis on the technofunctionality and the avoidance of a bitter taste formation. *Food science & technology, 68*, 707-716.

Mercuri, A., Curto, A., Wickham, M., Craig, D., & Barker, S. A. (2008, 01/01). Dynamic gastric model (DGM): A novel in vitro apparatus to assess the impact of gastric digestion on the droplet size of self-emulsifying drug-delivery systems. *J. Pharm. Pharmacol., 60*.

Minekus, M., Alminger, M., Alvito, P., Ballance, S., Bohn, T., Bourlieu, C., Carrière, F., Boutrou, R., Corredig, M., Dupont, D., Dufour, C., Egger, L., Golding, M., Karakaya, S., Kirkhus, B., Le Feunteun, S., Lesmes, U., Macierzanka, A., Mackie, A., Marze, S., McClements, D. J., Ménard, O., Recio, I., Santos, C. N., Singh, R. P., Vegarud, G. E., Wickham, M. S. J., Weitschies, W., & Brodkorb, A. (2014). A standardised static in vitro digestion method suitable for food - an international consensus. *Food Funct, 5*(6), 1113-1124.

Minekus, M., Marteau, P., Havenaar, R., & Veld, J. (1995, 03/01). A multicompartmental dynamic computer-controlled model simulating the stomach and small intestine. ATLA Altern Lab Anim. *Alternatives to laboratory animals: ATLA, 23*, 197-209.

Miranda, G., Haze, G., Scanff, P., & Pelissier, J. P. (1989). Hydrolysis of α-lactalbumin by chymosin and pepsin. Effect of conformation and pH. *Lait, 69*(6), 451-459.

Nguyen, T. T. P., Bhandari, B., Cichero, J., & Prakash, S. (2015, 2015/10/01/). Gastrointestinal digestion of dairy and soy proteins in infant formulas: An in vitro study. *Food Research International, 76*, 348-358.

Onoue, S., Takahashi, H., Kawabata, Y., Seto, Y., Hatanaka, J., Timmermann, B., & Yamada, S. (2010). Formulation design and photochemical studies on nanocrystal solid dispersion of curcumin with improved oral bioavailability. *Journal of pharmaceutical sciences, 99*(4), 1871-1881.

Porkka, L., Salminen, E., & Salminen, S. (1988). The effects of lactulose-sweetened yoghurt on the rate of gastric emptying and intestinal transit in healthy human volunteers. *Zeitschrift fuer Ernaehrungswissenschaft, 27*(3), 150-154.

Ravindranath, V., & Chandrasekhara, N. (1981, 1981/01/01/). Metabolism of curcumn-studies with [3H]curcumin. *Toxicology, 22*(4), 337-344.

Ross-Murphy, S. B., Morris, V. J., & Morris, E. R. (1983). Molecular viscoelasticity of xanthan polysaccharide. *Faraday symposia of the Chemical Society, 18*, 115.

Rumsey, D. (2005). SMALL INTESTINE | Structure and Function. In B. Caballero (Ed.), *Encyclopedia of Human Nutrition (Second Edition)* (pp. 126-133). Elsevier.

Sahu, A., Kasoju, N., & Bora, U. (2008, 2008/10/13). Fluorescence Study of the Curcumin−Casein Micelle Complexation and Its Application as a Drug Nanocarrier to Cancer Cells. *Biomacromolecules, 9*(10), 2905-2912.

Sauter, M., Curcic, J., Menne, D., Goetze, O., Fried, M., Schwizer, W., & Steingoetter, A. (2012). Measuring the interaction of meal and gastric secretion: a combined quantitative magnetic resonance imaging and pharmacokinetic modeling approach. *Neurogastroenterology & Motility, 24*(7), 632-e273.

Schulze, K. (2006). Imaging and modelling of digestion in the stomach and the duodenum. *Neurogastroenterol Motil, 18*(3), 172-183.

Shen, C.-R., Liu, C.-L., Lee, H.-P., & Chen, J.-K. (2013). The Identification and Characterization of Chitotriosidase Activity in Pancreatin from Porcine Pancreas. *Molecules, 18*(3), 2978-2987.

Siegel, J. A., Urbain, J. L., Adler, L. P., Charkes, N. D., Maurer, A. H., Krevsky, B., Knight, L. C., Fisher, R. S., & Malmud, L. S. (1988, Jan). Biphasic nature of gastric emptying. *Gut, 29*(1), 85-89.

Sneharani, A. H., Karakkat, J. V., Singh, S. A., & Rao, A. G. (2010, Oct 27). Interaction of curcumin with β-lactoglobulin-stability, spectroscopic analysis, and molecular modeling of the complex. *J Agric Food Chem, 58*(20), 11130-11139.

Wang, J., Wu, P., Liu, M., Liao, Z., Wang, Y., Dong, Z., & Chen, X. D. (2019). An advanced near real dynamic in vitro human stomach system to study gastric digestion and emptying of beef stew and cooked rice. *Food & function, 10*(5), 2914-2925.

Worning, H., Müllertz, S., Hess Thaysen, E., & Bang, H. O. (1967). pH and Concentration of Pancreatic Enzymes in Aspirates from the Human Duodenum during Digestion of a Standard Meal: In Patients with Duodenal Ulcer and in Patients Subjected to Different Gastric Resections. *Scand J Gastroenterol, 2*(1), 23-28.

Xu, X., Xu, J., Zhang, Y., & Zhang, L. (2008, 2008/07/01/). Rheology of triple helical Lentinan in solution: Steady shear viscosity and dynamic oscillatory behavior. *Food hydrocolloids, 22*(5), 735-741.

Ye, Q., Ge, F., Wang, Y., Woo, M. W., Wu, P., Chen, X. D., & Selomulya, C. (2020). On improving bioaccessibility and targeted release of curcumin-whey protein complex microparticles in food. *Food Chem, 346*, 128900-128900.

Chapter 6

Conclusions and Recommendations

6.1 Conclusions

The coupling between desolvation, crosslinking, and spray drying was proposed as a microencapsulation strategy for improving bioaccessibility and controlled release of active food components. Upon encapsulation with WPI, the potential application range of core materials covers bioactive hydrophilic and hydrophobic small molecules, *i.e.,* amino acids, minerals, cholines, sugar alcohols, vitamins, carotenoids, polyphenols and phytosterols. A comparison of the digestion behaviours in the DIVHS to those in the static INFOGEST protocol suggested that the yogurt digestion and curcumin release depended on the physiological process of gastric emptying.

The main scientific outcomes from Chapter 3-5 are:

Modification of molecular conformation of spray-dried whey protein microparticles improving digestibility and release characteristics

Spray-dried WPI-riboflavin microparticles were prepared *via* the combination of ethanol desolvation and calcium ion bridging. Ethanol was introduced as a desolvating agent in the system, with four functions *i.e.,* lowering drying temperature, raising encapsulation efficiency, promoting the generation of ground-state riboflavin-WPI complexes, and exposing WPI cleavage sites to pepsin. The modification of WPI conformation and exposure of cleavage sites to pepsin upon desolvation were observed in the dry powder form after spray drying. The release profiles and digestibility of microparticles could be adjusted by varying the concentrations of ethanol and calcium ions. Microparticles generated from 30% v/v ethanol at 1 and 2 mM Ca^{2+} possessed gastric resistance and sustained intestinal release. The coupling between desolvation and spray drying has huge potential for food application as a versatile and low-cost method of microencapsulation with proteins for controlled release.

On improving bioaccessibility and targeted release of curcumin-whey protein complex microparticles in food

WPI-curcumin complexation *via* desolvation was retained and in fact improved upon spray drying to prepare complex microparticles. After desolvation, the maximum total curcumin amount entrapped reached up to approximately 3.47 mg/g particle, nearly one order of magnitude higher that of the microparticles without desolvation. The spray-dried complex samples had higher solubility and stability under physiological environments than raw curcumin, improving the bioaccessibility. The radical scavenging activity of curcumin was successfully retained in the complex microparticles upon spray drying. The integration of complex samples into yogurt reduced the curcumin release percentages in early gastric digestion and increased the release in the intestinal condition. However, the samples to some extent still retained their release profiles (rapid and targeted formulations). The complex powders present in the yogurts only showed a marginal effect on most of the yogurt properties, except for colour and curcumin flavour. This strategy shows the potential to integrate functional small molecules with low water solubility and bioaccessibility into foods without negative influences on consumer acceptance.

Digestion of curcumin-fortified yogurt in before/after-meal states: A study using a near-real dynamic *in vitro* human stomach

The DIVHS, reproducing the anatomical structures, gastric peristalsis, and biochemical environments of a real stomach as practically as possible, was employed to simulate the gastric processes (emptying and pH variations) during yogurt digestion in before- and after-meal states. The effects of gastric peristalsis, digestive fluid dilution, and enzymatic hydrolysis on digesta viscosity were evaluated respectively, suggesting the predominant role of proteolysis and dilution. After integrating curcumin-WPI complex microparticles into the yogurt, the slower gastric emptying in the after-meal state resulted in the delay of curcumin release, particle disintegration, and enzymatic hydrolysis in both RR-yogurt and TR-yogurt. The ingestion pattern influenced the viscosity of gastric and duodenal digesta, intestinal release kinetics of functional components, food matrix breakdown, and digestion pattern, which was difficult to be observed using traditional *in vitro* digestion methods. The DIVHS can be applied to study digestion more easily from various perspectives with high reproducibility, comparing to the *in vivo* procedures with many limitations.

The following is a summary of the key findings from Chapter 3-5:

1) The combination of ethanol desolvation and calcium ion bridging has allowed the production of crosslinked riboflavin-WPI microparticles upon spray drying.
2) Ethanol, as a desolvating agent in the system, has four basic functions *i.e.,* reducing drying temperature, increasing encapsulation efficiency, facilitating the formation of ground-state riboflavin-WPI complexes, and exposing WPI cleavage sites to pepsin.
3) The modification of WPI conformation and accessibility to cleavage sites for pepsin *via* desolvation is successfully retained in the dry state using spray drying.
4) The release characteristics and digestibility of WPI-riboflavin microparticles can be easily tuned by ethanol content and calcium ion concentration.
5) The complexation between WPI and curcumin upon desolvation is retained and in fact enhanced *via* spray drying to produce microparticles.
6) Upon desolvation, the maximum total curcumin content loaded in the WPI-curcumin microparticles could be up to around 3.47 mg/g particle, almost one order of magnitude higher than that of the sample without desolvation 0.37±0.03 mg/g.
7) The curcumin-WPI complex microparticles would possess better solubility and stability at physiological conditions compared to curcumin alone, enhancing the bioaccessibility.
8) The addition of curcumin-WPI microparticles into yogurt had negligible effects on the sensory properties of yogurt, except for colour and curcumin flavour.
9) The DIVHS is able to reproduce the *in vivo* gastric emptying and pH changes in before/after-meal states.
10) The curcumin release from yogurt can reach a maximum of 43% at 120 min in the before-meal state, and only 16% at 180 min in the after-meal state using the DIVHS, compared to 80% release at 90 min using the INFOGEST protocol. The release differences between the static protocol and the DIVHS, and between the two states, were attributed to the emptying kinetics in each state.
11) The slower gastric emptying would cause the delay of microparticle disintegration and proteolysis in yogurt.
12) The effects of enzymatic hydrolysis and dilution play a predominant role in reducing the viscosity of the gastric digesta.

6.2 Recommendations

This project presented the microencapsulation strategies of bioactive small molecules in solids using WPI *via* ethanol-induced desolvation. After incorporation into yogurt, the digestion behaviours and release mechanisms were studied in the absence of solid meals. The future work needed for more in-depth understanding in various areas is listed as follows:

1) Due to the protein amphiphilicity by nature and the adjustable solvent polarity by desolvation, this methodology has the potential to prepare WPI microparticles loaded with functional oils (*e.g.,* unsaturated fatty acids and essential oils) upon spray drying.
2) A similar strategy could be applied to other proteins with similar or different features. As stated above, polyphenols possess an excellent binding affinity for proteins, particularly proline-rich proteins, promoting the formation of polyphenol-protein complexes. A typical dairy protein of β-casein is rich in proline but highly susceptible to digestive enzymes due to the flexible and open structure. Therefore, polyphenol-β-casein microparticles prepared using the strategy in this thesis would be expected to show stable complexation with improved water solubility, chemical stability, and thus bioaccessibility of polyphenols, as well as tunable gastric resistance of microparticles as a function of crosslinking extent.
3) The addition of desolvating agent with a relatively low boiling point led to a low drying temperature and a fast drying rate of feed solutions. As a heat-sensitive polyphenol, curcumin retained its radical scavenging property in the form of spray-dried microparticles. This raises the possibility that heat-labile macromolecules like β-galactosidase may be incorporated into the WPI microparticles *via* spray drying without reducing its enzymatic activity.
4) Bioactive small molecules like vitamins and phytochemicals possess different binding affinities for various proteins, depending on the hydrogen bond pairing. To optimise the pairing and thus increase the water solubility, stability, and bioaccessibility of the small molecules, screening on proteins is a widely used method. Desolvation process can adjust the H-bond interaction between proteins and ligands, based on the results of the research reported in this thesis. Therefore, a screening of desolvating agents with different polarities

could be an alternative solution to prepare protein-ligand complexes with improved physicochemical properties.

5) No solid meals were loaded in the dynamic digestion experiments. The gastric contents from solid foods may have a buffering effect on the pH profiles, microparticle disintegration, complex dissociation, curcumin release, and proteolysis pattern of yogurt chyme. To investigate the above influences, three types of solid food rich in carbohydrates, lipids, and proteins can be ingested along with the curcumin-fortified yogurt, separately.

Appendix. The front pages of the published papers of this project during the enrolment

Trends in Food Science & Technology 78 (2018) 167–179

Contents lists available at ScienceDirect

Trends in Food Science & Technology

journal homepage: www.elsevier.com/locate/tifs

Review

Microencapsulation of active ingredients in functional foods: From research stage to commercial food products

Qianyu Ye[a], Nicolas Georges[b], Cordelia Selomulya[a,*]

[a] Department of Chemical Engineering, Monash University, Clayton Campus, Victoria 3800, Australia
[b] School of Chemistry, Monash University, Clayton Campus, Victoria 3800, Australia

ARTICLE INFO

Keywords:
Functional food
Microencapsulation
Active ingredients
Functional properties

ABSTRACT

Background: Twelves categories of active ingredients have been recognised to enhance human health. They are to some extent susceptible to certain conditions such as heat, light and low pH. To reduce their susceptibility and achieve controlled release at the target site, various microencapsulation strategies have been introduced.
Scope and approach: In this review, the chemical structures, physicochemical properties and beneficial effects of the active components are summarised. Different encapsulation techniques and tailored shell materials have been investigated to optimise the functional properties of microcapsules. Several encapsulated constituents (e.g., amino acids) have been successfully incorporated into food products while others such as lactic acid bacteria are mostly used in the free format. Encapsulating some of these active ingredients will extend their ability to withstand process conditions such as heat and shear, and prolong their shelf stability.
Key findings and conclusions: The functional properties of a microcapsule are encapsulation efficiency, size, morphology, stability, and release characteristics. Several microencapsulation strategies include the use of double emulsions, hybrid wall materials and crosslinkers, increasing intermolecular attraction between shell and core, physical shielding of shell materials, and the addition of certain ions. Other approaches such as the use of hardening agents, nanoencapsulation, or secondary core materials, and the choice of shell materials possessing specific interactions with the core may be used to achieve targeted release of active ingredients. The physicochemical properties of shell materials influence where the active ingredients will be released *in vivo*. A suitable microencapsulation strategy of active ingredients will therefore expand their applications in the functional foods industry.

1. Introduction

In the last decades, the concept of food has changed greatly. Nutrition is not only to sustain life, supply energy, or promote growth, but also to prevent disease and enhance physical and mental health. In the latter fields, "functional food" especially has attracted increasing attention.

Generally, functional foods are closely regulated but not recognised by law in most countries, resulting in no statutory definition. There is a working definition adopted by the European Commission Concerted Action i.e., "a food can be regarded as 'functional' if it satisfactorily demonstrates to improve beneficially one or more target functions in the body, beyond the adequate nutritional effects in a way that is relevant to either an improved state of health and well-being and/or reduction of risk of disease" (Action, 1999). With respect to legal supervision, functional foods are regulated by Food and Drug Administration (FDA) in the USA but they are not specifically defined by law. Food Standards Australia New Zealand defines novel foods and food for special medical purposes. Japan regulates and oversees functional foods, named "Foods with Health Claims," under the provision of a specific regulatory approval process. According to the Japanese Ministry of Health and Welfare, twelve broad categories of ingredients have been regarded to promote human health: dietary fibre; oligosaccharides; sugar alcohols; amino acids, peptides and proteins; glucosides; alcohols; isoprenes and vitamins; cholines; lactic acid bacteria; minerals; unsaturated fatty acids; and others e.g., phytochemicals and antioxidants (Goldberg, 2012).

The supplementation of these active ingredients into food and dairy products is a commonly used method in the food industry to improve the nutritional value. Many of the ingredients have been researched and manufactured to produce functional foods such as orange juice with added calcium, eggs with increased omega-3 content, and sunflower seeds with guarana. In some of the cases, however, the active ingredients and their true effects on physiological functions in humans

* Corresponding author.
E-mail address: Cordelia.Selomulya@monash.edu (C. Selomulya).

https://doi.org/10.1016/j.tifs.2018.05.025
Received 8 January 2018; Received in revised form 29 May 2018; Accepted 31 May 2018
Available online 06 June 2018
0924-2244/

Food Chemistry 280 (2019) 255–261

Contents lists available at ScienceDirect

Food Chemistry

journal homepage: www.elsevier.com/locate/foodchem

Modification of molecular conformation of spray-dried whey protein microparticles improving digestibility and release characteristics

Qianyu Ye, Meng Wai Woo, Cordelia Selomulya*

Department of Chemical Engineering, Monash University, 18 Alliance Lane, Clayton, VIC 3800, Australia

ARTICLE INFO

Keywords:
Microencapsulation
Desolvation
Spray drying
Targeted release
Riboflavin

ABSTRACT

This study reports on the preparation of riboflavin-loaded whey protein isolate (WPI) microparticles, using desolvation and then spray drying. Ethanol desolvation led to the exposure of embedded hydrophobic amino acids of WPI to riboflavin, facilitating the formation of riboflavin-WPI complexes. The extent of desolvation and cross-linking influenced the morphology of the spray-dried microparticles, while the moisture content of microparticles decreased with desolvation and increased with crosslinking. The modification of WPI conformation upon desolvation could be retained in the dry state *via* spray drying. The gastric resistance, release site and release characteristics of microparticles were readily adjusted by varying the ethanol and calcium ion contents from 0 to 50% v/v and from 0 to 2 mM, respectively. The sample prepared from 30% v/v ethanol without calcium crosslinking displayed rapid peptic digestion in less than 30 min. The samples from 30% v/v ethanol at 1 and 2 mM Ca^{2+} exhibited excellent gastric resistance and intestinal release.

1. Introduction

Many efforts have been devoted to the research, design, and production of nutraceuticals and functional foods to provide public health benefits such as enhanced cognitive performance, gut immune function and improved anti-oxidant capabilities (Duffy, Wiseman, & File, 2003). However, a great number of active components lack bioavailability by oral administration because of poor solubility and/or permeability in the gut (Varma et al., 2004). Moreover, some bioactives are unstable during food processing (exposure to heat, oxygen, light) or in the gastro-intestinal tract (due to acid, proteolysis, or interactions with other substances) (Arbos, Arangoa, Campanero, & Irache, 2002).

In the past decades, encapsulation strategies using food-grade carriers have been proposed to protect and incorporate active ingredients into functional foods. Whey protein isolates (WPI) are one type of extensively used milk proteins, considered as water-soluble, cheap, safe (GRAS *i.e.*, Generally Recognized As Safe, an American Food and Drug Administration designation), and nutrient-dense coating materials. It is a mixture of around 60% β-lactoglobulin, 22% α-lactalbumin, 5.5% bovine serum albumin and 9.1% immunoglobulins (Bryant & McClements, 1998). As the principal component, native β-lactoglobulin is not digested by pepsin since most cleavage sites of this globular protein for pepsin are buried in its hydrophobic cores (Dalgalarrondo, Dufour, Chobert, Bertrand-Harb, & Haertlé, 1995; Kitabatake & Kinekawa, 1998). The low peptic digestion of WPI is regarded as the leading cause of its allergenicity (Schmidt, Meijer, Slangen, & Van Beresteijn, 1995). Many means *e.g.*, heat treatment, high pressure, esterification, sulfitolysis and desolvation, have been applied to improve the WPI susceptibility to enzymatic hydrolysis (Dalgalarrondo et al., 1995; Maynard, Weingand, Hau, & Jost, 1998). Desolvation induced by alcohols is proven to change the solvent bulk dielectric constant and form competing hydrogen bonds with proteins, causing the shift of protein secondary structure and exposure of cleavage sites of β-lactoglobulin for pepsin (Dalgalarrondo et al., 1995; Hirota-Nakaoka & Goto, 1999). The effect of desolvation on protein susceptibility to pepsin hydrolysis has been investigated in the aqueous suspension state but rarely in the dry state. The first aim of this study was to investigate the reversibility of protein susceptibility to pepsin *via* desolvation in the aqueous suspensions *versus* in the dry state.

Meanwhile, desolvation leads to the coacervation of protein molecules in the aqueous phase and formation of nanoparticles, which can act as drug delivery devices (Soppimath, Aminabhavi, Kulkarni, & Rudzinski, 2001). It has been reported that WPI can bind and transport various ligand molecules such as riboflavin (Diarrassouba, Liang, Remondetto, & Subirade, 2013) and resveratrol (Liang, Tajmir-Riahi, & Subirade, 2007). However, very few studies have investigated the binding behaviour and generation of ligand-WPI complexes under desolvation condition. It is reported that a part of WPI and ligands

* Corresponding author.
E-mail address: Cordelia.Selomulya@monash.edu (C. Selomulya).

https://doi.org/10.1016/j.foodchem.2018.12.074
Received 15 October 2018; Received in revised form 14 December 2018; Accepted 14 December 2018
Available online 22 December 2018

Food Chemistry 346 (2021) 128900

Contents lists available at ScienceDirect

Food Chemistry

journal homepage: www.elsevier.com/locate/foodchem

On improving bioaccessibility and targeted release of curcumin-whey protein complex microparticles in food

Qianyu Ye [a], Fangzi Ge [b], Yong Wang [c], Meng Wai Woo [d], Peng Wu [b], Xiao Dong Chen [b], Cordelia Selomulya [c,*]

[a] Department of Chemical Engineering, Monash University, Clayton 3168, Australia
[b] Suzhou Key Laboratory of Green Chemical Engineering, School of Chemical and Environmental Engineering, College of Chemistry, Chemical Engineering and Materials Science, Soochow University, Suzhou 215123, China
[c] School of Chemical Engineering, UNSW Sydney, NSW 2052, Australia
[d] Department of Chemical & Materials Engineering, The University of Auckland, Auckland, New Zealand

ARTICLE INFO

Keywords:
Curcumin
Complexation
Bioaccessibility
Food matrix
Targeted release
Sensory

ABSTRACT

Curcumin is a bioactive food component, with poor bioaccessibility due to low water solubility and stability. Spray drying retained and in fact enhanced curcumin-whey protein isolate (WPI) complexation *via* desolvation, lowering the amount of unbound curcumin to <5% wt after drying, forming microparticles with better water solubility, stability, and bioaccessibility than raw curcumin. The desolvated microparticles encapsulated 3.47 ± 0.05 mg/g curcumin, almost one order of magnitude higher than the un-desolvated sample 0.37 ± 0.03 mg/g. After incorporation into yogurt, the rapid-release formula liberated 87% curcumin, whereas the targeted-release one discharged 44% before entering the simulated intestinal condition. Most of the yogurt sensory properties were not adversely affected, except for colour and curcumin flavour. This study proposed a strategy in which food ingredients containing hydrophobic bioactive small molecules can be incorporated into a food matrix to improve bioaccessibility and targeted release, without affecting their sensory properties.

1. Introduction

Curcumin is a hydrophobic polyphenol extracted from the rhizome of turmeric plant, reported to be around 3% by dry weight (Wang et al., 2008). Chemically, it is composed of two aryl rings with one hydroxyl and one methoxy substituents on individual moiety, connected with a seven-carbon chain in keto or enol form according to the medium pH. The keto/enol moiety and two phenolic groups of curcumin are considered as reactive functional groups, responsible for its pharmacological effects such as anti-inflammatory, antioxidant, anti-tumour, anti-proliferative, and anti-angiogenic activities (Khan, Zafaryab, Mehdi, Ahmad, & Rizvi, 2016). Several issues still limit the application of curcumin in food and pharmaceutical industry. These include a short shelf life from chemical instability, and low bioaccessibility due to poor aqueous solubility, low absorption, rapid metabolism, and elimination.

The technique of nano/microencapsulation is recognised as a feasible method to control release characteristics, and to increase solubility, stability, and resulting bioavailability of curcumin. It has been reported that curcumin entrapped within chitosan nanoparticles *via* ionic gelation exhibited sustained release and anti-proliferative activity (Khan et al., 2016). Curcumin coated within complexed biopolymers of zein and alginate/gelatin using electrostatic deposition and solvent evaporation, showed improved stability, bioaccessibility and antioxidant activity (Yao, Chen, Song, McClements, & Hu, 2018). However, most of these formulations were prepared in batch processes, which are challenging to scale up. Only a few cases were made in a continuous process of spray drying (Liu, Chen, Cheng, & Selomulya, 2016; Pan, Zhong, & Baek, 2013), which is extensively used in the food industry. These previous efforts focused on increasing solubility and dispersibility of curcumin, with little attention paid to incorporate curcumin-loaded microparticles into a food matrix, to investigate their targeted-release behaviour in food with improved bioaccessibility and without diminishing its sensory properties.

It has been extensively reported that polyphenols have a characteristic binding affinity for proteins, especially proline-rich proteins (*e.g.*, salivary proteins), resulting in the generation of polyphenol-protein complexes (Carnovale, Britten, Couillard, & Bazinet, 2015; Guo et al., 2020; Kaspchak, Goedert, Igarashi-Mafra, & Mafra, 2019). The extent of

* Corresponding author.
E-mail address: cordelia.selomulya@unsw.edu.au (C. Selomulya).

https://doi.org/10.1016/j.foodchem.2020.128900
Received 1 July 2020; Received in revised form 2 October 2020; Accepted 16 December 2020
Available online 29 December 2020
0308-8146/